THE REPORT OF STUDY RESULT BY SUBSIDY

助成研究成果報告書

第26回

The Watanabe Foundation
公益財団法人 渡邉財団

助　成　研　究　成　果

報　告　書

第26回

（研究期間：令和2年4月1日～令和3年3月31日）

公益財団法人 渡邉財団

目　　次

巻　頭　言

公益財団法人 渡邉財団

理事長　小　谷　　誠

今から45年程前に私は米国のマサチューセッツ工科大学（MIT）に留学して、人間の身体から発生する微弱な磁気を計測して、病気の診断に役立てようとする研究を2年間行い、帰国後も生体磁気計測の研究を続けてきた。

人間の心臓や脳からは微弱な磁気が発生していることは以前から推定されていたが、この微弱な磁気を計測できる磁束計がなかった。ところが、1970年代に超伝導技術を応用した超高感度のSQUID磁束計が米国立研究所とMITの共同研究で開発された。

MITではこのSQUID磁束計を用いて、心臓から発生する磁気の計測に成功し、更に心臓磁気の千分の1程度の脳から発生する磁気計測に挑戦している頃、私はMITに留学した。

私がMITに留学した頃、MITの研究所では大変なことが起っていた。それは、米国の著名な医師が、「MITのグループは心臓や脳の神経活動に伴って発生する磁気を計測していると言っているが、それは間違いである。彼らの計測している磁気は血液の中の鉄分が地磁気を乱している磁気を計測しているのにすぎない」と新聞で批判された。その結果、MITの生体磁気計測の研究への米国の公的研究費は大幅に削減されていた。

私は、この医師の意見は理にかなっていると思って、十数名の健常者の血液を採取してSQUID磁束計で計測したが、血液は全く磁性がないことがわかった。

その理由は、鉄自体は常に磁性を持っているが、鉄が酸素と結合する仕方によって強い磁性を持ったり、全く磁性を持たなくなる。血液中の鉄は全く磁性を持たないように酸素と結合しているのである。

人間の祖先がこの世に登場し、立って歩き、言葉を交わすようになったのは、今から200万年程前と云われている。この間に、地磁気の大きさと方向が10回ほど変わっている。このように地磁気の大きさや方向が大きく変わる環境の中で人間は進化してきたので、地磁気の影響はあまり受けないように人体はできている。

ところが、人間が電気を使うようになったのは、僅か200年ほど前からである。そのため、人体は電気に対しては防衛能力が進化しておらず、大変敏感に反応する。例えば、心臓の表面に数ボルトの電圧を加えると心臓は正常に働かなくなる。ところが、外部から心臓に磁気を加えて心臓を止めることは大変困難である。

このような人体の特徴から電気治療器は即効性があるが、取り扱いを間違えると大変危険である。それに対して、磁気治療器は危険性は少ないが、時間をかけてじっくり治療する必要性があると思われる。

本財団は生体磁気現象を通して国民の医療と健康に貢献することを目的として、学術研究を助成し、講演会を開催するなど、社会に向けた活動をしている。しかし、磁気の作用は、基礎的現象から始まり、体内の複雑な相互作用への関与を通して生じるものであり、短期間の実験試行ではなく、長期間腰を落ち着けて追求して初めて明らかにされることが多い。

いっぽう昨今の学界においては、短期間に成果を挙げ、学位や業績に結びつけようとする雰囲気が強く、原因結果の関係が明白な現象や、客観的に説明できる現象に関心が集中するように見受けられる。これに対して本財団は、性急に成果を求めようとするよりも、長期間にわたる努力を覚悟して特定の問題に取り組む学究の徒を支援したいと考えている。

この報告書は、令和元年度に助成した研究の報告書を、原文のままにまとめたものである。基礎面から実際の応用にいたる広い範囲の研究が含まれているが、いずれもこの領域に新しい道を拓くことを目指している。この報告書が契機になって、志を同じくする研究者の間に連絡が始まり、磁気健康科学の発展に貢献することを期待している。

中枢神経障害に対する磁気刺激の治療的効果の検証

The effect of transcranial magnetic stimulation on neurodegeneration

藤田幸
Yuki Fujita

大阪大学大学院医学系研究科，〒565-0873　大阪府吹田市山田丘 2-2
Department of Molecular Neuroscience,
Graduate school of Medicine, Osaka University
2-2 Yamadaoka, Suita-shi, Osaka 565-0871, Japan

Abstract

Damaged axons in the adult central nervous system (CNS) fail to regenerate spontaneously due to several intrinsic and extrinsic factors that inhibit axon elongation. Transcranial magnetic stimulation (TMS) has been used as a form of rehabilitation, and accumulating studies have suggested that TMS is able to modulate neural plasticity of the cortex. Here, we conducted TMS in mice with CNS injury to investigate the potential effects on motor recovery.

Keywords: central nervous system, brain, spinal cord, neuron, TMS

1. 目的

脳血管障害や交通事故などにより中枢神経回路である皮質脊髄路が障害されると，神経細胞間の連絡を担う神経軸索が切断され，細胞間の連絡が途絶えてしまう．脊髄損傷などにより，運動機能を司る皮質脊髄路が一度損傷を受けると，著しい運動機能障害を生じ，ほとんど寝たきりの状態になることもしばしばある．脊髄損傷は国内に 10 万人以上の患者が存在する中枢神経障害であるにも関わらず，根本的な治療法の確立は困難を極めている．このような現状から，中枢神経損傷に対する新たな治療の開発は緊急の課題である．本研究は，損傷により破綻した神経回路の再形成促進という新たな観点から，中枢神経再生治療法の開発に貢献することを目指した

中枢神経損傷の治療のためには，切断された皮質脊髄路神経の軸索が再び伸長し，神経回路を再構築する必要がある．しかし，中枢神経の軸索は元のように再生しないため，回路を元通りにすることはできない．これは損傷を受けた中枢神経細胞周囲に，軸索再生を阻む機構が存在するためである．申請者はこれまでに中枢神経再生阻害の分子機序を明らかにしてきた (文献 1). また，一部の運動機能の回復には神経回路の再構築が関与することが明らかになってきた．つまり，損傷を免れた神経軸索が脊髄内で側枝を形成し，運動神経に投射している介在神経と接続することで，損傷部を避けた「迂回路」が構築され，運動機能の回復を担うことがわかってきた．このような「代償性神経回路」の形成を促すことは，神経細胞に備わった「可塑性」を活かした有効な手段であると期待される．

本研究では，脊髄損傷や頭部外傷により障害を受けた中枢神経回路の再形成を効果的に促すために，経頭蓋磁気刺激 (TMS)による効果的な治療法を確立することを目的とした．損傷を受けた中枢神経回路が再構築される過程を経時的に観察し，中枢神経回路修復過程の各ステップが時間

経過と共にどのように進行するか, 明らかにすることを試みた. また, TMS により生じる神経回路の修復促進効果について検証した. 神経可塑性を導く TMS により, 破綻した神経回路の再形成が促されるメカニズムを解明し, 動物モデルを用いて最適な TMS 施術条件を決定することが, 本研究の目標である.

2.方法

本研究では, TMS 施術が神経損傷後の回復過程へ与える影響を検証. これまで, 中枢神経損傷後の側枝伸張の促進や, 神経細胞保護, 過剰な免疫細胞の抑制などによって, 部分的に損傷後の運動機能の改善が見られた (文献 2). 本研究では, 回路修復の適切なタイミングで TMS を施術することで, 中枢神経障害後の神経機能の回復を効果的に促すことが可能かどうか検証した.

(1) 中枢神経回路修復のメカニズムとタイムコースの解析

マウスの大脳皮質運動野に由来する皮質脊髄路を, 胸部脊髄レベルで部分的に切断したモデルを用いた. このモデルでは, 胸部以下, 特に顕著に後肢の運動機能障害が観察される. 切断を免れた皮質脊髄路が頸髄において分枝を伸ばし, propriointerneurons を介して motor neurons に至る代償性神経回路を形成する. 本研究では,損傷前後の側枝数やシナプスの経時的な変化を検証するため, 中枢神経損傷モデルマウスを作製した後, 大脳皮質運動野に順行性トレーサーまたはウイルストレーサーを注入し, 皮質脊髄路からの側枝やシナプス結合を標識した. その後, 脊髄内において観察された側枝の数やシナプス結合を損傷前, 損傷後経時的に測定した.

(2) TMS による運動機能の回復

脊髄損傷後, TMS を施術することで運動機能回復が亢進するか, 検証した. コントロール群, TMS 群のマウスで, 損傷 1, 7, 14, 21, 28, 35, 42 日後, 以下の 3 種類の運動機能テストを行った. 目視による後肢可動域のスコア化を行う BMS score, 体幹バランスを要する運動機能評価を行う Rotarod test, はしご上を歩行中の後肢の踏み外し回数をカウントする Ladder walk test による後肢の運動機能評価を行った.

(3) TMS による神経マーカー発現の検討

最大効果の認められた TMS 施術条件において, 神経回路修復が促されているか, 検証する. 神経細胞マーカーとして利用される CaMK II の大脳皮質における発現について, 組織免疫染色によって検証した.

3. 結果

(1) 中枢神経回路修復のメカニズムとタイムコースの解析

これまでの申請者らの研究から, 損傷前には側枝がほとんど観察されなかったのに対し, 損傷後 14 日目までには側枝数が有意に増加していた. このことは, 損傷後 14 日目までに代償的に側枝が伸張し, その後, 標的細胞への結合, 刈り込みが生じることを示唆していた.

(2) TMS による運動機能の回復

これまでの申請者の研究結果から, TMS を脊髄損傷 3 日後より開始した群では, BMS score や Rotarod test では両群の間に有為な差は検出されなかった. Ladder walk test では, 若干の改善が見られたが, 優位な差は検出されなかった. 一方, 損傷後, 軸索伸長を促す既知の薬剤単独投与と比較して, この薬剤と TMS との併用によって, Ladder walk test によるより顕著な運動機能の改善が認められた.

(3) TMS による神経マーカー発現の検討

損傷後, 軸索伸長を促す既知の薬剤単独投与と比較して, この薬剤と TMS との併用によって, 神経マーカーCaMK II の発言が大脳皮質第 2/3 層で増加することがわかった.

4.考察

本研究の成果は, 磁気刺激の活用, および磁気刺激と薬剤との併用が中枢神経損傷後の運動機能

改善に貢献できることを示唆している.

5.謝辞

本研究をご支援くださいました公益財団法人渡邉財団 関係者各位に深く感謝申し上げます. また, これまでの研究遂行にあたり, 多くのご助言を戴きました大阪大学大学院医学系研究科分子神経科学教室の皆様に厚くお礼申し上げます.

文献

1) Fujita Y, Yamashita T: Axon growth inhibition by RhoA/ROCK in the central nervous system. Frontiers in neuroscience 8: 338, (2014).
2) Zhang S, Fujita Y, Matsuzaki R, Yamashita T: Class I histone deacetylase (HDAC) inhibitor CI-994 promotes functional recovery following spinal cord injury. Cell death & disease 9: 460, (2018).

単層カーボンナノホーンを用いたマグネタイト粒子による去勢抵抗性前立腺癌に対する温熱療法

Hyperthermia for castration-resistant prostate cancer using magnetite nanoparticle composed from single-walled carbon nanohorn

永井　隆* 河合 憲康*
Takashi Nagai* Noriyasu Kawai*

*名古屋市立大学大学院医学研究科腎・泌尿器科学分野,
〒467-0001　愛知県名古屋市瑞穂区瑞穂町川澄 1 番地

* Department of Nephro-urology, Nagoya City University, Graduate School of Medical Sciences
1 Kawasumi, Mizuho-cho, Mizuho-ku, Nagoya, Japan

Abstract

Single-walled carbon nanohorn (SWNH) can be used for drug delivery because of its high surface area. In this study, SWNH was applied for thermotherapy by combining Fe_3O_4 because Fe_3O_4 heat in an alternating magnetic field (AMF). Human castration resistant prostate cancer cells (22Rv1) were injected subcutaneously into nude mice. In treatment group mice, SWNH- Fe_3O_4 were injected into tumor nodule and the mice were exposed into AMF for 30 minutes. Tumor regression was observed in treatment group compared with control group.

Keywords: prostate cancer, single-walled carbon nanohorn, thermotherapy

1. 目的

前立腺癌の患者数は増加の一途を辿っている。一般的に転移のない限局性前立腺癌に関しては手術や放射線療法で良好な制癌性が報告されている。しかし、転移性前立腺癌の予後は不良であり、転移性前立腺癌の診断と治療こそが前立腺癌診療における課題である。また、前立腺癌の転移には治療に対する抵抗すなわち去勢抵抗性の獲得が大きく関わっている。そのため去勢抵抗性前立腺癌に対する治療も課題の一つである。

本邦では前立腺癌の転移巣の検索には CT や骨シンチグラフィーが一般的である。近年、前立腺膜抗原(PSMA: prostate specific membrane antigen)を標的とした PET(PSMA-PET)の有用性が報告されてきている。PSMA は前立腺癌において発現が上昇する抗原で、これを標的とすることで、前立腺癌により特異的な転移巣の発見を可能とするナノ粒子の開発を目指した。今回は、単層カーボンナノホーン(single-walled carbon nanohorn: SWNH)を用いることで、酸化鉄(Fe_3O_4)および PSMA を結合させ、腫瘍特異的な温熱療法の治療の開発を試みる。

上記計画の初期段階としてFe_3O_4含有 SWNH による温熱治療効果の検証を行ったので報告する。

2. 方法

Ⅰ. SWNH+Fe_3O_4 の作成

中部大学との共同研究で作成を行った。3-アミノプロピルトリエトキシシラン(APTES)を用いることで磁性を維持しながら分散性を持つナノ粒

子の開発を行った。

また in vitro での SWNH+Fe_3O_4 の発熱効率の検証を行った。

Ⅱ. SWNH+Fe_3O_4 の治療効果の検証

動物実験による温熱療法効果を検証するために、モデル動物として前立腺癌皮下移植モデルマウスを用いた。

6 週齢雄ヌードマウスの背部にヒト去勢抵抗性前立腺癌細胞株 22 Rv1 を皮下移植した。皮下移植後、3 週間(day21)経過時点で、コントロール(n=3) および加温群 (n=3) とし、加温群のモデルマウス腫瘍部位に SWNH+Fe_3O_4 (Fe 濃度:36.3mg/ml)を 300 μL 腫瘍部分に局所注入した。(図 1)

その後、コイル型交流磁場照射装置(図 2)を用いて、交流磁場下における SWNH+Fe_3O_4 の発熱による温熱療法を試みた。腫瘍内の温度は、いわゆる mild hyperthermia で定義される 42℃-46℃で維持し、30 分間の加温を行った。両群の経時的な腫瘍サイズの計測を行い、温熱治療効果の検証を行った。

3. 結果

Ⅰ. SWNH+Fe_3O_4 の作成

中部大学にて SWNH と Fe_3O_4 の間に APTES を介在させることで、磁性および分散性を有する磁性ナノ粒子(SWNH-APTES-Fe_3O_4)の開発に成功した。

Ⅱ. SWNH+Fe_3O_4 の治療効果の検証

皮下移植モデルマウスの温熱治療中の温度経過を示す。(図 3)マウス 1 においては温度上昇が緩やかであり、温度上昇も 42℃程度とやや低めであったが 3 匹とも 42℃以上を維持できた。なお、温度経過はサーモグラフィー(FLIR C5)を用いて測定した。(図 4)

腫瘍サイズの経時的な変化を図に示す。(図 5) 治療群では、麻酔により一匹死亡した。コントロール群では経時的な腫瘍サイズ増大を認めるのに対し、治療群では腫瘍縮小を認めた。皮下移植モデルマウスにおいて、SWNH+Fe_3O_4 を用いた磁性ナノ粒子を用いた交流磁場下の発熱で温熱治療効果が確認された。

4. 考察

本実験では、SWNH+Fe_3O_4 による去勢抵抗性前立腺癌温熱治療効果の検証を行った。

今回開発した SWNH+Fe_3O_4 は交流磁場下で発熱することが明らかになった。またこれを用いた温熱療法により腫瘍サイズの縮小を認めた。この結果は、我々がこれまでに行ってきた前立腺癌温熱療法 [1,2]と比較し遜色のない結果であった。

今後の課題として、より良好な治療効果を得るために、磁性ナノ粒子の鉄濃度を上昇させた試料の作成や、磁場照射条件がある。過去に私たちの施設では、複数回の温熱療法を行うことで前立腺癌皮下腫瘍が完全に退縮するという報告 [1]をしており、適正な治療間隔をおいた複数回治療の検討も行っていきたい。

また今回は、局所注入によるナノ粒子の投与を行ったが、ナノ粒子による温熱治療の課題点として drug delivery の問題がある。SWNH の特性として、様々な薬剤や抗体を結合させることで治療や診断への応用が可能 [3]であるため、今後は PSMA などを用い、より特異的な集積をもたらすナノ粒子の開発を行う必要がある。

謝辞

この研究は磁気健康科学研究振興財団(令和 2 年)の補助を受けて実施したものである. また, 名古屋市立大学実験動物センターの機器を使用した.

参考文献

1) Kawai N et al. Complete regression of experimental prostate cancer in nude mice by repeated hyperthermia using magnetite cationic liposomes and a newly developed solenoid containing a ferrite core. Prostate. 2006 May 15;66(7):718-27.
2) Kobayashi D et al. Thermotherapy using magnetic cationic liposomes powerfully suppresses prostate cancer bone metastasis in a novel rat model. Prostate. 2013 Jun;73(9):913-22.
3) Tsai HC et al. Drug-loading capacity and nuclear targeting of multiwalled carbon nanotubes grafted with anionic amphiphilic copolymers. Int J Nanomedicine. 2013;8:4427-40.

(図 1)

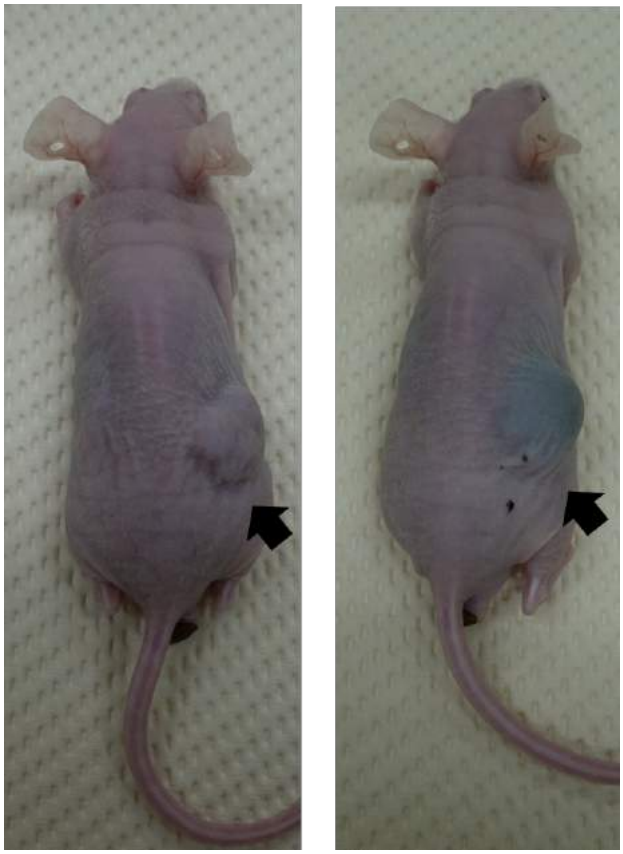

(図 2)

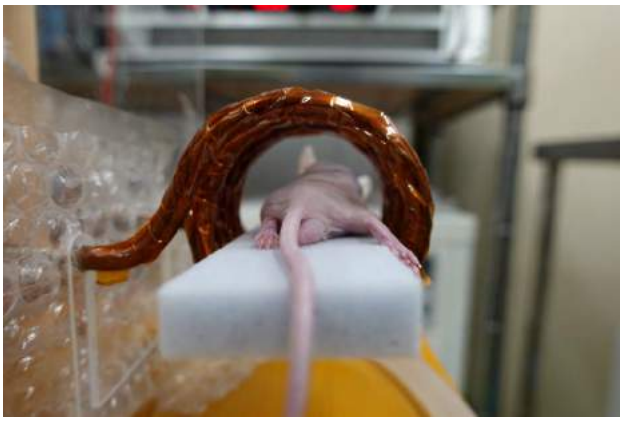

(図 3)

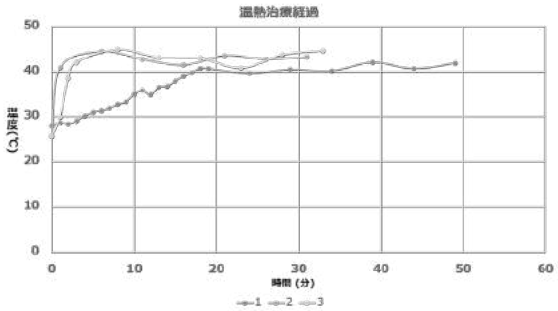
温熱治療経過
50
40
30
20
10
0
0
10
20
30
40
50
60
時間（分）
1
2
3

(図 4)


43.9°C
39.1
21.7
FLIR

(図 5)

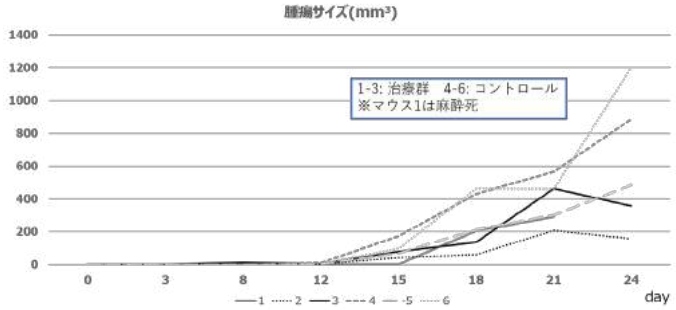
腫瘍サイズ(mm³)
1400
1200
1000
800
600
400
200
0
0
3
8
12
15
18
21
24
day
1-3: 治療群　4-6: コントロール
※マウス1は麻酔死
1
2
3
4
5
6

ABCA1 を介した細胞コレステロール搬出機構と脳内細胞新生反応への磁場効果

Effects of magnetic field on ABCA1-mediated cellular lipid release and adult brain cell generation

辻田麻紀 [1], 高瀬弘嗣 [1], 熊本奈都子 [1], 鵜川眞也 [1], 古家圭人 [2], 鍔木基成 [2]
Maki Tsujita[1], Hiroshi Takase[1], Natsuko Kumamoto[1], Shinya Ugawa[1], Yoshito Furuie[2], and Motonari Tsubaki[2]

[1] 名古屋市立大学大学院医学研究科, 〒467-8601 名古屋市瑞穂区瑞穂町川澄 1
[2] 神戸大学大学院理学研究科, 〒657-8501 神戸市灘区六甲台町 1-1
[1]Nagoya City University Graduate School of Medical Sciences
1 Kawasumi, Mizuho-cho, Mizuho-ku, Nagoya 467-8601 Japan
[2]Graduate School of Science and Technology, Kobe University
1-1 Rokkodai-cho, Nada-ku, Kobe 657-8501Japan

Abstract

This project aims to explore a novel magnetic field health care based on the cholesterol metabolism. Mouse peritoneal macrophage foam cells were incubated in CO_2-independent culture medium containing apoA-I and were exposed in a magnetic field (400 mT) using the electromagnet of an EPR spectometer. Cellular cholesterol release mediated by ABCA1 and apoA-I was not affected by the magnetic field treatment under our current condition. Furthermore, when C57BL/6N mice were exposed in the magnetic field under the identical condition, the PCSK9 expression was reduced in the hepatocytes and the newly generated hippocampal dentate gyrus cells were significantly reduced.

Keywords: macrophage foam cell, cholesterol, PCSK9, adult brain cell generation

1.目的

本研究課題は粥状動脈硬化病変のプラークの主要な領域を占める泡沫化マクロファージ細胞[1]からの ABCA1 を介した細胞コレステロール搬出に対する磁場の影響について検討し、細胞内コレステロール搬出機構[2,3]の磁場による促進の可能性をとその状況下での記憶に関与する海馬歯状回の細胞新生[4]反応を野生型マウスを用いて検証することを目的としている。

本研究課題においては、1) 動脈硬化病変プラークの主細胞である泡沫化マクロファージからの apoA-I による ABCA1 を介した細胞コレステロール搬出過程への磁場の影響、2)記憶の強化に関与し、ニューロステロイド産生の場である海馬歯状回に観察される生体新生細胞産生量への磁場の影響を観察する。本研究は EPR 測定装置の電動磁石による磁束密度 0〜400 mT の磁場を付加し、その効果を検討する新規の基礎研究課題である。

2.方法

1)マウス腹腔泡沫化マクロファージ細胞からの ABCA1 を介した細胞コレステロール搬出への磁場の効果

実験動物を用いた操作は全て名古屋市立大学

実験動物安全委員会に承認された手法を用いた。

マウス腹腔マクロファージ細胞の調製

安楽死させた C57BL/6N マウスの腹部皮膚を切開し腹腔膜を露出させた。PBS(フィルター滅菌済)を 10 mL/ 匹注入し、10 分後に清潔な注射器を用いて腹腔内遊離細胞液を採取し、低速遠心操作にてマクロファージ細胞を回収し、初代培養用コーティングを行ったフラスコ(Primaria)に播いた。20% FBS を含む RPMI1640 培地中に 5% CO_2 インキュベーターで 37℃で培養し、2 時間後に未結合細胞を洗浄し、アセチル化修飾 LDL と 0.2% BSA を含む培地へと交換した。48 時間培養で細胞を泡沫化させたのちに細胞を洗浄し、0.2% BSA 添加培地で更に 24 時間培養した。[5]

ABCA1 依存的細胞コレステロール搬出の測定と磁場付加

ヒト apoA-I を 1-10 μg/mL を含む 0.02% BSA 添加 CO_2 independent 培地(Leibovitz's L-15) (富士フィルム和光純薬)をフラスコの蓋まで入れ、振動による細胞の剥離を防いだ。保温状態で研究施設へ移動し(30 分以内)、EPR 装置内に設置し、磁場を付加した。実験 1 と実験 2 では 0.4 T の 2 時間継続付加を 2 回行った。実験 3 では 0 T と 0.4T 間を 30 分間で上昇、30 分間固定、30 分間で低下させる系を 3 往復行った(図 1)。磁場付加後、培地を回収し遠心操作にて浮遊細胞を除去し、凍結乾燥により粉末を得た。細胞は-30℃に保存した。脂質は有機溶剤にて抽出し、酵素反応法による Cholesterol 測定(LabAssay™ Cholesterol) (富士フィルム和光純薬)を行った。

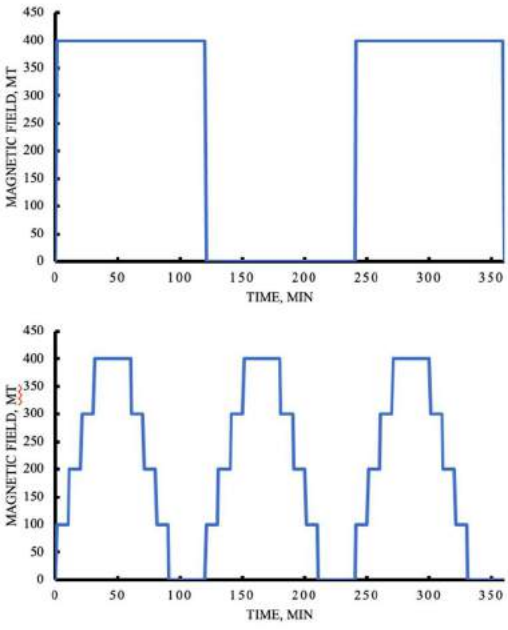

Fig 1. Magnetic field level during the treatment.
Upper panel indicates the magnetic field level for the Experiment 1 and 2. Lower panel indicates the magnetic field level condition for the Experiment 3.

2) 生体マウス海馬における新生細胞産生能への磁場付加効果の検討

野生型マウスの F-ara-EdU の標識と磁場付加

C57BL/6N 野生型マウス(8 週令)をイソフルランで麻酔し、腹腔内へ (2′S)-2′-Deoxy-2′-fluoro-5-ethynyluridine (F-ara-EdU) /PBS (133μg / マウス体重 g)を投与した。磁場付加群と対照群を別々の小型輸送用段ボール箱(幅 12cm)へ入れ EPR 測定装置内に設置し磁場(0.4T)を 90 分間付加した。対照群は磁場以外の条件を一致させ、その後 4 週間通常飼育を行った。

血清・脳脊髄液・肝臓の回収と脳の固定

安楽死させ、採血後に PBS+0.5mM EDTA で全身灌流し、脳脊髄液と肝臓片を採取した。その後 4%PFA/0.1MPB にて灌流固定し脳を摘出した。4℃において 24 時間の後固定と 30%ショ糖/PBS 中での置換を 3 日間行い-80℃に保存した。クリオスタット Leica CM1900 にて 40μm 厚の切片を作成した。全ての切片は 24-well plate に回収し PBS 1mL 中に 4℃に静置し、24 時間後に PBS を入れ替えて更に洗浄した。

Click Chemistry 法を用いた F-ara-EdU の蛍光標識と観察

非得意的な吸着を避ける目的で 24-well plate へ 3% BSA/TBS を 1 mL 入れ、小筆を使用してそこへ脳切片を移動させた。0.1% TritonX-100/TBS を入れた well へ脳切片を移動させた。20 分間室温で透過を行い、再び 3% BSA/TBS 1mL へ脳切片を移動し、次に同水溶液 2 mL 中へ移動させ更に洗浄した。Alexa-488 アザイド、銅、アスコルビン酸ナトリウムを含む TBS 反応液へ脳切片を移動し室温で 30 分間反応させた。再び 3% BSA/TBS 中 2mL に脳切片を移動し洗浄した[6]。Hoechst 33342(同仁化学)を含む 3%BSA/TBS へ移動し、4℃一昼夜静置する。海馬歯状回並びに嗅球領域を共焦点超解像顕微鏡 SpinSR10 (Olympus)を用いてバーチャルスライドイメージファイルを作成し、OlyVIA アプリケーション(Olympus)にて蛍光標識

された染色体を有する細胞を観察した。

血清リポタンパク質プロファイル・アミロイド β ペプチド・肝臓における関連タンパク質発現の定量

血清はスカイライトバイオテック（株）にてゲル濾過 HPLC を用いたリポタンパク脂質分析（LipoSEARCH™）[7]を行った。脳脊髄液・血清のアミロイド β40 並びに 42 は ELISA キットワコー測にて定量した(富士フィルム和光純薬)[8]。肝臓での関連タンパク質の発現は ISOGEN(ニッホンジーン)にて RNA を回収し、ランダムプライマーを用いて fscDNA を作成し、鋳型とした。定量リアルタイム PCR は StepOnePlus™ リアルタイム PCR システム(Thermo Fisher 社)を用い、各ウエルの PCR 最終産物はメルトカーブ分析で確認した。標的遺伝子のプライマーペアーはイントロンを含む配列を用いた[9]。

統計学的解析

統計学的解析では Microsoft Excel 付属の統計機能(*t* 検定)を利用した。

3.結果

細胞コレステロール搬出への磁場の効果

泡沫化マクロファージ細胞の細胞膜に局在する ABCA1 トランスポーターの細胞コレステロール搬出能への磁場の影響を検討するために実験 1 ではフラスコの設置方向による差を比較した。細胞の上部から培養フラスコ方向 Top to Bottom (T to B)、その逆(B to T)、フラスコ接着面に対して平行(Side to side)、に磁場を付加した。ApoA-I の添加により全ての条件で培地中へ細胞コレステロールの搬出が観察された (図 2[1])が、磁場を付加しなかった対照の細胞が最も効果的に細胞コレステロールを搬出し、培養フラスコ面と平行に磁場を付加した場合には apoA-I 添加による細胞コレステロール搬出は大きく低下した。実験 2(図 2[2])と実験 3(図 2[3])では細胞上部から磁場を付加し、apo A-I の濃度依存的なコレステロール搬出を評価した。実験 2 と実験 3 の結果は ABCA1-apoA-I 特異的な細胞コレステロール搬出が 0.4T の磁場の付加で低下するか変化しない事を示した。

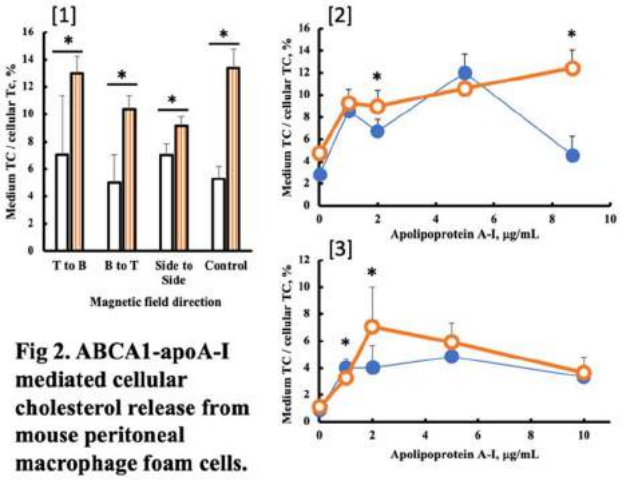

Fig 2. ABCA1-apoA-I mediated cellular cholesterol release from mouse peritoneal macrophage foam cells.

[1]; Experiment 1, Effect of magnetic field direction on cellular cholesterol efflux. Open bar; no apoA-I. Stripe bar; with apoA-I (6 μg/mL). [2]; Experiment 2, Dose dependent cholesterol efflux. Open circle; control cells, solid circles; magnetic field exposed cells. [3]; Experiment 3, Dose dependent cholesterol efflux. Open circle; control cells, solid circles; magnetic field exposed cells. *; Asterisks indicate statistic significance.

磁場付加によるマウス血清リポタンパク質プロファイルの変化と肝臓での関連遺伝子発現

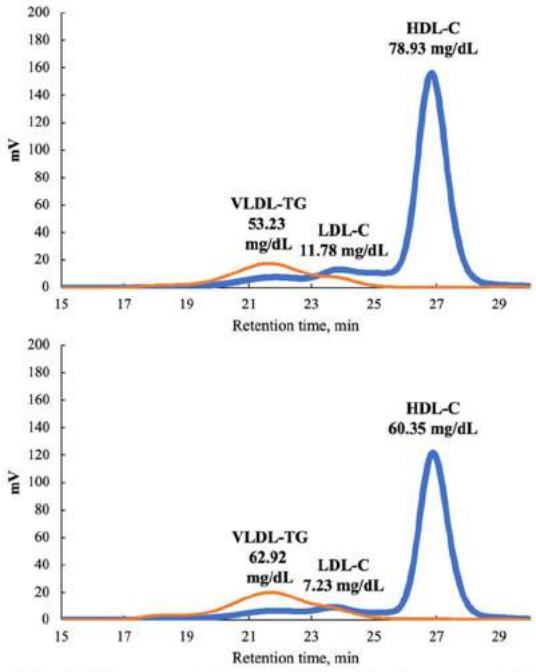

Fig 3. Lipoprotein profiles of mice treated with magnetic field. Upper panel indicates control wild type mice. Lower panel indicates mice exposed to 0.4 T magnetic field for 2 hours. Mice serum were harvested on the day 28. Bold line shows total cholesterol and thin line shows triacylglycerol level.

0.4T の磁場に 2 時間暴露された野生型マウスは 4 週間通常飼育後に採血し、血中リポタンパク質の解析を行った(図 3)。対照マウス(図 3 上)は典型的な野生型マウスのリポタンパク質パターンを示している。今回磁場を付加したマウス(図 3 下)は磁場付加後 4 週間が経過していたが HDL コレステロールの低下と VLDL 中性脂肪の増加が観察

された。これらマウス肝臓における関連遺伝子を検討した結果、HMGCoA 還元酵素並びに ABCA1 の発現が β アクチンに対して有意に低下し、apo A-I 並びに SR-BI の発現が GAPDH に対して有意に増加していたが、異なるハウスキーピング遺伝子では有意差は得られなかった。一方、LDL 受容体の分解やアテローム性動脈硬化プラーク内の T 細胞を活性化する作用のある PCSK9[10,11]の発現は磁場付加マウスで両ハウスキーピング遺伝

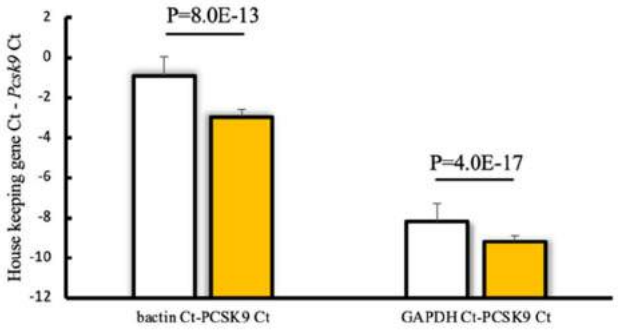

Fig 4. *Pcsk9* expression level in liver. Open column, control mice liver. Solid column, magnetic field treated, 0.4 T for 2 hrs, mice liver. Statistical significance were examined by two-tailed Student's-*t* test.

子に対して有意に低下していた。

磁場照射によるマウス脳脊髄液中・血清中のアミロイド β40 と 42 の変化

磁場付加群と対照群のマウス脳脊髄液並びに結成中のアミロイド β40 とアミロイド β42 ペプチドの定量結果を図 5 に示す。これらの結果には有意差は観察されなかった。

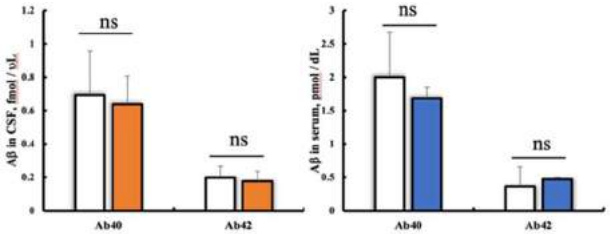

Fig 5. Amyloid-β level in cerebrospinal fluid and in serum. Open column, control mice biofluid. Solid column, magnetic field exposed, 0.4 T for 2 hrs, mice biofluid. ns; indicates no statistical significance.

生体マウス海馬における新生細胞産生能への磁場の影響

マウス腹腔内へ投与した核酸修飾化合物 F-ara-EdU は神経幹細胞の分裂において染色体の複製に利用される。その時点で新生された細胞を 28 日後に脳を回収し脳切片(40μm 厚)を作成、蛍光標識した。次に海馬歯状回を観察し蛍光標識された核を有する細胞数をカウントした(図 6)。対

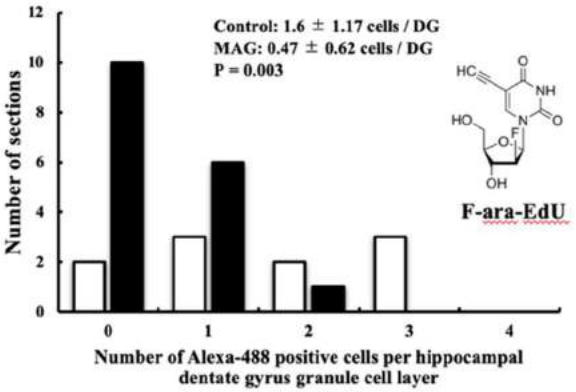

Fig 6. F-ara-EdU incorporated cells in hippocampal dentate gyrus. Open bar; control mice group. Solid bar; magnetic field treated mice group.

照マウスでは海馬歯状回の顆粒層と顆粒層基底部に 0 から 3 個の陽性細胞が見られた。1 枚のスライスに観察される歯状回あたり平均 1.6 個が陽性細胞として検出できた。これに対して磁場照射群由来の海馬歯状回では大半が 0 または 1 個であり、海馬スライス当たり平均 0.47 個の陽性細胞に留まった(P=0.003)。海馬歯状回以外で細胞新生が認められる嗅球中央部の顆粒細胞領域では対照群と磁場付加群共に陽性細胞が多数観察された。

4.考察

本研究成果ではマウス腹腔マクロファージ細胞への磁場付加で細胞コレステロール搬出の実質的な増加は観察されなかった。また 0.4 T の磁場に 2 時間暴露したマウス血中リポタンパク質プロファイルは 28 日後でも HDL コレステロールが低下していた。肝臓での遺伝子発現の結果は HDL 新生と代謝に関与する ABCA1 の発現の低下と SR-BI 発現の増加傾向が観察され、HDL コレステロールの低下は ABCA1 低下による HDL 新生反応の減少並びに SR-BI 増加による HDL 代謝の亢進の両者に起因する機序が推察される。肝臓での PCSK9 の低下はもしかするとヒトでは LDL 受容体の増加による LDL コレステロール代謝促進[12]につながる現象である可能性が考えられる。残念ながらマウス LDL では LDL 受容体との結合領域を欠いた apoB48 も LDL の構造タンパク質とする[13]為、LDL 代謝についての議論には更に詳細な検討が必要である。

脳内 HDL コレステロールと血中 HDL コレステロールの機能に関する関連はその構造タンパク質の組成の違いから直接的な比較は困難である[14]が、血中 HDL の高い時に脳内 apoA-I 量が上昇することを本課題代表研究者は報告している[15]。今回血中 HDL の低下から脳内 apoA-I 量が低下していることが推察される。海馬歯状回において顆粒層並びに顆粒層基底部に検出された新生細胞数が磁場付加を行ったマウスで有意に低下している事と何からの関連があるのかもしれない。今後この新生細胞が神経細胞であるかグリア細胞であるか詳細な検討が必要である。

5. 研究助成・利益相反

本研究は公益財団法人渡邉財団(助成番号 01104)、一般財団法人日本健康開発財団(2020 年度)、並びに名古屋市立大学特別研究奨励費(交付決定番号 2050002)の助成並びに補助を受けて実施したものである。

本研究に関連し、発表者らが開示すべき COI 関係にある企業等はない。

参考文献

[1] Kruth, H.S. (2001). Macrophage foam cells and atherosclerosis. Front Biosci 6, D429-55.

[2] Yokoyama, S. (1998). Apolipoprotein-mediated cellular cholesterol efflux. Biochim Biophys Acta 1392, 1-15.

[3] Yokoyama, S. (2006). ABCA1 and biogenesis of HDL. J Atheroscler Thromb 13, 1-15.

[4] Matsumoto, M. et al. (2019). Dynamic Changes in Ultrastructure of the Primary Cilium in Migrating Neuroblasts in the Postnatal Brain. J Neurosci 39, 9967-9988.

[5] Tsujita, M. and Yokoyama, S. (1996). Selective inhibition of free apolipoprotein-mediated cellular lipid efflux by probucol. Biochemistry 35, 13011-20.

[6] Neef, A.B. and Luedtke, N.W. (2011). Dynamic metabolic labeling of DNA in vivo with arabinosyl nucleosides. Proc Natl Acad Sci U S A 108, 20404-9.

[7] Okazaki, M. and Yamashita, S. (2016). Recent Advances in Analytical Methods on Lipoprotein Subclasses: Calculation of Particle Numbers from Lipid Levels by Gel Permeation HPLC Using "Spherical Particle Model". J Oleo Sci 65, 265-82.

[8] Sano, O. et al. (2016). ABCG1 and ABCG4 Suppress γ-Secretase Activity and Amyloid β Production. PLoS One 11, e0155400.

[9] Tsujita, M., Matsushita, S. and Takase, H. (2021). Modulation of lipoprotein profiles by the WAON treatment in mice. *Nihonkenkoukaihatsuzasshi* 42

[10] Seidah, N.G., Awan, Z., Chrétien, M. and Mbikay, M. (2014). PCSK9: a key modulator of cardiovascular health. Circ Res 114, 1022-36.

[11] Liu, A. and Frostegård, J. (2018). PCSK9 plays a novel immunological role in oxidized LDL-induced dendritic cell maturation and activation of T cells from human blood and atherosclerotic plaque. J Intern Med

[12] Cohen, J., Pertsemlidis, A., Kotowski, I.K., Graham, R., Garcia, C.K. and Hobbs, H.H. (2005). Low LDL cholesterol in individuals of African descent resulting from frequent nonsense mutations in PCSK9. Nat Genet 37, 161-5.

[13] Yamanaka, S., Balestra, M.E., Ferrell, L.D., Fan, J., Arnold, K.S., Taylor, S., Taylor, J.M. and Innerarity, T.L. (1995). Apolipoprotein B mRNA-editing protein induces hepatocellular carcinoma and dysplasia in transgenic animals. Proc Natl Acad Sci U S A 92, 8483-7.

[14] Hirsch-Reinshagen, V. et al. (2004). Deficiency of ABCA1 impairs apolipoprotein E metabolism in brain. J Biol Chem 279, 41197-207.

[15] Tsujita, M., Vaisman, B., Chengyu, L., Vickers, K.C., Okuhira, K.I., Braesch-Andersen, S. and Remaley, A.T. (2020). Apolipoprotein A-I in mouse cerebrospinal fluid derives from the liver and intestine via plasma high-density lipoproteins assembled by ABCA1 and LCAT. FEBS Lett

合成生物学的アプローチによるDNA光修復反応に対する磁場の影響評価

Synthetic Biology Approach for Evaluating Magnetic Field Effects on DNA Photorepair Reactions

岡　芳美
Yoshimi Oka

大分大学 全学研究推進機構，〒870-1192　大分県大分市大字旦野原 700
Promotion Research Institute, Oita University
700 Dannoharu, Oita-city, Oita 870-1192 Japan

Abstract

Geomagnetic field, along with water and air, is an environmental factor that affects human health. The aim of this study was to evaluate the effect of weak magnetic field on flavin-mediated DNA. The generation of radical pair between flavin and guanine (G) in DNA oligomer upon irradiation with blue light were observed by time-resolved electron spin resonance (TREPR) spectroscopy. The TREPR result can be evaluated as a direct observation for the oxidation of G, which is the initial intermediate in oxidative damage of DNA.

Keywords: radical pair, DNA, flavin, blue light, weak magnetic field

1. 目的

近年，青色光受容体タンパク質，クリプトクロムが，渡り鳥などの磁気コンパスとして働く可能性が強く示唆されている [1)-4)]．その機構は，クリプトクロム中のフラビンアデニンジヌクレオチド（FAD）が青色光により励起されたとき，アミノ酸（トリプトファン，Trp）との間で電子移動が起こり，その結果生じるラジカルペアのために，磁場による反応効率の差として検出できると推定されている．同様に，フラビンタンパク質の一種，フォトリアーゼ（光回復酵素）においても，青色光照射によるTrpからFADへの電子移動反応が磁場の影響を受けるという報告がある [2)]．フォトリアーゼの重要な機能は，紫外線によりDNA2重鎖中の隣り合う塩基間で生成した二量体を単量体へと戻すことであり，このDNA修復にまで磁場効果が関与するかは，明らかになっていない．また，DNAの酸化損傷（グアニン，Gの酸化が想定上の反応始点）がフラビン等の色素を介して可視光でも起こると報告があるが [5)]，磁場影響の可能性には着目されていない．

地磁気は，水や空気とともに健康にかかわる環境要因であり，本研究では，フラビンを介したDNAに対する微弱磁場の影響評価を目的とした．本研究において対象とするDNAを構築する途中で，青色光照射によるフラビンとグアニン（G）間のラジカルペア生成を観測したので，まずは，この点に着目して研究を遂行した．

2. 方法

水溶性のリボフラビンとグルタル酸無水物を出発原料として，比較的親水的なカルボン酸構造

を持つフラビン分子を合成し，3'–末端にリンカーを介して修飾されたアミノ基とアミド結合で連結させた11塩基からなるDNAオリゴマーを得た．3'–末端から 3 塩基目に G を含むオリゴマー（**DNA1**）と G を Inosine 置換したオリゴマー（**DNA1'**）を比較検討に用いた．**DNA1** と相補的で，5'–末端にリンカーを介して修飾されたアミノ基と 3-indolepropionic acid（Trp 誘導体）をアミド結合で連結させた DNA オリゴマー（**DNA2**）と無修飾オリゴマー（**DNA2'**）を得た．**上記** DNA2 重鎖について示差走査熱量（DSC）測定を行い，融解温度を求めた．ナノ秒光パルス（励起波長 450 nm，レーザーパワー～2 mJ，繰り返し周波数 30 Hz）照射後の X-band 時間分解電子スピン共鳴（TREPR）測定を行った．測定には，DNA 濃度 50 μM，10% DMSO 水溶液を用いた．

3. 結果

DSC 測定の結果から，Inosine 置換 DNA を用いた場合においても，室温ぐらいまでは DNA2 重鎖が維持されていることを確認した（$T_m \geq 25$ ℃）．5 ℃における TREPR 測定から，(1) 1 本鎖 DNA, **DNA1** について，光励起後，344 mT 付近の磁場領域に，図 1 のような分極パターンが観測できた（E:発光, A:吸収）. (2) 2 重鎖 DNA, **DNA1**/**DNA2'** でも同様の分極シグナルを観測した．(3) 1 本鎖 DNA, **DNA1'**では，シグナルは観測できなかった．(4) 2 重鎖 DNA，**DNA1'**/**DNA2'**でも同様に，シグナルは観測できなかった．しかしながら，(5) **DNA1** は，**DNA2** と 2 重鎖を形成することで（**DNA1**/**DNA2**），シグナルが打ち消されることが分かった．

4. 考察

上記(1)と(3)の比較から，フラビン修飾 DNA 鎖内で，フラビンーG・ラジカルペアが生成していることが分かった．クリプトクロムにおけるフラビンーTrp・ラジカルペアの報告 [6] と同様の E/E/A/A 分極パターンを示すことから 1 重項を前駆体とするスピン相関ラジカルペアが生成しているものと考えられる．また，3'–末端から 3 塩基目の G を Inosine に置換した場合には，ラジカルペア由来のシグナルが観測できなくなったことから，3 塩基目の G がフラビンとの電子移動反応の開始に必要不可欠であることを確認した．この TREPR の結果は，DNA の酸化損傷において， G の酸化が反応始点であることを直接観測できていると評価できる．

④では，分子間フラビンーTrp・ラジカルペアの生成を期待したが, TREPR の実測では捉えられなかった．しかしながら，①および②と⑤の比較から，分子間 Indole の寄与はあると考えられる．見方を変えれば，G の酸化を抑える効果があると解釈できる．

フラビンと G の光誘起電子移動反応が，クリプトクロムと同様の反応機構を辿ることから，原理的には，この反応にも微弱磁場が影響すると考えられる．フォトリアーゼの DNA 修復反応に対する磁場の影響についても，検討を進めていく予定である．本研究のような DNA に対する微弱磁場の影響評価のアプローチが，新たな健康科学や医療技術に繋がる一助となることを期待したい．

謝辞

本研究は，公益財団法人渡邉財団による第 26 回磁気研究助成の補助を受けて実施したものである．また，文部科学省ナノテクノロジープラットフォーム事業<分子・物質合成>の支援により，分子科学研究所機器センターで DSC 測定，TR-ESR 測定を実施した．

本研究の一部内容は，9 月に北海道で開催される『第 15 回分子科学討論会』で報告予定である．

参考文献

1) Schulten, K., Swenberg, C. E., Weller, A. A biomagnetic sensory mechanism based on magnetic field modulated coherent electron spin motion. *Z. Phys. Chem.* **111**, 1–5 (1978).
2) Maeda K., Robinson, A. J., Timmel, C. R., Hore, P. J. *et al.* Magnetically sensitive light-induced reactions in cryptochrome are consistent with its proposed role as a magnetoreceptor. *Proc. Natl. Acad. Sci. USA* **109**, 4774–4779 (2012).
3) Ritz, T., Wiltschko, R., Hore, P. J. *et al.* Magnetic

compass of birds is based on a molecule with optimal directional sensitivity. *Biophys. J.* **96**, 3451–3457 (2009).

4) Wiltschko, R., *et al.* Magnetoreception in birds: II. Behavioural experiments concerning the cryptochrome cycle. *J. Exp. Biol.* **217**, 4225–4228 (2014).
5) Wenninger, M., Carell, T. *et al.* Flavin-induced DNA photooxidation and charge movement probed by ultrafast transient absorption spectroscopy *ChemBioChem* **12**, 703–706 (2011).
6) Weber, S. *et al.* Origin of light-induced spin-correlated radical pairs in cryptochrome. *J. Phys. Chem. B* **114**, 14745–14754 (2010).

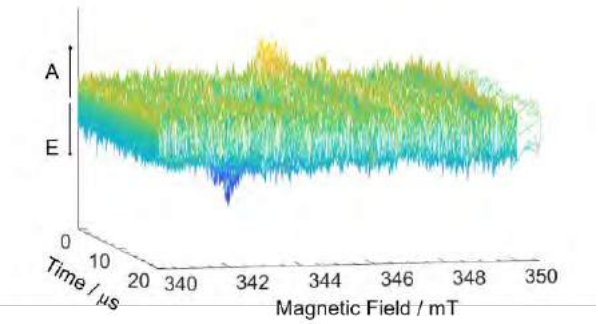

図 1：フラビンと G を含む DNA オリゴマーの TREPR スペクトル

細胞膜の分子認識に対する磁場効果の解明

～分離材料から細胞治療まで～

Investigation of magnetic field effects on the recognition ability of cell membrane
~From cell therapy to separation tool~

岡本行広
Yukihiro Okamoto

大阪大学 大学院基礎工学研究科，〒560-8531 大阪府豊中市待兼山町 1-3
Graduate School of Engineering Science Osaka University
1-3 Machikaneyama-cho, Toyonaka, Osaka 560-8531, Japan

Abstract

This report summarizes our research results on the effect of magnetic field on various lipid membrane. We prepared spherical and disk like lipid membrane, and then analyzed their specific properties. Based on obtained data, the effect of magnetic field was evaluated in the respect of lipid membrane properties and the reaction with lipid membrane. As a result, the magnetic field affected some lipid membrane properties, even if weak magnetic field, and enhanced the antioxidative effect. Thus, our results imply that the magnetic field affects cell membrane properties and also cell activity.

Keywords: magnetic field, lipid membrane, lipid membrane property, structure

1. 目的

磁場が細胞の機能に及ぼす効果に関して，多くの研究例がある．これらの研究の多くは，磁場の有無で，細胞の機能の違いを比較している例が多い．一方で，磁場が細胞膜自体に及ぼす効果に着目し，細胞機能に対する磁場効果を議論する研究は少ない．細胞膜は，バリアーとしての機能のみならず，分子認識においても重要な役割を担っており，この認識は，免疫・シグナル伝達などにも関係している．つまり，細胞膜の分子認識能に及ぼす磁場効果を解明することは，細胞機能への磁場効果の解明の一助となりうる．また，疑似細胞膜(以下，脂質膜と呼ぶ)は DDS 材料としても利用されており，磁場との併用による性能の向上が期待できる．

そこで，本提案では，様々な組成，形状の脂質膜を調製し，脂質膜に対する磁場効果の解明を目的とする．特に，分子認識に影響を及ぼす膜流動性や水和などの物性に対する磁場効果を中心に解析を行う．さらに，応用として，DDS 材料としてのリポソームに対する磁場効果を抗酸化反応の観点から評価を行うことを目的とした．

2. 方法

脂質膜の作製：以下のリポソームは既報により作製した．[1] 1,2-dioleoyl-*sn*-glycero-3-phosphocholine (DOPC), 1-palmitoyl-2-oleoyl-glycero-3-phosphocholine(POPC)，1,2-dipalmitoyl-*sn*-glycero-3-phosphocholine (DPPC)，1,2-diauroyl-*sn*-glycero-3- phosphocholine (DLPC)を用いて調製した脂質薄膜を超純水で水和させ，凍結融解法および extrusion 法により粒径 100 nm のリポソームを調製した．また，デンドリマーを有する脂質膜に関しては既報により作製

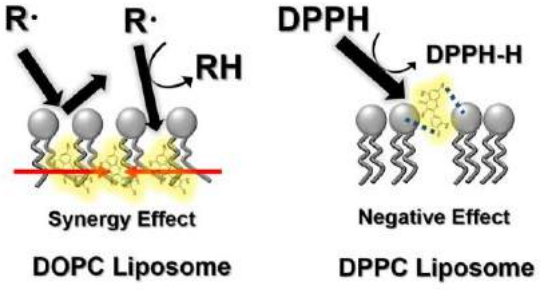

図 1 抗酸化効果の発現メカニズム

した．[2)]

脂質膜の解析: 脂質膜の解析として，膜流動性，極性の評価法に関しては蛍光プローブを利用した手法を用いた．粒子径は動的光散乱(DLS)，相転移温度は示差走査熱量測定(DSC)，脂質分子のパッキング状態はラマン分光法，脂質膜への抗酸化物質の吸着は紫外分光法と二次微分スペクトル法を用いた．磁場印加前後において，これらの解析法を適用して，磁場効果を評価した．磁場の印加は，ネオジウム磁石を用いた．

3.結果および考察

飽和脂質，不飽和脂質リポソームに対してケルセチン(抗酸化物質)を投与した結果，各膜に対してケルセチンの分配係数，配向位置が異なることを明らかとした．また，DPPH ラジカルアッセイに関しては，リポソームにケルセチンを含有した場合でも，ラジカル消去能に変化は観測されなかった．一方で，ケルセチンを含有することで，脂質の過酸化を抑制可能であることを実証した(図 1)．この検討において，磁場を印加した際，特定の脂質膜において DPPH ラジカル消去能の向上が観測された．今後は，さらならラジカル消去能の向上を目指して，条件の検討を実施予定である．

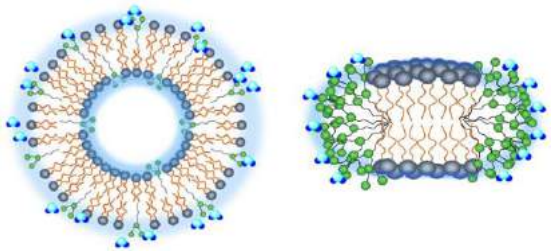

図 2 脂質デンドリマー/脂質分子が形成する集合体構造

デンドリマーを有する脂質膜は，薬物含有量を向上させ，細胞への取り込み量も多くなると期待できる．今回合成したデンドリマーを有する脂質膜は，デンドリマーの世代数やデンドリマー脂質の含有量により，形状が球状からディスク状へと変化することを明らかとした．ディスク状の脂質膜は磁場応答性が高いと報告されているため，現在，磁場応答性を評価している段階である．

最後に，構造の異なる脂質を用いてリポソームを作製し，磁場による膜特性への変化を解析した．その結果，磁場により膜流動性や極性に変化が生じる脂質膜は一部の脂質に限定されていた．現在，この磁場効果が誘起される因子の特定を行っている段階である．また，前述したように，本研究で合成したディスク状の集合体は磁場応答性が高いと考えられる．自然界でもディスク状の脂質集合体は観測されるため，構造の違いによる磁場応答という観点でも今後研究を進めていく予定である．さらに，ナノ粒子と脂質膜との併用による高機能性材料に関して我々は報告しているが，[3)]磁場印加による機能付与により，高機能性材料の作製を目指して研究を実施している．

謝辞

本研究は公益財団法人渡邉財団の助成を受けて実施したものであり，厚く御礼申し上げます．

本論文の内容は 2020 年 11 月 12 日(木)・13 日(金)にオンラインで開催された『膜シンポジウム 2020』で報告したものを一部含むものである．

参考文献

1) Jin Han, Misaki Amau, Yukihiro Okamoto, Keishi Suga, Hiroshi Umakoshi; *J. Biosci. Bioeng.,in press*.

2) Jin Han, Yosuke Iimure, Yukihiro Okamoto, Keishi Suga, Hiroshi Umakoshi: *Chemistry Letters*, 50, 187-190 (2021).

3) Miftah Faried, Seiya Ando, Keishi Suga, Yukihiro Okamoto, Hiroshi Umakoshi: *Chemistry Letters*, 49(9), 1107-1110 (2020)

魚のウロコ（骨モデル）を用いた磁場による骨形成機構の解析：渦電流による新規機構の解明

Analysis of bone formation by magnetic field using fish scales (bone model): Elucidation of a new mechanism by eddy currents

鈴木信雄*，山田外史，平山　順***，田渕圭章****，柿川真紀子*******

Nobuo Suzuki*, Sotoshi Yamada**, Jun Hirayama***, Yoshiaki Tabuchi****
and Makiko Kakikawa*****

*金沢大学 環日本海域環境研究センター臨海実験施設，〒927-0553 石川県能登町ム小木 4-1

**公立小松大学 生産システム科学部，〒923-8511 石川県小松市四丁町ヌ 1 番地 3

***公立小松大学 保健医療学部，〒923-0961 石川県小松市向本折町へ 14 番地 1

****富山大学 研空推進機構，〒930-0194 富山県富山市杉谷 2630 番地

*****金沢大学 生命理工学系，〒920-1192 石川県金沢市角間町

*Noto Marine Laboratory, Institute of Nature and Environmental Technology, Kanazawa University, Mu4-1, Ogi, Noto-cho, Ishikawa 927-0553, Japan

**Faculty of Production Systems Engineering and Sciences, Komatsu University, Nu1-3, Shicho-machi, Komatsu-city, Ishikawa 923-8511, Japan

***Faculty of Health Sciences, Komatsu University, He14-1, Mukaihon-ori-machi, Komatsu-city, Ishikawa 923-0961, Japan

**** Life Science Research Center, University of Toyama, 2630 Sugitani, Toyama-city, Toyama 930-0194, Japan

***** Institute of Science and Engineering, Kanazawa University, Kakuma-machi, Kanazawa-city, Ishikawa 920-1192, Japan

Abstract

The purpose of this study is to analyze bone formation caused by eddy currents. A culture system has been developed with fish scales in which osteoblasts and osteoclasts coexist on calcified bone matrix protein. In the present study, we examined the effect of extremely low–frequency (ELF) magnetic fields that generate eddy currents for bone formation using cultured fish scales. The static magnetic fields changed neither osteoblastic or osteoclastic activity. However, ELF magnetic fields increased the activities of both osteoblasts and osteoclasts. Therefore, we noted eddy currents generated by ELF magnetic fields. We found that a large amount of eddy currents function to activate both osteoblasts and osteoclasts. This indicates that eddy currents may be related to the activation of both osteoblasts and osteoclasts. On the basis of our present data, we will develop an apparatus for bone therapy with ELF magnetic fields in the future.

Keywords: eddy currents, osteoblasts, osteoclasts, fish scales

1. 目的

磁場が骨組織に作用して，骨形成を促すことは報告されている．しかしながら，骨形成を促す機構については不明な点が多い．生体内（*in vivo*）での骨形成を詳細に調べることができる試験管内（*in vitro*）でのモデルシステムの欠如により，研究が進んでいない現状にある．即ち，人体の骨組織を再現させるためには，骨芽細胞（骨を作る細胞）と破骨細胞（骨を壊す細胞），骨基質（コラーゲンやオステオカルシンなどのタンパク質とそのタンパク質に結合したハイドロキシアパタイト）を共存させる必要がある．特に磁場や重力等の物理的な刺激には，骨基質が重要な役割を果たしている．これら全て共存させて培養する必要があるが，このような共存培養が難しく，優れた *in vitro* での培養システムが切望されている．

骨粗鬆症等の骨疾患に対する治療薬を開発するためには，卵巣を除去して，骨が折れやすくしたラットを用いて，時間と多額の費用を投資して開発しているのが現状である．そこで磁場が骨形成を促すことから，磁場のような物理的な刺激により，骨疾患の治療を行うことができれば，高価な薬を購入する必要もなく，さらに副作用もなく，高齢者にはとても適した治療になる．そこで我々は，魚のウロコには骨芽細胞，破骨細胞及び骨基質タンパク質が共存し，カルシウムもハイドロキシアパタイトの状態で存在すること（図１）に着目した．このような特徴をもつウロコを用いて，ヒトの骨に代わる *in vitro* のウロコの培養システムを開発した[1-3]．

本研究では、このシステムを用いて、誘導電流（渦電流）が発生する 60Hz の極低周波磁場（変動磁場）に対する作用と，渦電流が発生しない永久磁石を用いた静磁場に対する作用をキンギョのウロコの *in vitro* 培養で比較した．さらに渦電流の作用をキンギョのウロコ（*in vitro*）で解析した．また，ゼブラフィッシュのウロコ（*in vitro*）においても，60Hz の極低周波磁場に対する骨芽細胞と破骨細胞の作用を確認した．

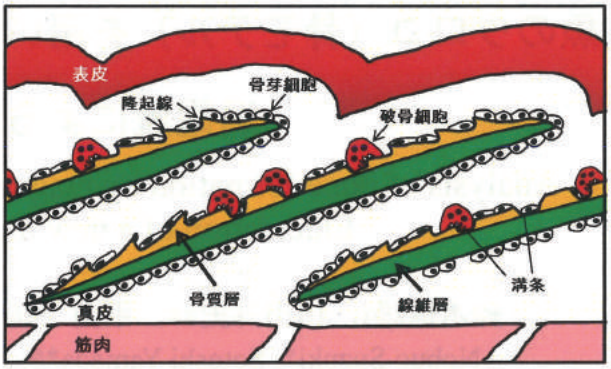

図1　魚類のウロコの模式図
魚のウロコには、骨を作る細胞（骨芽細胞）と骨を壊す細胞（破骨細胞）が共存しており、骨モデルとして使用可能。

2. 方法

キンギョ（*Carassius auratus*）を MS-222 で麻酔し，麻酔下でウロコを取り，2 ml 用のエッペンドルフチューブに入れた．次にそのチューブに HEPES（20 mM）（pH 7.0）及び抗生物質（1%）を含む培地を 500 µl 加えた．そのチューブを極低周波磁場（60 Hz）あるいは永久磁石を用いた静磁場に 15℃，24 時間曝露した．なお，極低周波磁場と静磁場は，同じ磁場強度で骨芽細胞及び破骨細胞の活性に及ぼす影響を調べた．本研究では，破骨細胞の活性の指標として酒石酸抵抗性酸フォスファターゼを用い，骨芽細胞の活性の指標としてアルカリフォスファターゼを使用し，磁場の骨組織に対する作用を調べた[1-3]．

キンギョからウロコを抜き，3D プリンターにより作成した容器（図２）に入れて 60Hz の極低周波磁場（3 mT）を照射した．直径の異なる穴にウロコを入れたので，直径の大きな穴に入ったウロコには，直径の小さな穴に入ったウロコと比較して大きな渦電流が流れる．これらの渦電流の差による骨芽細胞と破骨細胞の活性の変化を調べた．

さらにゼブラフィッシュのウロコに 60Hz の極低周波磁場（3 mT 及び 30mT）を照射して，その応答をキンギョのウロコと比較した．なお，ゼブラフィッシュの骨芽細胞と破骨細胞の活性測定は，Suzuki et al. (2016)[4]に従って測定した．

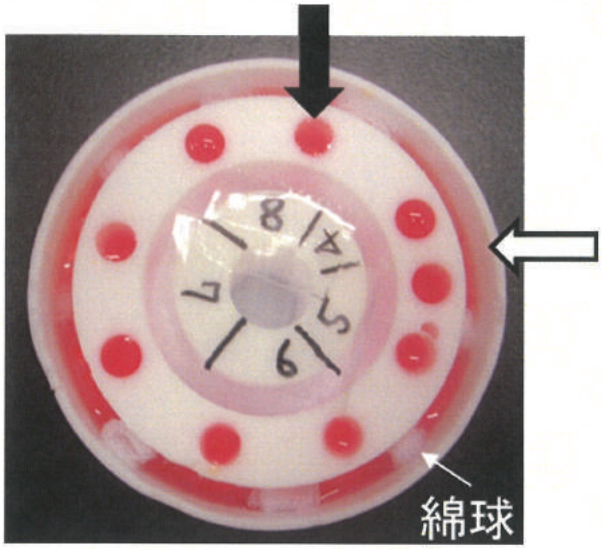

図2 渦電流の実験に用いた容器
ウロコを黒矢印と白矢印の穴に入れて実験を行った。綿球は、各個体のウロコを仕切るために使用した。

3. 結果

極低周波磁場（60 Hz）で 30 mT の磁場強度で 24 時間曝露した結果，骨芽細胞及び破骨細胞の活性が有意に上昇することがわかった．しかしながら，静磁場（30 mT）で 24 時間曝露しても骨芽細胞及び破骨細胞の活性は有意な変化を示さなかった．

次に，直径の異なる穴にウロコを入れて異なる大きさの渦電流が流れるようにすると，直径が大きい方では，骨芽細胞及び破骨細胞の活性が上昇することがわかった．一方，長径が小さい方では，そのような変化は生じなかった．直径が大きい場合は，3 mT であるにもかかわらず，30 mT と同じような変化を誘導することがわかった．

さらに，キンギョのウロコで得られた結果が，ゼブラフィッシュのウロコでも再現できるのかを調べた結果，30 mT の極低周波磁場により，骨芽細胞及び破骨細胞が活性化することが判明した．

4. 論議

同じ強度の磁場に曝露されても，極低周波磁場と静磁場では，骨芽細胞及び破骨細胞の応答が異なっていることが，本研究で明らかになった．この応答の違いは，渦電流の違いによる可能性が高い．次に，直径の異なる穴にウロコを入れて異なる大きさの渦電流が流れるようにした結果（図2），直径が大きい場合は，3 mT であるにもかかわらず，30 mT と同じような変化を誘導することがわかった．したがって，骨芽細胞及び破骨細胞を活性化させ，骨形成を促進させるには，磁場強度を上昇させるのではなく，より大きな渦電流を流すことが重要である．

一方，キンギョのウロコで得られた結果が，ゼブラフィッシュのウロコでも再現でき，30 mT の極低周波磁場により，骨芽細胞及び破骨細胞が活性化することが判明した．今後は，ゼブラフィッシュ用いて，*in vivo* の実験により，骨芽細胞及び破骨細胞に対する渦電流の作用を詳細に調べていく予定である．

謝辞

本研究は公益財団法人 渡邉財団からの補助を受けて実施したものである．

参考文献

1) Suzuki, N., Suzuki, T. and Kurokawa, T.: Suppression of osteoclastic activities by calcitonin in the scales of goldfish (freshwater teleost) and nibbler (seawater teleost). *Peptides*, **21**, 115-124 (2000)
2) Suzuki, N. and Hattori, A.: Melatonin suppresses osteoclastic and osteoblastic activities in the scales of goldfish. *J. Pineal Res.*, **33**, 253-258 (2002).
3) Suzuki, N., Somei, M., Seki, A., Reiter, R.J. and Hattori, A.: Novel bromomelatonin derivatives as potentially effective drugs to treat bone diseases. *J. Pineal Res.*, **45**, 229-234 (2008).
4) Suzuki, N., Hanmoto, T., Yano, S., Furusawa, Y., Ikegame, M., Tabuchi, Y., Kondo, T., Kitamura, K., Endo, M., Yamamoto, T., Sekiguchi, T., Urata, M., Mikuni-Takagaki, Y. and Hattori, A.: Low-intensity pulsed ultrasound induces apoptosis in osteoclasts: Fish scales are a suitable model for analysis of bone metabolism by ultrasound. *Comp. Biochem. Physiol. Part A*, **195**, 26-31 (2016).

神経磁場３次元定量計測による線虫の温度感受性メカニズム解明

Three-dimensional neuronal magnetic field measurement for the study of thermosensation of *C. elegans* worms

藤原正澄*，中台枝里子**
Masazumi Fujiwara*, Eriko Kage-Nakadai**

*大阪市立大学大学院理学研究科，〒558-8585　大阪市住吉区杉本 3-3-138
*Graduate School of Science, Osaka City University
3-3-138 Sugimoto, Sumiyoshi-ku, Osaka 558-8585 Japan
**大阪市立大学大学院生活科学研究科，〒558-8585　大阪市住吉区杉本 3-3-138
**Graduate School of Human Life Science, Osaka City University,
3-3-138, Sugimoto, Sumiyoshi-ku, Osaka 558-8585, Japan.

Abstract

The purpose of this research is to develop a real-time three-dimensional vector magnetic field imaging system that can simultaneously measure the temperature under the microscope. Such a measurement system may probe thermo-sensitive neuronal cells of *C. elegans*, one of the best studied multicellular model organism. By heating the neurons with laser, the action potential of cells can be measured via generated magnetic field, which allows for the precise temperature measurement at the same time. With the magnetic information and temperature information of neuron activities, we will quantify the activity of the neural network of *C. elegans*. To achieve this ultimate goal, we developed an artifact-free temperature method in diamond quantum thermometry. We also tried to label *C. elegans* with fluorescent nanodiamonds.

Keywords: *C. elegans*, nanodiamond, nanothermometry, nanomagnetometry

1. はじめに

蛍光ナノダイヤモンド（ND）粒子は，細胞や生物個体の内部にまで無毒性で導入可能な上，輝度が高く長期間安定な蛍光プローブである [1]．さらに蛍光起源である窒素欠陥（NV）中心が有する電子スピン共鳴の量子制御・量子計測を用いた超高感度磁場・温度センシングが報告されている [2]．この計測法は，マイクロ波照射によるスピン共鳴を蛍光強度の変化として捉え，その共鳴周波数が磁場や温度によってシフトする事を利用する．最近では申請者らによって幹細胞の再生機能温度依存性定量化などへの応用 [3]や，線虫 *C. elegans* 体内での温度計測も捉えられている [4]．また，本手法を磁場計測モードに切り変えて測定した場合，イカの軸索が活動する際のアクションポテンシャルが磁場変化として捉えられている [5]．

このマルチモーダルな計測技術を用いれば，温度計測と磁場計測を統合して生体活動情報を得ることが可能となると期待される．この技術は例えば，線虫の温度感受神経メカニズムを調べることに応用可能である．線虫では，温度を感知して走行する温度走性が研究されており [6]、完全に明らかとなった神経コネクトーム [7]を踏まえた神経ネットワークの研究が期待される．しかしながら，鍵となる神経細胞が時空間的にどの程度相互作用して温度走性という一つの行動を織りなす

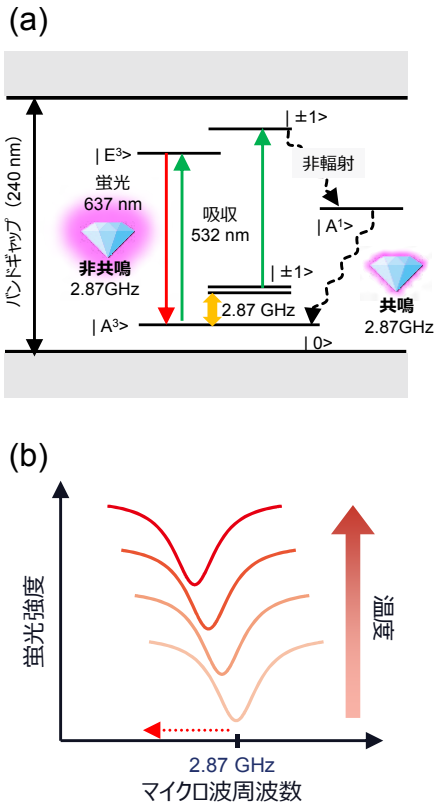

図１：(a) 蛍光 ND の ODMR 模式図と(b) ODMR スペクトルの温度依存性。

のか？という定量的な動力学描像は未だ明らかとなっていない．

本研究では，申請者らのリアルタイム *in vivo* 温度計測をさらに発展させ，線虫全体の 3 次元温度マッピングを一細胞レベルで可視化することを目的として研究を行った．この目的のために，特に以下の二つの課題に関して研究を行った．（1）光透過率が時々刻々と変化するリアルタイム *in vivo* 環境において温度計測の正確性を向上させる技術，（2）蛍光 ND を線虫にラベリングする技術．

2. 実験

NV センターによる温度量子センシングでは，ODMR の共鳴周波数が温度によって周波数シフトすることを利用する（図 1(a), (b)）．ODMR スペクトルのピークシフトを測定する上でもっともシンプルなのはスペクトルフィッティングを行って中心周波数を決定し，シフト量から温度変化を決定する手法である．しかしながら，この手法では測定時間が長くなり，現実的な測定時間では高い測定精度が得られない．本研究では高速化のために，スペクトル全体を測定するのではなく，スペクトル上の 4 点を測定する多点 ODMR 測定を導入した [8]．蛍光 ND を線虫にラベリングする点に関しては，ポリグリセロール修飾蛍光 ND（PG-ND）の表面電荷状態を制御して線虫に投与し，その線虫内挙動を観察した．

3.結果と議論

図 2(a)は 37℃において蛍光 ND を用いて温度計測を行っている状態で，人為的に励起レーザー光強度を変化させた時の温度測定値を示したものである．温度変化を加えていないにもかかわらず温度指示値に変化が現われるアーティファクトが観測された．ODMR スペクトル全体の形状が示す励起光強度依存性を別の実験で詳細に測定したところ，これは蛍光 ND の電子スピン緩和時間やスピン準位間のスピン混合による複合的な効果であることが明らかとなった．このアーティファクトは温度測定の前に事前に評価して数値的に取り除くことが可能である．この数値フィルターを適用した結果が図 2(a)である．光強度の変化に対しても安定した温度計測ができるようになった．

蛍光 ND による線虫ラベリングに関しては，PG-ND の表面をさらに-COOH, -NH_2 で修飾し [9]，表面電荷をそれぞれ負・正に帯電させたものを線虫に投与して，蛍光 ND の挙動を観察した．このような表面電荷の制御によって，培養細胞などでは細胞へのナノ粒子の取り込み量が変化することが知られている．図 2(b)は，-COOH で修飾した蛍光 ND を投与した線虫の蛍光顕微鏡画像である．蛍光 ND の赤と自家蛍光の青を重ねた画像である．蛍光 ND は腸管内には確認できたが，腸管細胞からの取り込みは見られなかった．この原因として，表面電荷制御が適切でなかった可能性以外に，使用した蛍光 ND のサイズが 50 nm と小さく，線虫の赤色領域自家蛍光に埋もれて蛍光 ND を明確に観察できなかったことも考えられる．-NH_2 によって正に帯電させた蛍光 ND では，投与する際に線虫培養専用培地に分散させた時点で凝集が開始してしまった．現在，これを解決するために適切な条件を探索しているが，線虫の餌である大腸菌が正に帯電したナノ粒子を凝集させる

ことが報告されており，その点に関する対応などもする予定である.

謝辞

本研究で使用した PG-ND は京都大学の Zou Yajuan 大学院生、小松直樹教授から提供して頂いた。本研究は渡邊財団磁気健康科学助成からの支援、および、科学研究費補助金の支援を受けて実施したものである.

参考文献

1. Masfer H. Alkahtani, Fahad Alghannam, Linkun Jiang, Abdulrahman Almethen, Arfaan A. Rampersaud, Robert Brick, Carmen L. Gomes, Marlan O. Scully and Philip R. Hemmer, *Nanophotonics* **7**, 1423 (2018).

2. Romana Schirhagl, Kevin Chang, Michael Loretz, and Christian L. Degen, *Annu. Rev. Phys. Chem.* **65**, 83 (2014).

3. Hiroshi Yukawa, Masazumi Fujiwara, Kaori Kobayashi, Yuka Kumon, Kazu Miyaji, Yushi Nishimura, Keisuke Oshimi, Yumi Umehara, Yoshio Teki, Takayuki Iwasaki, Mutsuko Hatano, Hideki Hashimoto and Yoshinobu Baba, *Nanoscale Adv.* **2**, 1859 (2020).

4. Masazumi Fujiwara, Simo Sun, Alexander Dohms, Yushi Nishimura, Ken Suto, Yuka Takezawa, Keisuke Oshimi, Li Zhao, Nikola Sadzak, Yumi Umehara, Yoshio Teki, Naoki Komatsu, Oliver Benson, Yutaka Shikano, and Eriko Kage-Nakadai, *Sci. Adv.* **6**, eaba9636 (2020).

5. John F. Barry, Matthew J. Turner, Jennifer M. Schloss, David R. Glenn, Yuyu Song, Mikhail D. Lukin, Hongkun Park, and Ronald L. Walsworth, *Proc. Natl. Acad. Sci. U.S.A.* **113**, 14133 (2016).

6. Tsubasa Kimata, Hiroyuki Sasakura, Noriyuki Ohnishi, Nana Nishio, and Ikue Mori, *Worm* **1**, 31 (2012).

7. Steven J. Cook, Travis A. Jarrell, Christopher A. Brittin, Yi Wang, Adam E. Bloniarz, Maksim A. Yakovlev, Ken C. Q. Nguyen, Leo T.-H. Tang, Emily A. Bayer, Janet S. Duerr, Hannes E. Bülow, Oliver Hobert, David H. Hall & Scott W. Emmons, *Nature* **571**, 63 (2019).

8. Masazumi Fujiwara, Alexander Dohms, Ken Suto, Yushi Nishimura, Keisuke Oshimi, Yoshio Teki, Kai Cai, Oliver Benson, and Yutaka Shikano, *Phys. Rev. Research* **2**, 043415 (2020).

9. Yajuan Zou, and Naoki Komatsu, *Carbon* **163**, 395 (2020).

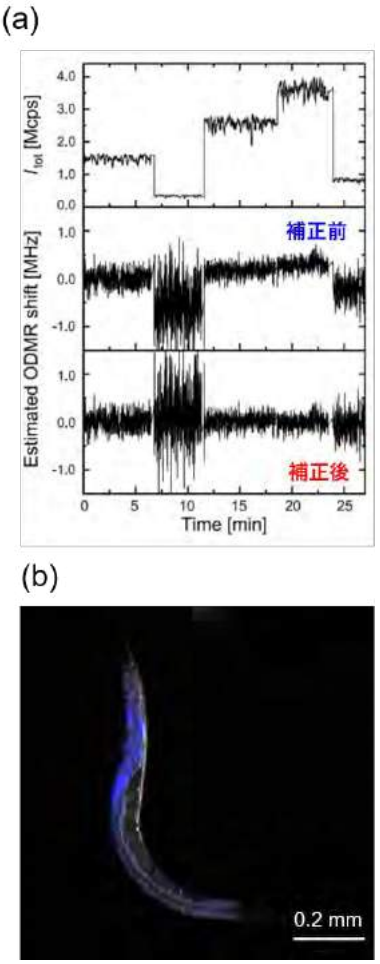

図 2：(a) 蛍光 ND 温度計測中に人為的に励起レーザー光強度を変化させた時の温度測定値を示したもの。上から蛍光強度、アーティファクト補正前温度データ、補正後温度データ。(b) 蛍光 ND を投与した線虫の蛍光顕微鏡画像（青：自家蛍光、赤：蛍光 ND、灰：明視野のマージ画像）。

医療応用のための高周波パルスマグネットの開発

Development of the high frequency pulse magnetic fields generator for medical applications

浜崎亜富
Atom Hamasaki

信州大学理学部，〒390-8621　長野県松本市旭 3-1-1
Faculty of Science, Shinshu University
3-1-1 Asahi, Matsumoto, Nagano 390-8621 Japan

Abstract

An oscillating strong magnetic field can be easily generated compared to the conventional magnetic field generation using an AC power supply by using a pulsed magnetic field. Increasing of the generated magnetic field intensity leads to an increase in the efficiency of heat generation, which can shorten the treatment time. In this study, an oscillating pulsed magnetic field of 3 kHz was generated with a simple circuit and relatively low energy, and heat generation in an aluminum block was observed.

Keywords: oscillating strong magnetic field, pulsed magnet, heat generation

1. 目的

近年，経頭蓋磁気刺激（TMS）や温熱療法（ハイパーサーミア）など，パルス磁場を利用した治療法が増加しており，細胞の発育や，心筋の血管新生を促進する方法としても研究が進められている．この中でハイパーサーミアは、がん細胞が 42 度以上で死滅するという特徴から、磁場による誘導加熱によって選択的に細胞を加熱して死滅させる治療法である．生体深部まで浸透する磁場の特徴を生かして、直接穿刺せずに非接触で治療可能なため患者にとっても身体的、精神的負担を減らすことから注目されている．

ハイパーサーミアは磁場に曝露するだけで患部が加熱されてガン細胞が死滅するので、操作が簡便で、従来の放射線治療や中性子補足療法（BNCT）と比べ、比較的安価に設備を導入できる利点がある．しかし，この手法の普及が進んでいるとは，現状では言いがたい．その要因のひとつに、磁場による患部の加温が充分でないことが挙げられている．最近では磁性微粒子をガン細胞に付着させ、磁性微粒子を磁場で加熱して細胞を死滅させるのが一般的であるが [1]，実際の患部における磁場強度が不足していることが原因の一つであるとされている．

磁性微粒子の研究は数十 mT 程度で行われており，これは直径 500 nm 程度の磁性微粒子（マグネタイト）の飽和磁化に相当する．例えば，コイルの端から 30mm の位置に患部がある場合，中心磁場では患部の数倍から数十倍の磁場強度を出さなければならない．従来の方法でこれを発生させることも可能であるが，大出力の電源が必要となるので過剰な設置スペースが必要となり、導入コストも高くなるので、普及の妨げになることが懸念される．そこで，一般的な交流電源を用いるところを，パルス磁場を用いた磁性微粒子を加熱する方法を提案した．2020 年度は，振動磁場を発生させるシステムを作成し，発生磁場の特性について検討したので，報告する．

2. 方法

設計，製作したパルスマグネットシステムの回路図を図1に示す．システムは，充電回路，蓄電回路，放

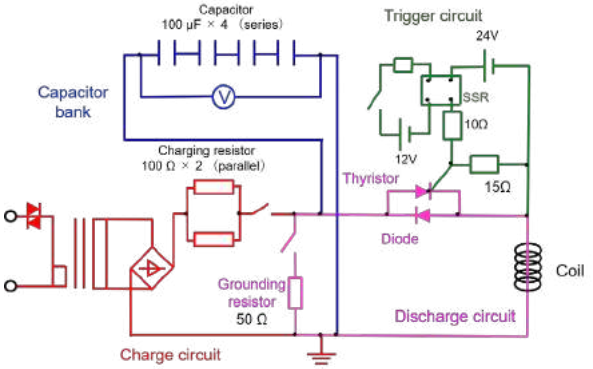

図 1. パルスマグネットシステムの回路図

Figure 2. 作成した振動バルス磁場発生装置

電回路，および制御回路に分けることができる．振動磁場を発生させるために，従来の回路[2), 3)]からクローバー回路をなくし，サイリスタと逆向きにダイオードを設置した．図 2 の写真は蓄電設備および放電スイッチ以外の部分で，交流電源の回路と比べても単純な作りである．サーチコイルを用いて、この装置で発生する誘導起電力を測定し、コイル内に発生する磁場強度を測定した．コイルは巻き数や線の太さ、径の大きさなど形状が異なるものを用意してコイルの形状の違いによる振動磁場の影響について調べた．また、コイルの径内に熱電対を差し込んだアルミニウムのサンプルを入れ、磁場を発生させた際の温度変化についても調べた．

3. 結果

インダクタンス(L)と抵抗がそれぞれ 125 μH, 93 mΩ のコイルを 100 μF のコンデンサバンクに接続し，100 V の電圧を充電して放電スイッチをONにすると、1 回の放電で図 3 のように最大約 0.2 T の磁場が約 3kHz の周期で 4 回連続して発生した．充電電圧によって周波数は変化せず、振幅は充電電圧に比例した．次に，100 V の充電電圧で 30 秒ごとに振動パルス磁場を発生させ，ボア中央に設置したアルミブロック (φ8, l=10) の昇温を観測した．図 4 のように，5 分程度で約 2.5 K 上昇した．

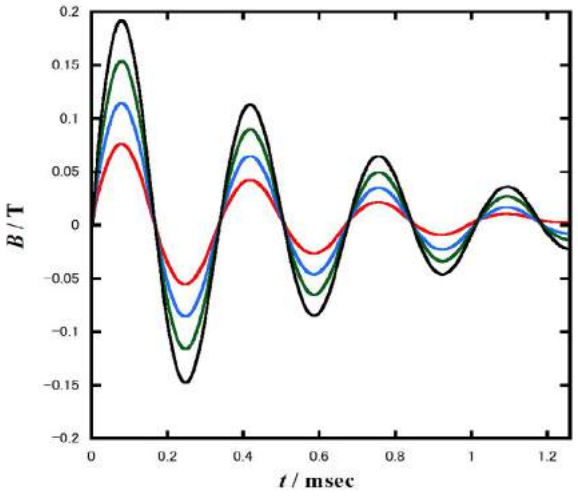

図 3. 振動パルス磁場の時間変化

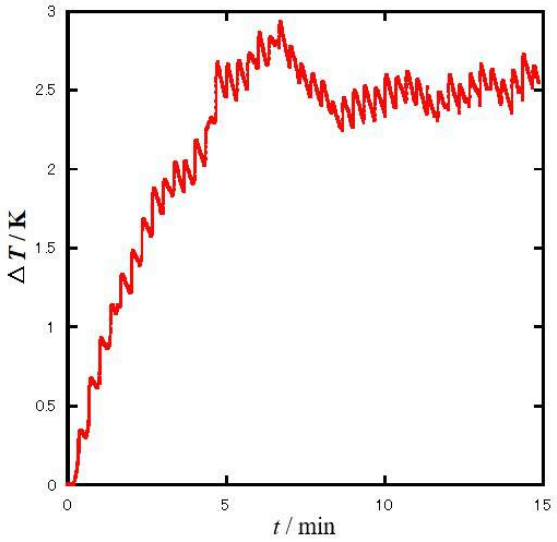

図 4. アルミブロック温度の時間変化

4. 考察

今回，3 kHz の振動磁場が発生し，2 周期目，3 周期目になるにつれて減衰したが、抵抗を小さくし、インダクタンスを大きくすることで減衰を押さえることができる．そのためには、コイルの線を太くする、径を小さくすることで改善できる．また，磁気刺激による温度の上昇については，磁場強度を引き上げることが必須であるが，こ

れも充電電圧の向上で対応可能である. 一方, 振動の向上も効果的であり, 周波数を 10 倍程度まで向上させると, 磁性微粒子の飽和磁化付近に到達することになる. 静電容量を下げて高圧充電する必要があり, 大容量のコンデンサを直列につないで実質的な静電容量を下げることで実現できる. 今後, 今回準備した光学系を用いて熱の発生を光学的に非接触で測定する設備の使用の下, コンデンサの拡充による発熱効率の向上を目指し, 開発を継続する.

謝辞

本研究は公益財団法人渡邉財団の補助を受けて実施した.

参考文献

1) Swee Kuan Yen, et al. *Theranostics* 2013, 3, 986-1003

2) Atom Hamasaki, et al., *IEEE Transactions on Magnetics*, 2016, 52, 9401704

3) Atom Hamasaki, et al., *IEEE Transactions on Magnetics*, 2017, 53, 6500504

脳磁図を用いたLewy小体型認知症の視覚情報処理障害の検出と早期診断マーカーとしての有用性

Detection of disturbances of visual perception processing using magnetoencephalography in patients with Lewy body disease

篠原もえ子[1, 2], 小池暢人[1, 3], 森瀬博史[3], 工藤究[3], 小松潤史[1, 2], 阿部智絵美[1, 2], 山田正仁[1]
Moeko Shinohara[1, 2], Masato Koike[1, 3], Hirofumi Morise[3], Kiwamu Kudo[3], Junji Komatsu[1, 2], Chiemi Abe[1, 2], and Masahito Yamada[1]

[1]金沢大学医薬保健学総合研究科　脳老化・神経病態学（脳神経内科学）
[2]金沢大学医薬保健学総合研究科　認知症先制医学，〒920-8640　石川県金沢市宝町 13-1
[3]株式会社リコー　リコーフューチャーズ BU　メディカルイメージング事業センター，〒920-0177　石川県金沢市北陽台 2-3
[1]Department of Neurology and Neurobiology of Aging, Kanazawa University Graduate School of Medical Sciences, Kanazawa University, Kanazawa, Japan
[2]Department of Preemptive Medicine of Dementia, Kanazawa University Graduate School of Medical Sciences, Kanazawa University, Kanazawa, Japan
[3]Medical Imaging Business Center, Ricoh Futures BU, Ricoh Company, Ltd., Tokyo, Japan

Abstract

Lewy body disease (LBD) includes Parkinson's disease and Dementia with Lewy bodies (DLB). DLB is the second most common neurodegenerative disease, which cause dementia, after that due to Alzheimer's disease (AD). Early diagnostic methods of DLB have not been established. Since DLB is characterized by visual processing disturbance, we analyzed the neural responses to the optic flow and evaluated the visual perception processing using magnetoencephalography (MEG). The analysis was performed for patients with LBD (n = 4) and normal controls (n = 6). This study demonstrated that the maximum power in the left lateral occipital significantly correlated with the Trail making test-A score. Further studies are necessary to verify whether MEG during the optic flow task is useful for early diagnosis of DLB, and differentiation of DLB and AD.

Keywords: Lewy body disease, magnetoencephalography, optic flow

1. 目的

Lewy body disease（LBD）はαシヌクレインを主要構成成分とするLewy小体の存在を神経病理学的特徴とする病態のすべてを包含する疾患概念で、Lewy小体型認知症（DLB）の他にParkinson病（PD）なども含まれる。DLBは認知症の約20%を占めAlzheimer病に次いで2番目に多い神経変性疾患である。軽度認知障害（MCI）とは、社会生活や日常生活上の支障はなく、認知症の診断基準をみたさないが正常とも言い難い状態を指す。

適切な認知症治療のためには MCI 段階以前での早期診断が重要である。しかし、DLB は病初期には認知機能障害が目立たず早期診断が困難な場合がある。

DLB の幻視は後頭葉の視覚情報処理障害により生じると考えられている。SPECT、FDG-PET で後頭葉の活性低下を伴う全般性の取り込み低下は DLB の指示的バイオマーカーとされているが[1]、病初期の DLB を対象とした研究では診断マーカーとしての精度が十分あるとは言い難いことが指摘されている[1)2)3)]。ヒトの視覚情報処理において空間や動きの認知に関わる背側路（Where 経路）には、一次・三次・五次視覚野（後頭葉外側部）及び上頭頂小葉、下頭頂小葉が含まれている[4]。脳磁図（MEG）は時間・空間分解能に優れた非侵襲的脳機能計測法であり、視覚情報処理過程の評価に有用とおもわれる。

本研究の目的は LBD 患者の視覚情報処理にかかる Where 経路の神経ネットワークについて MEG を用いて定量的に評価することである。

2. 方法

本研究は金沢大学医学倫理審査委員会に承認をうけ（承認番号 3041）、被験者に十分な説明を行った上で文書にて参加同意取得を行った。

2.1. 対象

60 歳以上の高齢者を対象とする。LBD 群は金沢大学附属病院脳神経内科に通院中の PD または DLB とする。正常認知機能高齢者（NC）群は LBD 群と年齢をマッチさせる。

2.2. Optic flow 課題

画面中央から放射状に周囲に拡大するように流れる点群と静止した点群の表示が 4:11 の割合でランダムに生じるタスクを用いた。Optic flow 課題の所要時間は 15 分であった。

2.3. 解析

Optic flow 課題の際の脳磁図の加算波形を記録し、各被験者の頭部 MRI 構造画像より信号源推定を行った。Desikan-Killiany アトラスの Lateral Occipital, Inferior Parietal, 及び Superior Parietal を関心領域（ROI）とし、解析には Matlab の無料ツールボックスである Brainstorm を用いた。

3. 結果

LBD 群は PD 4 例（中央値 72.5 歳, 71-74 歳, 女性 2 例）、全例が International Parkinson and Movement Disorder Society（MDS）診断基準（2015）で clinically established Parkinson’s disease と診断された。The Unified Parkinson’s Disease Rating Scale （UPDRS）part III スコアは中央値 26.5 点（19-30 点）であった。Mini-mental state examination（MMSE）は中央値 27.7 点（27-28 点）で NC 群に比して有意に低値だった（$P = 0.019$）（表 1）。Trail making test (TMT)-A 及び TMT-B の中央値は NC 群に比して高値だが、有意差はみとめなかった（表 1）。LBD 群は Clinical dementia rating（CDR）0 で全例が正常認知機能と判断された。4 例中 3 例でレム期睡眠行動異常症をみとめ、うち 1 例では幻視があった。NC 群は 6 例（平均 74.5 歳, 64-80 歳, 女性 3 例）、UPDRS part III スコアは平均 0.5 点（0-2 点）でレム期睡眠行動異常症や幻視をみとめる方はいなかった。

LBD 群のうち、1 例は筋電図の混入が強く脳磁図解析から除外した。全被験者で Optic flow 開始 0.1～0.3 秒後に事象関連脳磁界を認めたため、この時間帯の各 ROI の最大信号強度を比較した。その結果、いずれの ROI においても LBD 群と NC 群の信号強度に有意差はみとめなかった。各 ROI の信号強度と MMSE, TMT-A 及び TMT-B スコアとの相関を検定したところ、左 Lateral Occipital の信号強度と TMT-A スコアに有意な負の相関を認めた（$r = -0.803$, $P = 0.009$）（図 1）。

4. 考察

TMT-A の成績は視知覚に関連した注意の選択性を反映するといわれている[5]。本研究より、注意機能の低下に関連して Optic flow 課題の際の左後頭葉外側部の脳活動が低下する可能性が示された。本研究は少数例での検討のため、今後さらに LBD や AD 症例を蓄積して症候や認知機能と MEG 所見との関連を解析することで、LBD 群の幻視など視覚情報処理過程の神経ネットワーク障害が明らかになるとともに、LBD の早期診断及び AD との鑑別における MEG の有用性が示されることが期待される。

謝辞

本研究は、公益財団法人渡邉財団の補助、及び株式会社リコーが金沢大学へ設置した寄附講座の研究経費にて実施したものである。

参考文献

1) McKeith IG, et al. Diagnosis and management of dementia with Lewy bodies: Fourth consensus report of the DLB consortium. Neurology, **89**: 88-100 (2017).

2) Lobotesis K, et al. Occipital hypoperfusion on SPECT in dementia with Lewy bodies but not AD. Neurology, **56**: 643-9 (2001).

3) O'Brien, JT, et al. ^{18}F-FDG PET and perfusion SPECT in the diagnosis of Alzheimer and Lewy body dementias. J Nucl Med, **55**: 1959-1965 (2014)

4) Tobimatsu S and Celesia GG. Studies of human visual pathophysiology with visual evoked potentials. Clin Neurophysiol, **117**: 1414-1433 (2006).

5) Sanchez-Cubillo I, et al. Construct validity of the Trail Making Test: Role of task-switching, working memory, inhibition/interference control, and visuomotor abilities. J Int Neuropsychol Soc, **15**: 438-450 (2009).

表1 NC と LBD の認知機能

	NC (n = 6)	LBD (n = 4)
MMSE (点), 中央値 (範囲)	29.4 (28-30)	27.7 (27-28)*
TMT-A (秒), 中央値 (範囲)	41.0 (25-59)	48.5 (31-94)
TMT-B (秒), 中央値 (範囲)	83.0 (39-129)	93.5 (88-146)

* $P < 0.05$; LBD: Lewy body disease; MMSE: Mini-mental state examination; NC: Normal control; TMT-A: Trail making test-A; TMT-B: Trail making test-B

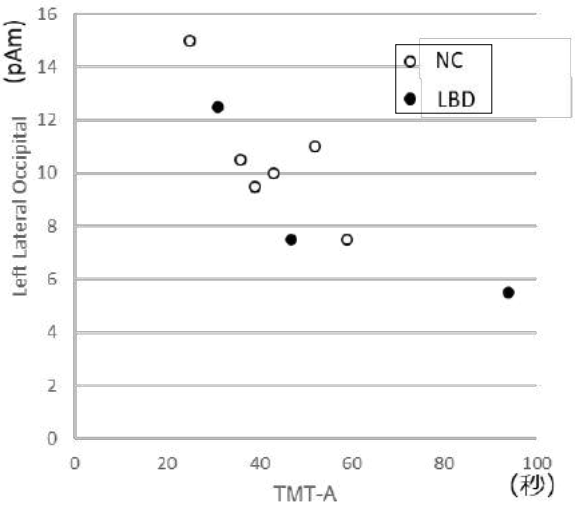

図 1 TMT-A スコアと左 Lateral Occipital 信号強度の相関

低周波磁場測定を応用した脊髄手術に適した手術ナビの研究開発

Development of navigation system for surgical operation of a spinal cord applying low-frequency-band magnetic field detection

足立善昭*, 小山大介*, 川端茂徳,**
中島義和*, 杉野貴明***, 松田美勇史***, 小野木真哉*****
Yoshiaki Adachi*, Daisuke Oyama*, Shigenori Kawabata**, Yoshikazu Nakajima***,
Takaaki Sugino***, Miyuji Matsuda***, Masaya Onogi***

*金沢工業大学先端電子技術応用研究所，〒920-1331 石川県金沢市天池町 3
**東京医科歯科大学先端技術医療応用学講座/整形外科，〒113-8519　東京都文京区湯島 1-5-45
***東京医科歯科大学生体材料工学研究所，〒101-0062 東京都千代田区神田駿河台 2-3-10
*Applied Electronics Laboratory, Kanazawa Institute of Technology
3 Amaike, Kanazawa, Ishikawa 920-1331 Japan
**Department of Advanced Technology in Medicine, Tokyo Medical and Dental University
1-5-45 Yushima, Bunkyo-ku, Tokyo 113-8519 Japan
***Institute of Biomaterials and Bioengineering, Tokyo Medical and Dental University
2-3-10 Kandasurugadai, Chiyoda-ku, Tokyo, 101-0062, Japan

Abstract

Conventional surgical navigation systems mainly rely on infrared stereographic camera technology and cannot track the position of the tools when optical markers are behind the body or hand of the surgeon. Furthermore, the dimensions of optical markers are often problematically large. To solve these inconveniences and satisfy the requirements of surgeons, which include a wide operative field and small markers, we developed a prototype of the new navigation system for spinal surgery based on low-frequency band magnetic field measurements. The developed system was equipped with a coil array implemented in a square frame surrounding the operative field. Instead of optical markers, surface-mounted inductors were used as markers to detect the magnetic fields generated from the coils. Real-time marker localization was successfully performed at approximately 1 Hz. As a result, we could expand the effective operative field to 300 mm×400 mm and reduce the dimensions of the marker to less than 3 mm×3 mm×3 mm.

Keywords: navigation system, marker localization, surface mounted inductor

1. 目的

整形外科の背骨の手術中の患者の脊椎骨の位置や術具の位置・向きを検出し，それらをあらかじめ撮像したX線像やCT画像などに，リアルタイムで重畳して画面上に表示するのが手術ナビゲーション（手術ナビ）であり，安全な手術には不可欠な技術となっている．従来の手術ナビは，患者の骨格や術具に装着した光学マーカーをステレオカメラで撮像し，双方の位置検出を行う光学式が主流である．しかし，カメラとマーカーの間に術中の医師の手や身体が入ると「手暗がり」の状態となり，ナビができなくなるという問題が

あった．また，この手暗がりのために装着する光学マーカーの配置に大きな制約があった．

マーカーから電磁場を発信し，アンテナコイルで受信する（あるいは逆にコイルから電磁場を発信し，マーカーで受信する）ことで位置検出する電波式には上記のような問題がないが，術野やその近傍に金属製の術具があると表皮効果の影響で電波の分布に歪みが生じ，正しく位置検出ができないという別の問題があり，普及には至っていない．

そこで，本研究では金属の表皮効果の影響を受けにくい 100 Hz～1 kHz の低い周波数帯域を利用し，従来の光学式や電波式の問題を解決する新しい磁場式の手術ナビの開発を行うことを目的とする．

2. 方法

われわれはこれまでに前述の磁場式手術ナビを実現するために，術野を囲むように 200 mm×200 mm の方形枠に複数配置した磁気センサアレイで，術具に装着した小さなコイルから発信した磁場信号を検出し，磁場源解析によりコイルの位置情報をリアルタイムに得るシステム(Ver. 0)を試作し，基礎的な開発を行なってきた [1]．

本助成事業による研究開始当初は，この Ver. 0 の高度化を進める計画であった．しかし，実際の脊髄手術での使用ケースを検討していく中で，頚椎骨や術具に装着するマーカーはさらに小さく，また術野をさらに広げたいというニーズが明らかになった．術野を広げると磁場源とセンサの距離が必然的に離れ，検出される信号が小さくなり，信号雑音比が低下する．これを補うために，磁場源となるコイルを大きくし，印加する電流量を増やすと，術具に装着するマーカーを小さくできなくなる．相反する問題を解決するために，発信と磁場検出を逆，すなわち枠に磁場発信用のコイルアレイを配置し，術具に磁気センサを配置したシステムが適当であるという結論に至った．

発信と磁場検出を逆にした場合，次のフローで方形枠に対するマーカーの相対位置を推定する．

1. 方形枠に配置した複数のコイル(本研究では 16 個）に異なる周波数の正弦波電流を同時に印加.
2. マーカーに装着した磁気センサで枠内の任意の位置で複数のコイルからの合成された磁場信号を測定する.
3. 磁気センサの出力を周波数解析し，各コイルからの周波数成分に分離する.
4. 分離された各コイルからの信号と，コイルの位置・向きの情報をもとに，磁気センサの位置を磁気センサアレイのキャリブレーションと同様の方法で推定する [2].

図 1 に示すようにシステムのブロック図は，発信と磁場検出のチャンネル数が異なる以外は，ほぼ同じである．コイルを枠側に配置することにより，コイルの大きさと電流値の条件が緩和された．そのため，従来よりも検出されるべき信号強度を増強でき，表面実装用インダクタ(インダクタンス

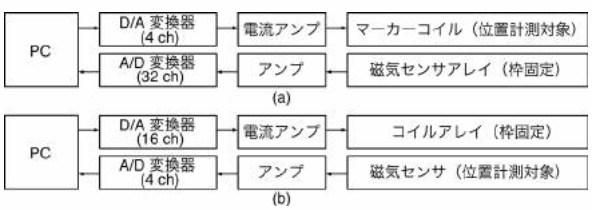

図 1 手術ナビシステムのブロック図, (a) 枠に磁気センサを配置した場合 (b) 枠にコイルを配置した場合

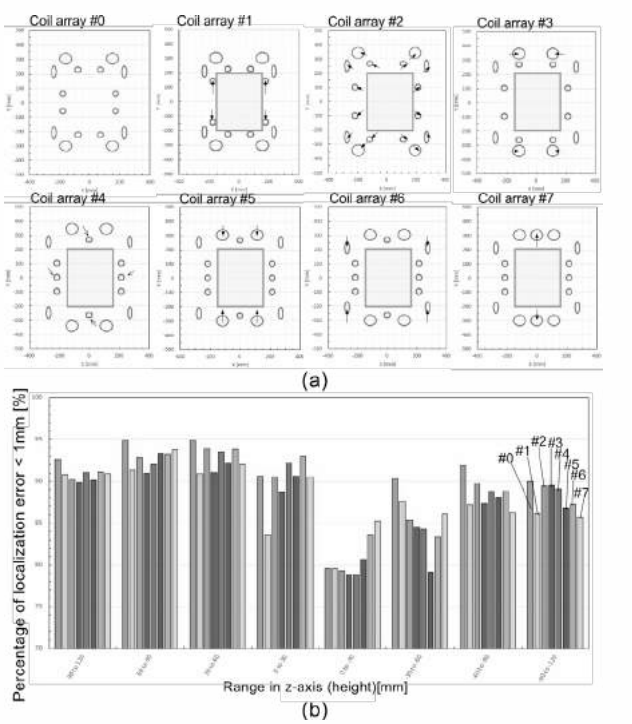

図 2(a) 方形枠コイル配置の候補例 (b) 各コイル配置で磁気センサ位置誤差が 1 mm 未満となる割合

100 μH, NLV25T101-PF, TDK 製)が磁気センサとして使用可能になった。これにより，マーカーのサイズを 3 mm 角以下と大幅に小さくできた.

コイル枠は術野を囲むように配置されるもので，枠内側のサイズは患者の体格や手術台の大きさを考慮して 300 mm×400 mm とした．また，手術時の邪魔にならないように，枠の厚みは 30 mm に抑えたが，鉛直方向の位置推定精度向上のために，長方形の枠の四隅の角はコイルを立体的に配置できるようにした．この制約の元で，コイルの最適配置を求めるために，図 2 (a)に示すようなさまざまなコイル配置に対してモンテカルロシミュレーションを適用した．図 2(b)から、枠内上下 120 mm の範囲で, 磁気センサの位置推定誤差が 1 mm 未満になる領域がもっとも大きくなるコイル配置として Coil array #0 を選択し、枠の四隅と辺にそれぞれ φ80 mm, φ40 mm, 巻き数 100 回巻きの円環コイルを 8 個ずつ配置するようにした.

各コイルに特定の周波数の電流を印加するための多チャンネル電流アンプと，磁気センサからの磁場信号を増幅する低雑音アンプを再設計・試作した．また，磁気センサ位置推定アルゴリズムを実装した位置検出ソフトウェアを新たに開発した．図 3 に試作した手術ナビシステムのコイルアレイ，電子回路，ソフトウェアの外観を示す.

予備実験として 16 個のコイルを 780 Hz～2 kHz の異なる周波数で同時に励振し，その合成磁場を枠内の任意の位置に配置した 4 個の磁気センサで検出，デジタルデータ収録した．各センサごとに逐次的にデータを特定の長さの時間窓で区切り，フーリエ解析で分離したコイル固有の周波数成分と，各コイルの位置，向きから磁気センサの位置推定を行った．その結果はソフトウェアの画面にリアルタイムで表示されるとともに, LAN 経由で医療画像と整合させるための計算機へ送信されるようになっている.

一方，検出したマーカーの位置をあらかじめ撮像した医療画像に重畳表示させるためには，検出した 3 次元空間中の位置座標を，医療画像上の座標に整合させる必要がある．この手続きはキャリブレーションと呼ばれるが，位置整合と表示ソフトウェアの開発のために，コイル枠に光学式マーカーを装着し，市販の 3 次元トラッキングシステム(Aurora, NDI 社製)と光学式手術ナビ(Polaris 社製)を用いてカメラ，コイル枠，術具の相対位置の検出試験を行った（図 4）.

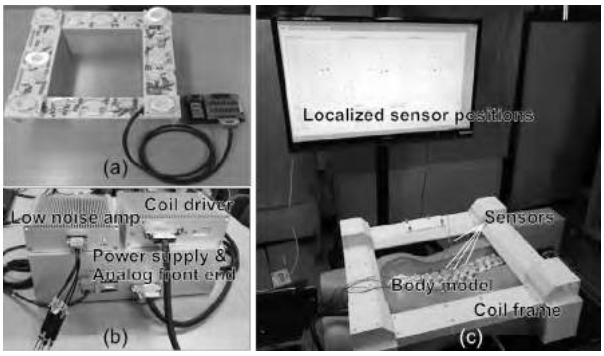

図 3 試作した手術ナビ（a）コイルアレイ（枠内部）(b）電子回路（c）磁気センサ位置推定のようす

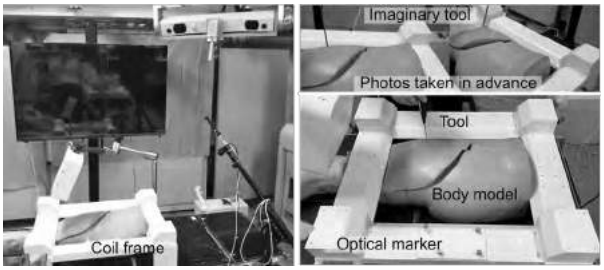

図 4 市販のシステムによるコイル枠のキャリブレーション実験

3. 結果

位置推定ソフトウェア上で, 16 個のコイルからの合成磁場を検出し，周波数解析した例を図 5 に示す．各コイルからの磁場が良好な信号雑音比で分離，検出できていることがわかる．各コイル固有の周波数成分とコイルの位置，向きから 4 個の磁気センサの位置を同時に推定した例が図 6 である．約 1 秒に 1 回の頻度で位置推定がなされており，術具に複数のマーカーが装着されることを想定して複数の磁気センサを同時に動かすと，動きに追従した位置推定ができることが確認できた.

4. 考察

従来の試作手術ナビシステム（Ver. 0）では，約 2 Hz 以上の頻度で位置推定ができていたが，本研究の試作機では同様の計算機環境で，約 1 秒に 1 回の頻度に留まった．これは，磁場源解析の際に，従来はマーカーコイルを近似的に磁気双極子と

して理論的な磁場を計算していたのに対して，円環コイルは磁気双極子で近似できず，その分負荷の高い計算方法で理論的磁場を計算せざるを得ないためである．実際には計算負荷を軽減するために，円環を多角形として近似して計算している．位置推定の頻度を上げるには，より少ない辺の多角形で近似する方が計算負荷が軽減するので有利だが，近似誤差による位置推定精度の劣化とのトレードオフとなる．

また，本研究では市販の手術ナビを用いてカメラ画像とコイル枠のキャリブレーションが可能であることを実証した．しかし，この方法ではコイル枠とカメラ以外にそれらのキャリブレーションを行う別のシステムが必要になる．カメラに映った画像からコイル枠の光学マーカーの位置を推定し，キャリブレーションすることは原理的に可能である．しかし，実際の手術ナビでは術具の位置をX線像に重畳して表示するため，コイル枠，X線照射機，X線撮像パネルとの位置合わせが必要になってくる．光学カメラと異なり，X線像は像自体にパースがほとんどつかないため，X線像に写るマーカーが必要になるのと同時に，キャリブレーションのアルゴリズムに新たな工夫が必要となってくる．これらは今後の課題とする．

5. 結語

本研究では生体磁気計測の技術を応用した「磁気計測による位置検出」を技術シーズとして，医工連携により医師目線で使いやすいナビをめざしたニーズオリエンテッドな開発を進めた．その結果, 術野を従来の200 mm×200 mmから300 mm×400 mmに広げ, マーカーの大きさも3 mm角以下にまで小さくすることができた．また，推定されたマーカーの位置にしたがって，医療画像の上に術具の位置を重畳表示するソフトウェアの開発も目処が立った．

今後は，マーカーの位置推定精度の評価と最適化，信号雑音比の向上による励振周波数の低減化，位置推定のさらなる高速化，X線像とのキャリブレーション，ユーザーインターフェースの整備など，実用化に向けた種々の課題について引き続き取り組む．

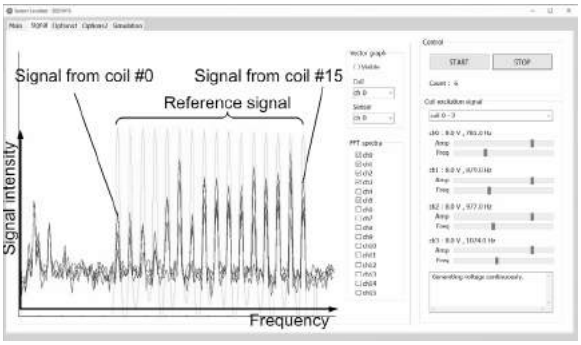

図5 合成磁場信号の周波数解析の例

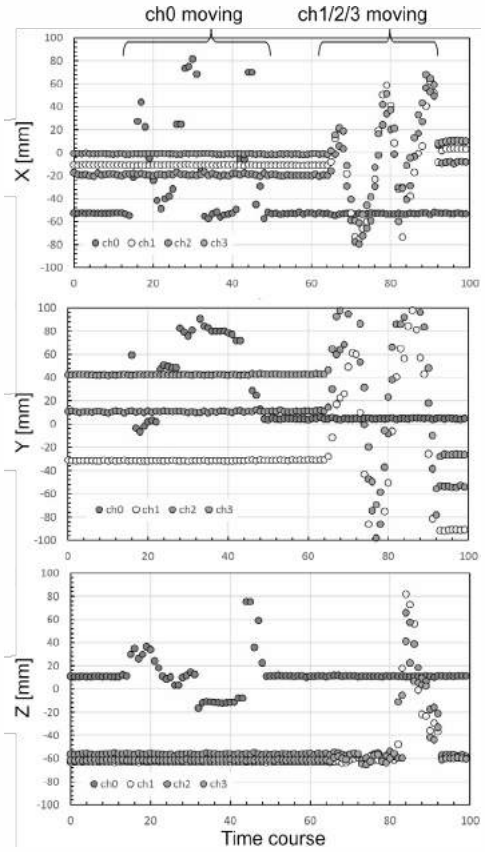

図6 磁気センサの位置推定結果の例

謝辞

本研究は公益財団法人渡邉財団からの研究助成金を受けて実施した．

参考文献

1) Daisuke Oyama et al, IEEE Trans Magn, vol. 50 (11), 5101604 (2014).
2) Yoshiaki Adachi et al, IEEE Trans Magn, vol. 55(7), 5000506 (2019).

新規生体透視ナノイメージングを可能とする磁性ナノ材料開発研究

Development of magnetic nanomaterials that
enable novel bioperspective nanoimaging

佐藤和秀*,**
Kazuhide Sato*,**

*名古屋大学高等研究院，〒466-8550 名古屋市昭和区鶴舞町 65
*Nagoya University Institute for Advanced Research (IAR)
**Dept of Respiratory Medicine, Nagoya University
65, Tsuruma-cho, Showa, Nagoya, Aichi, 466-8550, Japan

Abstract

In clinical medicine, diagnosis and evaluation based on imaging are essential for understanding pathological conditions, determining treatment methods, and measuring treatment effects. In this study, we develop the Gd encapsulated carbon nanotube (CNT), and investigate its biocompatible modification. We intend to develop this material for biological application with both Near infrared II (NIR-II) fluorescence and MRI-magnetic imaging.

Keywords: carbon nanotube, NIR-II, peapods, MRI, in vivo imaging

1. はじめに

臨床医学において、イメージングに依る診断・評価は病態の把握、治療法の決定、治療効果計測に必須である [1)]。近年、解剖学的なイメージングから病態、病気のみを診断し描出する分子イメージングが新しい分野、方法として知られている [2)]。その中でも蛍光を用いたイメージングは、広く細部生物実験や、遺伝子組み換え動物実験などに使用され、今日のバイオ系の研究の礎と成っている。その中でも、近赤外光の 1000nm を超える領域は NIR-II 領域(第 II 近赤外光領域)と呼ばれ近年注目を集めている。その特徴は、自家蛍光が極端に少なく、生体深部までの観察が可能であり、1320nm で 850nm とくらべて 100 倍の signal-noise ratio を得ることができ、インビボイメージングの新領域として期待されている [3)]。しかしながら、他の蛍光材料に比較して生体で用いることのできる蛍光材料が不足しているのが現状である。

2. 研究の目的

本研究提案の目的は、世界初の金属(Gd)内包カーボンナノチューブ(CNT)を開発し、その生体適合性修飾を検討し、最終的には MRI（磁性イメージング）も同時に行える NIR-II のイメージング材料としての生体応用を達成する。MRI を用いた CNT のリアルタイムイメージングのみならず、腫瘍血管の治療によるリアルタイムの変化、吸入イメージングの達成による肺疾患の効果測定へとつなげる。また、革新的治療として報道されている近赤外光線免疫療法の血流このように、自然由来の炭素素材を将来の医学臨床応用、生体応用を見据えたイメージング剤として開発を行う。

3.方法・結果・考察

単層カーボンナノチューブであるＭＥＩＪＯｅＤＩＰＳ　ＥＣ１．０（株式会社名城ナノカーボン）を準備した。なお、上記単層カーボンナノチューブの中心直径は１．０ｎｍである。中心直径の数値とは、含有されるカーボンナノチューブの中央値の数値であり、カイラル指数から算出した数値であるが、電子顕微鏡での観測においても同等の数値が確認できる [4)]。大気雰囲気下の電気

炉にて、単層カーボンナノチューブを６時間かけて５００℃まで昇温し、５００℃に達した時点で加熱を止めて、室温まで放冷した。この操作は、単層カーボンナノチューブ両端を開くためのものである[5]。室温まで冷却した石英管から生成物を取り出して水洗した。ここでの水洗にて、カーボンナノチューブに関与しなかったＧｄＩ$_3$、及び、カーボンナノチューブに内包されずにカーボンナノチューブの外表面に付着するＧｄＩ$_3$は除去される。水洗後のＧｄ内包カーボンナノチューブを、Ｇｄ内包カーボンナノチューブとした。Ｇｄ内包カーボンナノチューブにつき、透過型電子顕微鏡（以下、ＴＥＭと略すことがある。）での観察を行った。製造例１のＧｄ内包カーボンナノチューブのＴＥＭ像を図１に示す。

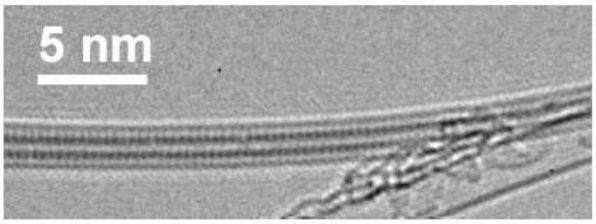

図１　TEM 像

図１のＴＥＭ像から、Ｇｄ内包カーボンナノチューブのいずれにおいても、カーボンナノチューブの内部にＧｄ含有物質が内包されているのが確認できる。カーボンナノチューブの内部でＧｄが連なったワイヤー状の構造が観察された。

なお、ＴＥＭ観察によれば、Ｇｄ内包カーボンナノチューブのいずれにおいても、存在するカーボンナノチューブのうち、概ね半数のカーボンナノチューブにＧｄ含有物質が内包されていると判断できた。

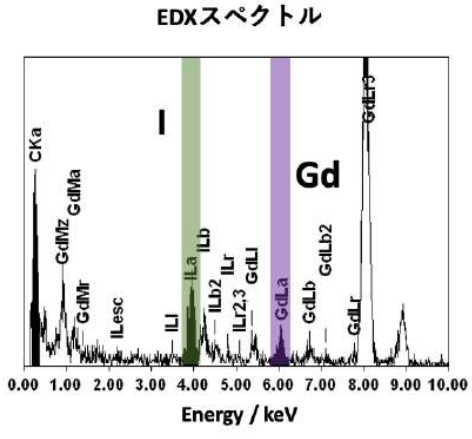

図２　　EDX スペクトル

次に透過型電子顕微鏡にエネルギー分散型Ｘ線分析装置を組み合わせたＴＥＭ－ＥＤＸにて、Ｇｄ内包カーボンナノチューブのうち、ＧｄI3 含有物質が内包されているのが確認されたカーボンナノチューブについての分析を行った(図 2)。その結果、ＧｄI3 内包カーボンナノチューブのＥＤＸスペクトルからは、Ｇｄ及びＣｌに由来するピークが観察された。

次に、５ｍｇのＧｄ内包カーボンナノチューブと、３ｍＬの１質量%コール酸ナトリウム水溶液を混合し、密閉式超音波分散装置Ｎａｎｏｒｕｐｔｏｒ　ＮＲ－３５０（東湘電機株式会社）を用いて、４時間超音波処理することで分散液とした。分散液を分離用小型超遠心機ＣＳ１００ＧＸＬ（日立工機株式会社）に供して、５２０００ｒｐｍで１時間、遠心分離をすることで、カーボンナノチューブ凝集体などを沈殿させた。遠心分離処理後の分散液における上部分散液を採取してその後の検討に用いた。

上記作成の、GdI3 溶液、水(陰性コントロール)の NIR- II 蛍光を評価するために、SHIMADZU の SAI-1000 を用いて蛍光を評価した（図 3）[6]。結果は GdI3 内包の CNT で十分な NIR-II 蛍光を認めた。次に、MRI での検討を行い、磁性イメージングについての可否を検討した。陽性コントロールとして造影剤のオムニスキャン、対比コントロールとして水を加えた。結果は、GdI3 は T1、T2 強調画像の両方で、水より濃く写り、陽性造影剤として利用できることが明らかとなった。

上記、作成した材料の NIR-II と MRI の造影能が明らかとなり、今後疾患動物モデルを用いた検討を行う。

図３　　NIR- II 蛍光の確認

4. 結論

GdCl２内包カーボンナノチューブの合成に成功し、イメージング性能を確認できた。今後、動物モデルでの利用検討を行う。

謝辞

この研究は公益財団法人渡邉財団の研究助成補助を受けて実施したものである.

参考文献

1) Kobayashi H, Longmire MR, Ogawa M, Choyke PL, Kawamoto S.
Lancet Oncol. 2010 Jun;11(6):589-95.

2) Kobayashi H, Choyke PL, Ogawa M.
Curr Opin Chem Biol. 2016 Aug;33:32-8.

3) Wang S, Li B, Zhang F.
ACS Cent Sci. 2020 Aug 26;6(8):1302-1316.

4) Nakanishi Y , Omachi H , Fokina NA , Schreiner PR , Becker J , Dahl JEP , Carlson RMK , Shinohara H .
Chem Commun (Camb). 2018 Apr 12;54(31):3823-3826.

5) Nagata M, Shukla S, Nakanishi Y, Liu Z, Lin YC, Shiga T, Nakamura Y, Koyama T, Kishida H, Inoue T, Kanda N, Ohno S, Sakagawa Y, Suenaga K, Shinohara H.
Nano Lett. 2019 Aug 14;19(8):4845-4851.

6)https://www.an.shimadzu.co.jp/bio/sai-1000.htm

令和2年度　研究助成テーマ

令和2年度は、以下のように、第27回 11名（基礎5名・応用3名・テーマ指定3名）30周年記念特別助成2020 2名の研究に対し助成が決定いたしました。

Ⅰ. 基礎研究

Ⅰ-1. 光線力学療法における磁場効果
崇城大学　工学部　ナノサイエンス学科／米村　弘明

Ⅰ-2. 超低周波変動する超微弱磁場が誘導するマイトファジーによる病態制御
名古屋大学　大学院医学系研究科　神経遺伝情報学分野／大野　欽司

Ⅰ-3. 磁場刺激による細胞配向特性を応用した人工骨組織の作製
九州情報大学　経営情報学部　情報ネットワーク学科／荒平　高章

Ⅰ-4. ベージュ脂肪の分布位置による形態および代謝特性の比較
日本体育大学／小川　まどか

Ⅰ-5. パルス磁場が培養骨格筋細胞の収縮機能獲得に及ぼす効果とそのメカニズム
東北大学　大学院医工学研究科／永富　良一

Ⅱ. 応用研究

Ⅱ-1. 脳波同時記録による新たな経頭蓋磁気刺激療法によるてんかんの新規バイオマーカー開発
東京大学　医学部附属病院　脳神経内科／小玉　聡

Ⅱ-2. コンパクトダイヤモンド磁気プローブのための永久磁石形状の最適化手法の開発
東京大学　大学院工学系研究科　電気系工学専攻／桑波田　晃弘

Ⅱ-3. Na-MRIを用いた全身性強皮症におけるナトリウム代謝異常の解明
横浜市立大学　大学附属病院　血液・リウマチ・感染症内科／峯岸　薫

Ⅲ. テーマ指定研究

Ⅲ-1. 脳の可塑的変化を誘導する磁気刺激と経皮的脊髄刺激の連合性ペア刺激における刺激パラメータの検討
東京大学　大学院総合文化研究科／金子　直嗣

Ⅲ-2. 磁気刺激による精神症状発症抑制効果の検討とそのメカニズムの解明
防衛医科大学校　精神科学講座／古賀　農人

Ⅲ-3. 頸部にある特定の神経節への低頻度磁気刺激による交感神経抑制効果に関する研究
大阪大学　医学系研究科　心臓血管外科／金田　恵理
＜この研究は岡井治特別研究助成に選ばれました＞

Ⅳ. 30周年記念特別助成2020

Ⅳ-1. ＜基礎研究＞磁場誘導加温による生体組織の凍結保存技術の開発
名古屋大学／井藤　彰

Ⅳ-2. ＜応用研究＞運動閾値未満の末梢磁気刺激を併用した上肢リハビリテーションの効果
藤田医科大学　医学部リハビリテーション医学Ⅰ講座／加賀谷　斉

なお、所属は研究助成決定当時のものです。

THE REPORT OF STUDY

RESULT BY SUBSIDY

26TH

(STUDY DURATION : April 1, 2020 - March 31, 2021)

The Watanabe Foundation

CONTENTS

Preface

About 45 years ago, I have been researching feeble magnetic measurements from the human body in order to help diagnose the disease at the Massachusetts Institute of Technology (MIT) in the United States for two years. I have been studying biomagnetism measurement after returning home.

It has been estimated that weak magnetism is generated from human heart and brain, but there was no magnetometer capable of measuring this weak magnetism. However, in the 1970s, an ultra-sensitive SQUID magnetometer using superconducting technology was developed in collaboration between US National Research and MIT.

When the magnetic measurement from heart using this SQUID magnetometer was successful and challenging magnetic measurements from the brain of about 1 / 1,000 of cardiac magnetism, I had been studying at MIT.

MIT laboratory was in big trouble during my study abroad. A prominent doctor in the United States criticized of MIT's research as follows. "They say that they measure the magnetism caused by nerve activity of heart and brain, but that is incorrect. They are only measuring the magnetism that the iron in the blood is disturbing the geomagnetism." As a result, the public research expenditure in the US for MIT biomagnetism research was greatly reduced.

I regarded his theory as correct. Therefore, I measured more than ten blood with SQUID magnetometer, but it turned out that blood had no magnetism at all.
The reason is that iron itself always has magnetism, but it has strong magnetism or no magnetism at all depending on the bonding method of iron and oxygen. Iron in the blood binds to oxygen so that it has no magnetism at all.
The evolution of mankind has progressed from birth to bipedalism to communication through spoken language over 2millions of years. The strength and directions of the geomagnetism have changed about ten times during the years. Since humans have evolved in such magnetic environment, human body have made to have little effect of geomagnetism.

On the other hand, it has been only 200 years or so since humans started using electricity. The humans have not developed full defensive capabilities against it. Therefore, a human body is vulnerable and sensitive to electricity: a heart stops beating once a couple of voltages are applied to the chest, however, it is quite difficult to stop a heart when magnetism is applied externally.
In view of this, it is fair to say that electric medical devices bring an immediate effect. However, they could be dangerous once misused. In contrast, magnetic medical devices are not dangerous, but they must be used for a long time for treatment.

Our foundation intends to contribute to the health and medical care of the nation, by subsidizing scientific research and appealing to the society through seminars. It should be noted, that the effect of the magnetic field is generated from some basic phenomena interacting with the complex mechanism of the body. The effect can only be clarified by a long-term persistent effort, not by short-sighted research.

It is a regrettable tendency in the present scientific sector that researchers are mostly interested in achieving successful results for acquiring a degree or achievement in a short period, focusing on obvious cause-effect relationship or phenomenon which invites quantitative descriptions. In view of such a tendency, our foundation prefers to support researchers who persistently attack a particular problem expecting long-term results rather than those who rush into short-term results.

This report is the summary of research which our foundation supported in the fiscal year 2019. It includes a wide range of topics from basic aspects to practical applications, intending to pave new ways in this area. It is our hope that the report will motivate researchers with similar interests to start communication and contribute to the development of magnetic health science.

Director Makoto Kotani
The Watanabe Foundation

The effect of transcranial magnetic stimulation on neurodegeneration

Yuki Fujita

Department of Molecular Neuroscience,
Graduate school of Medicine, Osaka University
2-2 Yamadaoka, Suita-shi, Osaka 565-0871, Japan

Abstract

Damaged axons in the adult central nervous system (CNS) fail to regenerate spontaneously due to several intrinsic and extrinsic factors that inhibit axon elongation. Transcranial magnetic stimulation (TMS) has been used as a form of rehabilitation, and accumulating studies have suggested that TMS is able to modulate neural plasticity of the cortex. Here, we conducted TMS in mice with CNS injury to investigate the potential effects on motor recovery.

Keywords: central nervous system, brain, spinal cord, neuron, TMS

1. PURPOSE

Central nervous system (CNS) injuries induce severe, longlasting neurological disabilities, including motor, sensory,
and cognitive dysfunctions.

Studies support the view that partial functional motor recovery can occur spontaneously after the injury. Such recovery is correlated with functional organization of remnant neuronal networks. It has been shown that reorganization of the corticospinal tract (CST), a major descending motor pathway in mammals which projects from the cortex to the spinal cord, can contribute to post-injury functional motor recovery. During reorganization, remnant CST fibers sprout collaterals, and then, they form synapses with interneurons to construct compensatory neural pathways.

Repetitive transcranial magnetic stimulation (rTMS) has been used as a form of rehabilitation, and accumulating studies have suggested that rTMS is able to modulate neural plasticity of the cortex. Here, we conducted rTMS treatment in mice with CNS injury to investigate the potential effects on motor recovery.

2. METHOD

1) Animal models

Adult C57BL/6 J female mice were used in this study. All experimental procedures were approved by the Institutional Ethics Committee of Osaka University and complied with the Osaka University Medical School Guidelines for the Care and Use of Laboratory Animals. Mice were anesthetized with a mixture of 0.5 mg/ml Vetorphale (Meiji Seika Pharma), 0.4 mg/ml Dormicum (Roche), and 0.03 mg/ml Domitor (Orion Pharma). For spinal cord injury, thoracic level 8 laminectomy was performed and a dorsal hemisection of the spinal cord was conducted with a surgical microknife at a depth of 1.0 mm. For controlled cortical impact (CCI), the scalp was retracted, then using a drill and a 23G needle, a 4mm diameter circular craniotomy was performed on the left side with the center at 0mm antero-posterior and 2mm lateral to bregma. Cortical traumatic injury was induced using a pneumatic impact device (Amscien

Instruments)11,13,14. The impactor tip (diameter, 3 mm) was set at 1 mm, and impact was induced at 4.0–4.5 m/s for 120 ms. Thereafter, the wound was sutured, and the mice were housed in their home cages.

2) Behavioral tests

Ladder walk test: The ladder walk test was used to assess precise limb placement and stepping while walking along a horizontal ladder with variable rung space. The ladder was designed as previously described. Mice received training three times per session the day before the injury; the percentage of foot-slips for each hindpaw was recorded.

Rotarod test: The rotarod is used to assess the motor recovery in rodents after the injury. Animals were placed on a rotating rod that gradually accelerated from 0 to 50 r.p.m. within 5 min. Mice were trained three times a day for 3 days before injury. Total time was recorded until the mouse fell off the rod or gripped and spun around two times. The baseline value (pre) was scored as the mean of three trials 1 day before the injury.

Basso mouse scale (BMS) score: The BMS score was used to assess the hindlimb motor function on the coordination in movement and stepping in mice. Each mouse was evaluated at the following time points: 1, 3, 7, 14, 21, 28, 35, and 42 days after the injury.

3) Immunohistochemistry

Mice were perfused transcardially with PBS followed by 4% paraformaldehyde in 0.1M phosphate buffer. Tissues were dissected, postfixed in the same fixative, immersed overnight in PBS containing 30% sucrose, and then embedded in Tissue-Tek OCT and frozen at −80 °C until use. Sections were prepared using a cryostat and mounted on adhesive-coated slides. Cryostat sections were incubated with blocking solution for 1 h at room temperature, followed by overnight incubation with primary antibodies anti-CaMKII for 2 days at 4 °C. Immunoreactivity was visualized using Alexa Flour 488-conjugated secondary antibodies. Coverslips were then placed on the slides with mounting medium. Images were captured using a laser scanning confocal microscope. The CAMKII fluorescence intensity was analyzed using ImageJ software.

3. RESULTS

1) Animal models

Following unilateral brain injury, the remnant CST fibers from the intact side extend axon collaterals into the denervated side of the spinal cord, and they form synapses with interneurons to reconstruct neural circuits. We injected pAAVphSyn1-tdTomato-T2A-SypEGFP into the motor cortex of intact hemisphere post-injury. We observed GFP-labeled synaptophysin-positive boutons on tdTomato-labeled CST axons in the cervical spinal cord 42 days post-injury; the number of GFP-positive puncta and tdTomato-labeled axons in the denervated side of the spinal cord was increased, consistent with the results of a previous studies.

2) Behavioral tests

We further examined whether rTMS treatment improved motor function after SCI since recent studies have shown that rTMS treatment improves motor recovery in rats and patients with SCI. Since axotomized corticospinal tract fibers form collaterals within 10 days following injury, we applied rTMS treatment to awake mice starting 3 days after SCI and repeated the treatment three times per week for 6 weeks. We also evaluated the motor function of mice with SCI. The rTMS-treated mice showed slightly better motor function in the ladder walk test and almost no difference in rotarod test in comparison with the control mice. Furthermore, the sequential treatment of Drug and rTMS showed better performance in the ladder walk test at 42 days after the injury compared with the mice that received a single Drug treatment.

3) Immunohistochemistry

We investigated the expression of CaMKII in the motor cortex 6 weeks after SCI using

immunohistochemistry. CaMKII is known to be a key mediator of long-term potentiation (LTP) by increasing the channel conductance of AMPA-type glutamate receptors (AMPAR). After the sequential treatment of Drug and rTMS, CaMKII intensity had increased compared to that in mice that received a single drug treatment in the cortical layer 2/3.

4. DISCUSSION

In the present study, we conducted TMS in mice with CNS injury to investigate the potential effects on motor recovery. The sequential treatment of Drug and rTMS can be able to modulate neural plasticity of the cortex.

Acknowledgements

We thank The Watanabe Foundation and all of Yamashita's lab members for their research assistance and helpful suggestions.

REFERENCES

1) Fujita Y, Yamashita T: Axon growth inhibition by RhoA/ROCK in the central nervous system. Frontiers in neuroscience 8: 338, (2014).

Hyperthermia for castration-resistant prostate cancer using magnetite nanoparticle composed from single-walled carbon nanohorn

Takashi Nagai* Noriyasu Kawai*

* Department of Nephro-urology, Nagoya City University, Graduate School of Medical Sciences
1 Kawasumi, Mizuho-cho, Mizuho-ku, Nagoya, Japan

Abstract

Single-walled carbon nanohorn (SWNH) can be used for drug delivery because of its high surface area. In this study, SWNH was applied for thermotherapy by combining Fe_3O_4 because Fe_3O_4 heat in an alternating magnetic field (AMF). Human castration resistant prostate cancer cells (22Rv1) were injected subcutaneously into nude mice. In treatment group mice, SWNH- Fe_3O_4 were injected into tumor nodule and the mice were exposed into AMF for 30 minutes. Tumor regression was observed in treatment group compared with control group.

Keywords: prostate cancer, single-walled carbon nanohorn, thermotherapy

1. Purpose

The number of patients with prostate cancer is increasing. In general, localized prostate cancer without metastasis has been reported to be well controlled by surgery and radiation therapy. However, the prognosis of metastatic prostate cancer is poor, and the diagnosis and treatment of metastatic prostate cancer is a problem in prostate cancer treatment. In addition, acquiring castration resistance plays a major role in the metastasis of prostate cancer. Therefore, the treatment of castration-resistant prostate cancer is also an issue.

In Japan, CT and bone scintigraphy are commonly used to detect metastatic sites of prostate cancer. In recent years, the utility of PET (PSMA-PET) targeting prostate specific membrane antigen (PSMA) has been reported. PSMA is an antigen that is upregulated in prostate cancer, and by targeting PSMA, more specific metastases can be detected. We aimed to develop nanoparticles that can detect metastatic lesions more specifically in prostate cancer by targeting PSMA.

In this study, we attempted to develop a tumor-specific thermotherapy treatment by using single-walled carbon nanohorn (SWNH) to bind iron oxide (Fe_3O_4) and PSMA. As an initial step of the above plan, we report the verification of the thermotherapeutic effect of SWNH containing Fe_3O_4.

2. METHODS

Ⅰ. Preparation of SWNH+Fe_3O_4

We developed dispersible magnetic nanoparticles by using 3-aminopropyltriethoxysilane (APTES) in collaboration with Chubu University.

Ⅱ. Therapeutic effects of SWNH+Fe_3O_4

To verify the effects of hyperthermia in animal experiments, a mouse model for subcutaneous implantation of prostate cancer was used as a model animal. A human castration-resistant prostate cancer cell line, 22 Rv1, was subcutaneously implanted into the back of 6-week-old male nude mice. At 3 weeks (day 21) after subcutaneous implantation, 300 μL of SWNH+ Fe_3O_4 (Fe concentration: 36.3 mg/ml) was injected locally into the tumor of the model mice in the control (n=3) and treatment group (n=3). (Figure 1)
Thereafter, hyperthermia due to the heat generated by

SWNH+ Fe_3O_4 under an alternating magnetic field (AMF) was attempted using a coil-type AMF irradiation device (Figure 2). The temperature in the tumor was maintained at 42°C-46°C, which is defined by so-called mild hyperthermia, and the heating was performed for 30 minutes. Tumor size in both groups was measured over time to verify the effect of hyperthermia.

3. RESULTS

Ⅰ. Preparation of SWNH+Fe_3O_4

Magnetic nanoparticles with magnetic properties and dispersibility (SWNH-APTES-Fe_3O_4) were successfully developed by intercalating APTES between SWNH and Fe_3O_4 at Chubu University.

Ⅱ. Therapeutic effects of SWNH+Fe_3O_4

The temperature course of the subcutaneously implanted model mice during the thermal treatment is shown. (Fig. 3) In mouse 1, the temperature rise was slow, and the temperature rise was a little low at about 42°C, but all three mice were able to maintain a temperature of 42°C or higher. The temperature progress was measured using a thermography camera (FLIR C5). (Figure 4)

The changes in tumor size over time are shown in the figure. (Figure 5)

In the treatment group, one mouse died due to anesthesia. The control group showed an increase in tumor size over time, whereas the treatment group showed a decrease in tumor size. In the subcutaneous transplantation model mice, the effect of thermotherapy was confirmed by heat generation under AMF using magnetic nanoparticles with SWNH+ Fe_3O_4.

4. DISCUSSION

In this study, we examined the effect of thermotherapy by using SWNH-APTES-Fe_3O_4 under an AMF for castration-resistant prostate cancer.

It was found that the SWNH+ Fe_3O_4 developed in this study generated heat under an AMF. In addition, the tumor size was reduced by hyperthermia using SWNH+ Fe_3O_4. These results are comparable to those of our previous thermotherapy for prostate cancer[1,2].

Future work includes the preparation of samples with increased iron concentration in magnetic nanoparticles and magnetic field irradiation conditions in order to obtain better therapeutic effects. In the past, our institution has reported that subcutaneous tumors of prostate cancer completely regressed after multiple cycles of hyperthermia[1], and we would like to investigate the possibility of multiple cycles with appropriate treatment intervals.

In this study, we administered nanoparticles by local injection, but there is a problem of drug delivery in thermotherapy using nanoparticles.[3] Since SWNH can be applied to therapy and diagnosis by binding various drugs and antibodies, we will develop nanoparticles with more specific accumulation by using PSMA. In the future, it is necessary to develop nanoparticles with more specific aggregation using PSMA.

ACKNOWLEDGEMENT

This study was supported by the Grant-in-Aid of Watanabe Foundation (2020). The equipment of the Laboratory Animal Center of Nagoya City University was used.

REFERENCES

1) Kawai N et al. Complete regression of experimental prostate cancer in nude mice by repeated hyperthermia using magnetite cationic liposomes and a newly developed solenoid containing a ferrite core. Prostate. 2006 May 15;66(7):718-27.
2) Kobayashi D et al. Thermotherapy using magnetic cationic liposomes powerfully suppresses prostate cancer bone metastasis in a novel rat model. Prostate. 2013 Jun;73(9):913-22.
3) Tsai HC et al. Drug-loading capacity and nuclear targeting of multiwalled carbon nanotubes grafted with anionic amphiphilic copolymers. Int J Nanomedicine. 2013;8:4427-40.

(Figure 1)

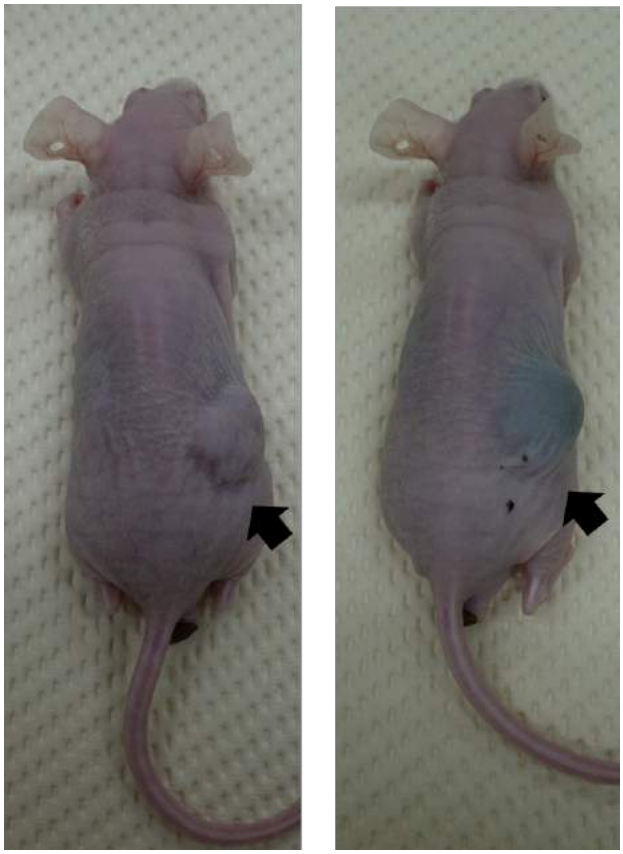

(Figure 2)

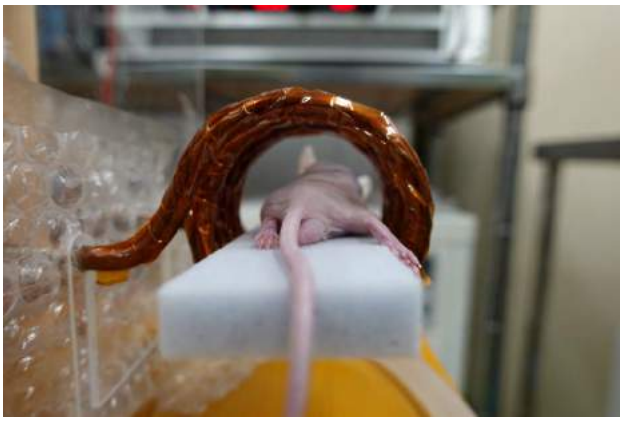

(Figure 3)

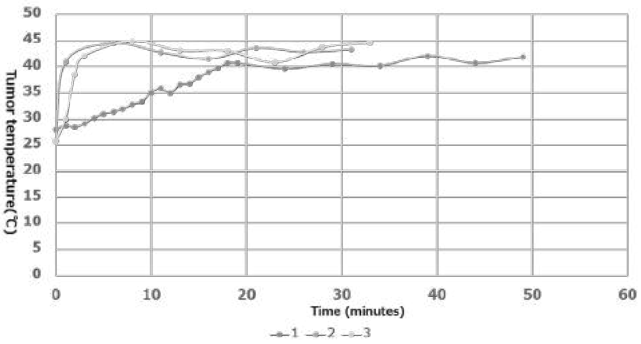

(Figure 4)

(Figure 5)

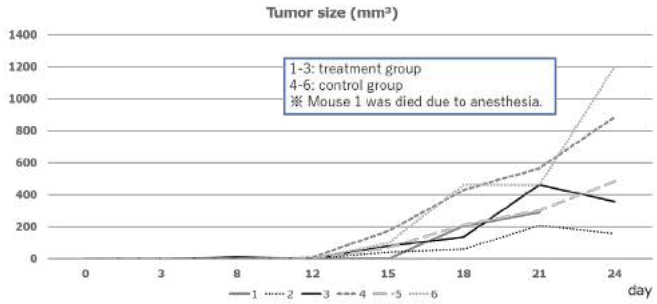

Effects of magnetic field on ABCA1-mediated cellular lipid release

Maki Tsujita[1], Hiroshi Takase[1], Natsuko Kumamoto[1], Shinya Ugawa[1], Yoshito Furuie[2], and Motonari Tsubaki[2]

[1]Nagoya City University Graduate School of Medical Sciences
1 Kawasumi, Mizuho-cho, Mizuho-ku, Nagoya 467-8601 Japan
[2]Graduate School of Science and Technology, Kobe University
1-1 Rokkodai-cho, Nada-ku, Kobe 657-8501Japan

Abstract

This project aims to explore a novel magnetic field health care based on the cholesterol metabolism. Mouse peritoneal macrophage foam cells were incubated in CO_2-independent culture medium containing apoA-I and were exposed in a magnetic field (400 mT) using the electromagnet of an EPR spectrometer. Cellular cholesterol release mediated by ABCA1 and apoA-I was not affected by the magnetic field treatment under our current condition. Furthermore, when C57BL/6N mice were exposed in the magnetic field under the identical condition, the PCSK9 expression was reduced in the hepatocytes and the newly generated hippocampal dentate gyrus cells were significantly reduced.

Keywords: macrophage form cell, cholesterol, PCSK9, adult brain cell generation

1. PURPOSE

The purpose of this research was to explore the effects of magnetic field on the efflux of cellular cholesterol via ABCA1 from foamed macrophage cells[1], which occupy a major part of the plaque in atherosclerotic lesions. We also examined the possibility of promotion of intracellular cholesterol export[2, 3] and the cell genesis[4] of the hippocampal dentate gyrus involved in memory by the exposure of wild-type mice in the magnetic field.

The specific subjects of this research are 1) effect of the magnetic field on the ABCA1-mediated cellular cholesterol export by apoA-I from foamed macrophages, which are major cells of atherosclerotic plaques, and 2) effect of the magnetic field on the newly generated cells observed in the dentate gyrus in hippocampus, which is involved in memory enhancement and is a site for neurosteroid production. This research is a new basic research to examine the effect of magnetic field using magnetic flux density from 0 to 400 mT generated by an EPR spectometer.

2. METHOD

1) Effect of magnetic field on ABCA1-mediated cell cholesterol export from mouse peritoneal foamed macrophage cells

All experimental procedures and laboratory animals used were approved by the Nagoya City University Laboratory Animal Safety Committee.

Preparation of mouse peritoneal macrophage cells

Incision of the abdominal skin of euthanized C57BL/6N mice was made to expose the peritoneal membrane. Injection of 10 mL/animal of PBS (filter sterilized) was made and, after 10 min, released cells in the abdominal cavity were collected using a clean syringe, followed by low-speed centrifugation, and were stored in a flask (Primaria) pre-coated for primary culture. The cells were cultured in RPMI1640 medium containing 20% FBS at 37 °C in 5% CO_2 incubator and, after 2 h, unbound cells were washed and transferred

into a medium containing acetylated-LDL and 0.2% BSA. After foaming the cells in the culture for 48 h, the cells were washed and cultured in 0.2% BSA-supplemented medium for another 24 h[5].

Measurement of ABCA1-dependent cellular cholesterol export and the effects of exposure in magnetic field

The culture flask was filled up to its lid with a CO_2-independent medium (Leibovitz's L-15) (Fuji Film Wako Pure Chemical Industries, Ltd.) containing 1-10 μg/mL of human apoA-I and 0.02% BSA to prevent cell detachment due to shaking vibration during the cultivation. Then, the cells were transferred to the research facility while keeping them warm (within 30 min), installed in the EPR device, and were exposed in the magnetic field. In Experiment 1 and Experiment 2, continuous exposure in 0.4 T for 2 h was performed twice. In Experiment 3, changing magnetic field that increase from 0 T and 0.4 T in 30 min, maintained for 30 min, and decrease in 30 min was applied three times (Fig. 1). Then, the medium was collected, and suspended cells were removed by centrifugation. Finally, the lyophilized powder was obtained.

Cells were stored at -30 °C. Lipids were extracted with an organic solvent, and cholesterol content was measured by an enzymatic reaction method (LabAssay ™ Cholesterol) (Fuji Film Wako Pure Chemical Industries, Ltd.).

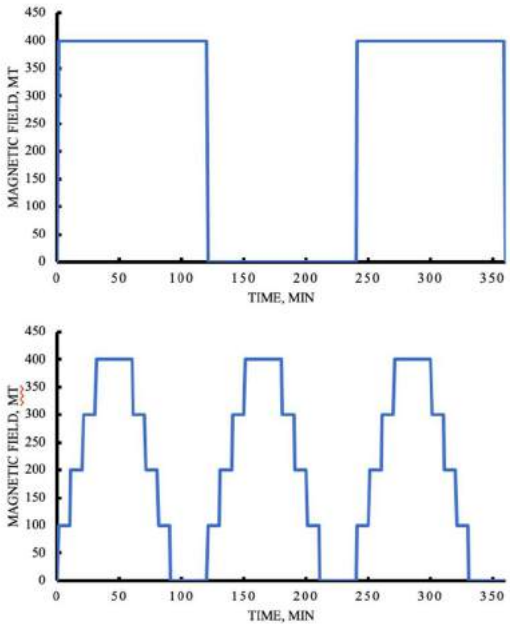

Fig 1. Magnetic field level during the treatment.
Upper panel indicates the magnetic field level for the Experiment 1 and 2. Lower panel indicates the magnetic field level condition for the Experiment 3.

2) Examination of the magnetic field effect on the ability to produce newborn cells in the hippocampus of living mice

Labeling of wild-type mouse with F-ara-EdU and exposure in magnetic field

C57BL/6N wild-type mice (8 weeks old) were anesthetized with isoflurane and (2'S)-2'-deoxy-2'-fluoro-5-ethynyluridine (F-ara-EdU) /PBS (133 μg/g mouse body weight) was administered intraperitoneally. The magnetic field exposure group mice were placed in separate small transport cardboard boxes (width 12 cm), placed in an EPR spectrometer, and exposed in a magnetic field (0.4 T) for 2 h. The control group mice were kept under the same conditions other than the magnetic field. Both group of mice were kept normal conditions for 4 weeks after the treatment.

Collection of serum, cerebrospinal fluid, liver and fixation of the brain from the treated mice

After euthanasia, blood was collected and perfused systemically with PBS+0.5 mM EDTA, and cerebrospinal fluid and liver fragments were collected. The brain was removed followed by fixation perfusion with 4% PFA/0.1 MPB. After the fixation for 24 h at 4 °C, and replacement in 30% sucrose / PBS were performed for 3 days and stored at -80 °C. A 40 μm thick section was prepared with a cryostat Leica CM1900. All sections were collected on a 24-well plate and allowed to stand at 4 °C in 1 mL of PBS, and after 24 h, PBS was replaced and sections were further washed.

Fluorescent labeling of brain sections and observation of F-ara-EdU using the Click Chemistry method

To avoid unfavorable adsorption, 1 mL of 3% BSA/TBS was placed in a 24-well plate and brain sections were transferred there using a small brush. Brain sections were transferred to wells containing 0.1% Triton X-100/TBS. Permeation was performed at room temperature for 20 min, the brain sections were transferred again to 1 mL of 3% BSA/TBS, then transferred into 2 mL of the same aqueous solution and

further washed. Then, the brain sections were transferred to a reaction solution (TBS containing Alexa-488 azide, copper and sodium ascorbate) and allowed to react at room temperature for 30 min. The brain sections were transferred to 2 mL in 3% BSA/TBS again and washed[6]. Then, they were transferred to 3% BSA/TBS containing Hoechst 33342 (Dojin Kagaku) and were kept at 4 °C for 24 h. A virtual slide image was created using a confocal super-resolution microscope Spin SR10 (Olympus) for the hippocampal dentate gyrus and the olfactory bulb region, and the image of the cells containing fluorescently-labeled chromosomes were observed using the OlyVIA application (Olympus).

Quantification of serum lipoprotein profile, amyloid β peptide, and related protein expression in the liver

Lipoprotein lipid analysis of serum was conducted using a gel filtration HPLC (Skylight Biotech Co., Ltd.) (LipoSEARCH™)[7]. Cerebrospinal fluid and serum amyloid β40 and 42 were quantified by ELISA Kit Wako measurement (Fuji Film Wako Pure Chemical Industries, Ltd.)[8] [9]. For the expression analyses of related proteins in the liver, total RNA was isolated by ISOGEN (Nippon Gene), and the first strand cDNA were prepared using random primers. They were used as a template. For the quantitative real-time PCR, StepOnePlus ™ real-time PCR system (Thermo Fisher) was used, and the PCR end product of each well was confirmed by melt curve analysis. A sequence containing an intron was used as the primer pair for the target gene[10].

Statistical analysis

For statistical analysis, the statistical function (t-test) equipped to Microsoft Excel was used.

3. RESULTS

Effect of magnetic field on cellular cholesterol export

In Experiment 1, in order to investigate the effect of the magnetic field on the cellular cholesterol export capacity of the ABCA1 transporter localized in the cell membrane of foamed macrophage cells, we examined the difference in the directions of flask installation against the magnetic field. A magnetic field was applied from the top of the cell in the direction of the culture

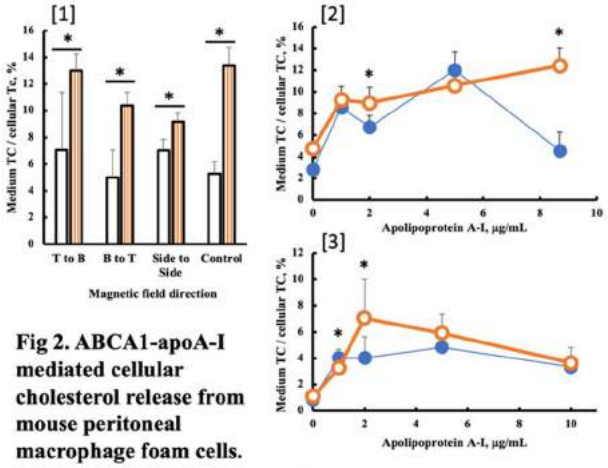

Fig 2. ABCA1-apoA-I mediated cellular cholesterol release from mouse peritoneal macrophage foam cells.

[1]; Experiment 1, Effect of magnetic field direction on cellular cholesterol efflux. Open bar; no apoA-I. Stripe bar; with apoA-I (6 μg/mL). [2]; Experiment 2, Dose dependent cholesterol efflux. Open circle; control cells, solid circles; magnetic field exposed cells. [3]; Experiment 3, Dose dependent cholesterol efflux. Open circle; control cells, solid circles; magnetic field exposed cells. *; Asterisks indicate statistic significance.

flask Top to Bottom (T to B), vice versa (B to T), and parallel to the flask adhesion surface (Side to side). Under all these conditions, addition of apo A-I caused the efflux of cellular cholesterol into the medium (Fig. 2 [1]). The control cells that were not exposed in the magnetic field showed the highest export of the cellular cholesterol. When a magnetic field was applied parallel to the surface of the culture flask, the export of cellular cholesterol was significantly reduced. In Experiment 2 (Fig. 2 [2]) and Experiment 3 (Fig. 2 [3]), the magnetic field was applied in vertical direction to the cells to evaluate the concentration-dependent cholesterol export upon addition of apo A-I. The results showed that the ABCA1-apoA-I-specific cellular cholesterol exports were reduced or unchanged by the exposure in the magnetic field of 0.4 T.

Changes in mouse serum lipoprotein profile and expression of related genes in the liver by exposure in a magnetic field

Wild-type mice exposed in the magnetic field of 0.4 T for 2 h were collected after normal breeding for 4 weeks, and their blood lipoproteins level were analyzed (Fig. 3). Control mice (Fig. 3, top) showed typical wild-type mouse lipoprotein patterns. In the mice exposed in the magnetic field (Fig. 3, bottom), followed by normal breeding of 4 weeks, showed a decrease in HDL cholesterol and an increase in VLDL triglyceride. Examinations of related genes in these mouse livers

revealed that the expression of HMGCoA reductase and

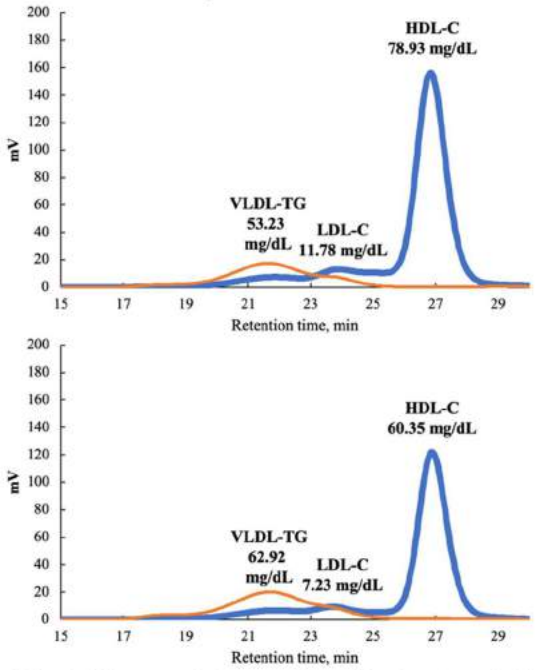

Fig 3. Lipoprotein profiles of mice treated with magnetic field. Upper panel indicates control wild type mice. Lower panel indicates mice exposed to 0.4 T magnetic field for 2 hours. Mice serum were harvested on the day 28. Bold line shows total cholesterol and thin line shows triacylglycerol level.

ABCA1 were significantly decreased against β-actin, whereas the expressions of apoA-I and SR-BI were significantly increased against GAPDH. However, for other house-keeping genes, there was no significant difference. On the other hand, the expression of PCSK9, which has the potency of degrading LDL receptors and activating T cells in atherosclerotic plaques[11, 12], was significantly reduced against both types of the house-

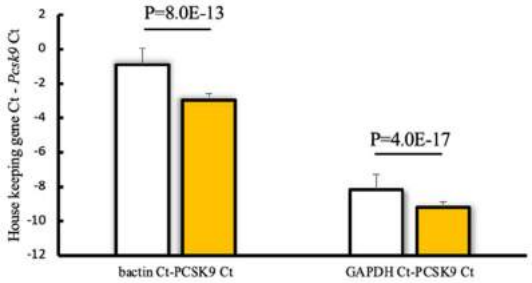

Fig 4. *Pcsk9* expression level in liver. Open column, control mice liver. Solid column, magnetic field treated, 0.4 T for 2 hrs, mice liver. Statistical significance were examined by two-tailed Student's-*t* test.

keeping genes in the magnetic field-exposed mice.

Changes in amyloid β40 and 42 in mouse cerebrospinal fluid and serum by exposure in the magnetic field

Figure 5 shows the quantitative results of the mouse cerebrospinal fluid and serum upon the magnetic field treatment. No significant difference was observed in the levels of amyloid β40 and amyloid β42 peptides.

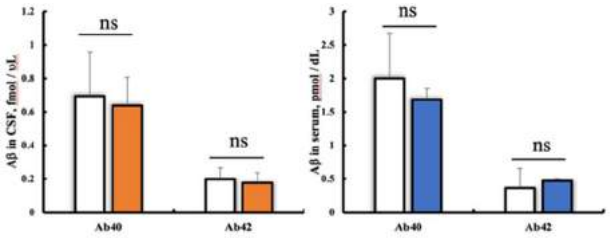

Fig 5. Amyloid-β level in cerebrospinal fluid and in serum. Open column, control mice biofluid. Solid column, magnetic field exposed, 0.4 T for 2 hrs, mice biofluid. ns; indicates no statistical significance.

Effect of the magnetic field on newborn cell-producing ability in living mouse hippocampus

The nucleic acid-modifying compound F-ara-EdU administered intraperitoneally in mice would be used for chromosome replication in neural stem cell division. The newly born cells incorporated with F-ara-EdU were fluorescently labeled on the 28th day. Then, the hippocampal dentate gyrus was observed and the number of the cells having a fluorescently-labeled nucleus was counted (Fig. 6). In control mice, 0 to 3 positive cells were found in the granular zone and in the subgranular zone of the hippocampal dentate gyrus. An

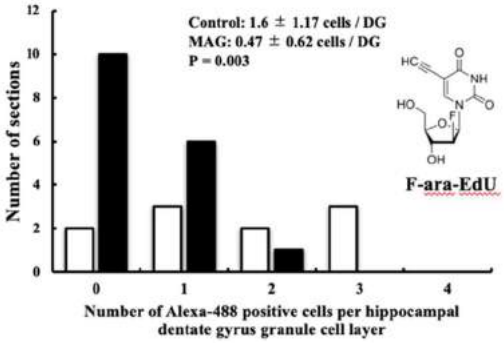

Fig 6. F-ara-EdU incorporated cells in hippocampal dentate gyrus. Open bar; control mice group. Solid bar; magnetic field treated mice group.

average of 1.6 cells per dentate gyrus in one slice could be detected as positive cells. In contrast, most hippocampal dentate gyrus prepared from the magnetic field exposed mouse group had 0 or 1 cells, with an average of 0.47 positive cells per hippocampal slice (P = 0.003). In the granule cell region of the central part of the olfactory bulb where newly generated cells are observed other than the hippocampal dentate gyrus, many positive cells were observed in both the control group and the magnetic field exposed group.

4. DISCUSSION

In this research, no substantial increase in cellular cholesterol export was observed for mouse peritoneal macrophage cells upon exposure in magnetic field. In addition, the lipoprotein profile in the blood of the mice exposed in a magnetic field of 0.4 T for 2 h showed a decrease in HDL cholesterol level even after 28 days. Our analyses on the gene expression in the liver showed a decrease in ABCA1 expression and an increase in SR-BI expression, which are involved in HDL assembly and metabolism. From these observations it was inferred that the mechanism is maintained by both the decrease in HDL new assembly by lowering of ABCA1 expression and the enhancement of HDL metabolism caused by increase in SR-BI. Decreased PCSK9 in the liver may be a phenomenon that promotes LDL cholesterol metabolism[13] by increasing LDL receptors in humans. Unfortunately, in mouse LDL, apoB48, which lacks a binding region to the LDL receptor, is also one of structural proteins of LDL[14], further detailed studies are needed to discuss about the LDL metabolism.

The functional relationship between brain HDL cholesterol and blood HDL cholesterol is still unclear due to the differences in the composition of their structural proteins[15]. On the other hand, the representative researcher of this project has reported tha the amount of apoA-I in the brain increases when blood HDL is high[8]. It is inferred that the amount of apoA-I in the brain becomes decreased by the decrease in blood HDL level in the current study. This observation may be related to the fact that the number of newly generated cells detected in the granular zone and the subgranular zone in the dentate gyrus of the hippocampus was significantly reduced in the mice subjected to the magnetic field treatment. In the future, it is necessary to investigate in detail whether these newborn cells are neuron or glial cells.

5. RESEARCH GRANTS / CONFLICT OF INTEREST

This research was carried out with the support and assistance of the Watanabe Foundation (Grant No. 01104), the Japan Health Development Foundation (FY2020), and the Nagoya City University Special Research Incentive Fund (Grant Decision No. 2050002).

There are no companies with COI relationships that the presenters should disclose in relation to this research.

REFERENCES

[1] Kruth, H. S. (2001) Macrophage foam cells and atherosclerosis, *Front Biosci 6*, D429-455.

[2] Yokoyama, S. (1998) Apolipoprotein-mediated cellular cholesterol efflux, *Biochim Biophys Acta 1392*, 1-15.

[3] Yokoyama, S. (2006) ABCA1 and biogenesis of HDL, *J Atheroscler Thromb 13*, 1-15.

[4] Matsumoto, M., Sawada, M., García-González, D., Herranz-Pérez, V., Ogino, T., Bang Nguyen, H., Quynh Thai, T., Narita, K., Kumamoto, N., Ugawa, S., Saito, Y., Takeda, S., Kaneko, N., Khodosevich, K., Monyer, H., García-Verdugo, J. M., Ohno, N., and Sawamoto, K. (2019) Dynamic Changes in Ultrastructure of the Primary Cilium in Migrating Neuroblasts in the Postnatal Brain, *J Neurosci 39*, 9967-9988.

[5] Tsujita, M., and Yokoyama, S. (1996) Selective inhibition of free apolipoprotein-mediated cellular lipid efflux by probucol, *Biochemistry 35*, 13011-13020.

[6] Neef, A. B., and Luedtke, N. W. (2011) Dynamic metabolic labeling of DNA in vivo with arabinosyl nucleosides, *Proc Natl Acad Sci U S A 108*, 20404-20409.

[7] Okazaki, M., and Yamashita, S. (2016) Recent Advances in Analytical Methods on Lipoprotein Subclasses: Calculation of Particle Numbers from Lipid Levels by Gel Permeation HPLC Using "Spherical Particle Model", *J Oleo Sci 65*, 265-282.

[8] Tsujita, M., Vaisman, B., Chengyu, L., Vickers, K. C., Okuhira, K. I., Braesch-Andersen, S., and Remaley, A. T. (2020) Apolipoprotein A-I in mouse cerebrospinal fluid derives from the liver and intestine via plasma high-density

lipoproteins assembled by ABCA1 and LCAT, *FEBS Lett*.

[9] Sano, O., Tsujita, M., Shimizu, Y., Kato, R., Kobayashi, A., Kioka, N., Remaley, A. T., Michikawa, M., Ueda, K., and Matsuo, M. (2016) ABCG1 and ABCG4 Suppress γ-Secretase Activity and Amyloid β Production, *PLoS One 11*, e0155400.

[10] Tsujita, M., Matsushita, S., and Takase, H. (2021) Modulation of lipoprotein profiles by the WAON treatment in mice, *Nihonkenkoukaihatsuzasshi 42*.

[11] Seidah, N. G., Awan, Z., Chrétien, M., and Mbikay, M. (2014) PCSK9: a key modulator of cardiovascular health, *Circ Res 114*, 1022-1036.

[12] Liu, A., and Frostegård, J. (2018) PCSK9 plays a novel immunological role in oxidized LDL-induced dendritic cell maturation and activation of T cells from human blood and atherosclerotic plaque, *J Intern Med*.

[13] Cohen, J., Pertsemlidis, A., Kotowski, I. K., Graham, R., Garcia, C. K., and Hobbs, H. H. (2005) Low LDL cholesterol in individuals of African descent resulting from frequent nonsense mutations in PCSK9, *Nat Genet 37*, 161-165.

[14] Yamanaka, S., Balestra, M. E., Ferrell, L. D., Fan, J., Arnold, K. S., Taylor, S., Taylor, J. M., and Innerarity, T. L. (1995) Apolipoprotein B mRNA-editing protein induces hepatocellular carcinoma and dysplasia in transgenic animals, *Proc Natl Acad Sci U S A 92*, 8483-8487.

[15] Hirsch-Reinshagen, V., Zhou, S., Burgess, B. L., Bernier, L., McIsaac, S. A., Chan, J. Y., Tansley, G. H., Cohn, J. S., Hayden, M. R., and Wellington, C. L. (2004) Deficiency of ABCA1 impairs apolipoprotein E metabolism in brain, *J Biol Chem 279*, 41197-41207.

Synthetic Biology Approach for Evaluating Magnetic Field Effects on DNA Photorepair Reactions

Yoshimi Oka

Promotion Research Institute, Oita University
700 Dannoharu, Oita-city, Oita 870-1192 Japan

Abstract

Geomagnetic field, along with water and air, is an environmental factor that affects human health. The aim of this study was to evaluate the effect of weak magnetic field on flavin-mediated DNA. The generation of radical pair between flavin and guanine (G) in DNA oligomer upon irradiation with blue light were observed by time-resolved electron spin resonance (TREPR) spectroscopy. The TREPR result can be evaluated as a direct observation for the oxidation of G, which is the initial intermediate in oxidative damage of DNA.

Keywords: radical pair, DNA, flavin, blue light, weak magnetic field

1. PURPOSE

Recently, it has been strongly suggested that cryptochrome, a blue-light photoreceptor protein, may act as a magnetic compass for migratory birds.[1)–4)] The reaction mechanism is presumed to be that when flavin adenine dinucleotide (FAD) in the cryptochrome is irradiated by blue light, electron transfer occurs from an amino acid (tryptophan, Trp), and the resulting radical pair can be detected as a reaction efficiency even in weak magnetic field. Similarly, in photolyase, a family of flavoprotein, it has been reported that the electron transfer reaction from Trp to FAD by blue light irradiation is affected by magnetic field.[2)] An important function of photolyase is to revert the dimer, generated between neighboring bases in DNA duplexes by UV light, to a monomer, and it is not clear whether the magnetic field effect is involved in this DNA repair. Furthermore, guanine (G) is the most readily oxidized base and the putative initial intermediate in the oxidative cleavage of DNA, which is also induced by visible light through dyes such as flavin.[5)] However, the possibility of magnetic field effects on the reaction has not been studied.

Geomagnetic field, along with water and air, is an environmental factor that affects human health. The aim of this study was to evaluate the effect of weak magnetic field on flavin-mediated DNA. In the process of constructing the target DNA, the generation of radical pairs between flavin and G upon irradiation with blue light were observed. The first step in this research was to focus on this point.

2. METHOD

A new flavin derivative with a relatively hydrophilic carboxylic acid structure was synthesized using water-soluble riboflavin and glutaric anhydride as starting materials, and then obtained DNA oligomers consisting of 11 bases linked by an amide bond to an amino group modified via a linker at the 3'-end. The oligomer containing G at the third base from the 3'-end (**DNA1**) and the oligomer with G replaced by inosine (**DNA1'**) were used for comparison. DNA oligomers (**DNA2**) and unmodified oligomers (**DNA2'**) were obtained by amide linkage of a modified amino group

and 3-indolepropionic acid (Trp derivative) at the 5'-end. The melting temperatures of the above DNA duplexes were determined by differential scanning calorimetry (DSC). X-band time-resolved electron spin resonance (TREPR) measurements were performed after irradiation with nanosecond laser pulses (excitation wavelength 450 nm, laser power ~2 mJ, repetition rate 30 Hz). DNA concentration of 50 μM in 10% DMSO solution was used for the measurement.

3. RESULTS

From the DSC results, it was confirmed that the DNA duplex was maintained up to room temperature (Tm ≥ 25 °C) even in the case of Inosine-substituted DNA. TREPR measurements at 5 °C displayed (1) a spin-polarized signal in the magnetic field region around 344 mT after photoexcitation of a single-stranded DNA, **DNA1** , as shown in Figure 1 (E: emission, A: absorption). (2) The similar polarized signal was observed for the DNA duplex, **DNA1**/**DNA2'**. (3) No polarized signal was observed for a single-stranded DNA, **DNA1'**. (4) Similarly, no polarized signal was observed in the DNA duplex, **DNA1'/DNA2'**. However, (5) the signal of the **DNA1** was canceled by forming the duplex DNA with **DNA2** (**DNA1/DNA2**).

4. DISCUSSION

From the comparison of (1) and (3), a flavin–G radical pair was generated in the flavin-modified DNA strand. The E/E/A/A polarization pattern is similar to that reported for the flavin–Trp radical pair in cryptochrome,[6] suggesting the formation of the flavin–G spin-correlated radical pair via the singlet precursor. When the third G base from the 3'-end was substituted by inosine, the polarized signal from the radical pair was no longer observed, confirming that the third G base is essential for the initiation of the electron transfer reaction with flavin. This TREPR result can be evaluated as a direct observation for the oxidation of G, which is the initial intermediate in oxidative damage of DNA.

In (4), the formation of an interstranded flavin–Trp radical pair was expected, but this was not captured by the TREPR measurements. However, the comparison of (1) and (2) with (5) suggests that the contribution of intermolecular indole unit is present, which can be interpreted as an effect of suppressing the oxidation of G.

Since the photoinduced electron transfer reaction between flavin and G follows the similar mechanism as that of cryptochrome, in principle, a weak magnetic field should also affect this reaction. The effect of magnetic field on the DNA repair reaction of photolyase will also be investigated. This approach to the evaluation of the effects of weak magnetic fields on DNA is expected to contribute to the development of health science and medical technology.

ACKNOWLEDGEMENT

This work was supported by the 26th Research Grant from the Watanabe Foundation. DSC and TR-ESR measurements were conducted in Instrument Center, Inst. Mol. Sci. Okazaki, supported by Nanotechnology Platform Program <Molecule and Material Synthesis> of the Ministry of Education, Culture, Sports, Science and Technology (MEXT), Japan.

Part of this study will be reported at the "15th Annual Meeting of Japan Society for Molecular Science" held in Hokkaido in September.

REFERENCES

1) Schulten, K., Swenberg, C. E., Weller, A. A biomagnetic sensory mechanism based on magnetic field modulated coherent electron spin motion. *Z. Phys. Chem.* **111**, 1–5 (1978).
2) Maeda K., Robinson, A. J., Timmel, C. R., Hore, P. J. *et al.* Magnetically sensitive light-induced reactions in cryptochrome are consistent with its proposed role as a magnetoreceptor. *Proc. Natl. Acad. Sci. USA* **109**, 4774–4779 (2012).
3) Ritz, T., Wiltschko, R., Hore, P. J. *et al.* Magnetic compass of birds is based on a molecule with optimal directional sensitivity. *Biophys. J.* **96**,

3451–3457 (2009).

4) Wiltschko, R., *et al.* Magnetoreception in birds: II. Behavioural experiments concerning the cryptochrome cycle. *J. Exp. Biol.* **217**, 4225–4228 (2014).
5) Wenninger, M., Carell, T. *et al.* Flavin-induced DNA photooxidation and charge movement probed by ultrafast transient absorption spectroscopy *ChemBioChem* **12**, 703–706 (2011).
6) Weber, S. *et al.* Origin of light-induced spin-correlated radical pairs in cryptochrome. *J. Phys. Chem. B* **114**, 14745–14754 (2010).

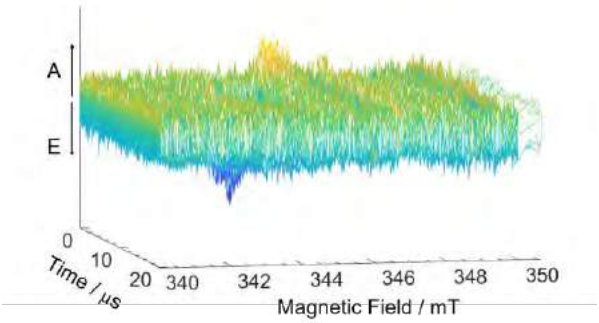

Fig. 1 TREPR spectrum of DNA oligomer containing flavin moiety and G bases.

Investigation of magnetic field effects on the recognition ability of cell membrane ~From cell therapy to separation tool~

Yukihiro Okamoto

Graduate School of Engineering Science Osaka University
1-3 Machikaneyama-cho, Toyonaka, Osaka 560-8531, Japan

Abstract

This report summarizes our research results on the effect of magnetic field on various lipid membrane. We prepared spherical and disk like lipid membrane, and then analyzed their specific properties. Based on obtained data, the effect of magnetic field was evaluated in the respect of lipid membrane properties and the reaction with lipid membrane. As a result, the magnetic field affected some lipid membrane properties, even if weak magnetic field, and enhanced the antioxidative effect. Thus, our results imply that the magnetic field affects cell membrane properties and also cell activity.

Keywords: magnetic field, lipid membrane, lipid membrane property, structure

1. PURPOSE

Much research studied about the effect of magnetic field on cell function. On the other hand, there is not so much about the magnetic field effect on the cell functionality, focusing on the magnetic field effect on cell membrane itself. Cell membrane plays the role not only as barrier but molecular recognition. This molecular recognition relates to immunity and signal transduction. Thus, if the effect of magnetic field on molecular recognition is clarified, it will be helpful for clarification of its effect on the cell function. In addition, the study about magnetic field effect on the cell membrane can be applied to liposomes, which mimic cell membrane. Therefore, the performance of liposomes as DDS carrier can be expected to be enhanced by magnetic field application.

This research purpose is to clarify the magnetic field effect on lipid membrane itself by preparation of various structured lipid membrane in various composition. Especially, during this research period, the magnetic field effect on lipid membrane properties was analyzed before and after application. Furthermore, as the application research, antioxidation by liposome containing antioxidants was evaluated with and without magnetic field.

2. METHOD

Preparation of lipid membrane: Following liposomes were prepared according to our reported paper.[1)] Briefly, the thin membrane of 1,2-dioleoyl-*sn*-glycero-3-phosphocholine (DOPC), 1-palmitoyl-2-oleoyl-glycero-3-phosphocholine (POPC), 1,2-dipalmitoyl-*sn*-glycero-3-phosphocholine (DPPC), 1,2-diauroyl-*sn*-glycero-3- phosphocholine (DLPC) were prepared and hydrated with ultrapure water. These liposomes were frozen, thawed, and extruded with 100 nm membrane. Fatty acid-dendrimer molecules were synthesized according to our reported paper. [2)]

Analysis of lipid membrane: The lipid membrane was analyzed by following methods: The fluidity and polarity of lipid membrane, fluorescence spectroscopy with fluorescent probes; the size of lipid membrane, dynamic light scattering method (DLS); the variation of phase transition temperature, differential scanning calorimetry (DSC); the packing of lipid molecules,

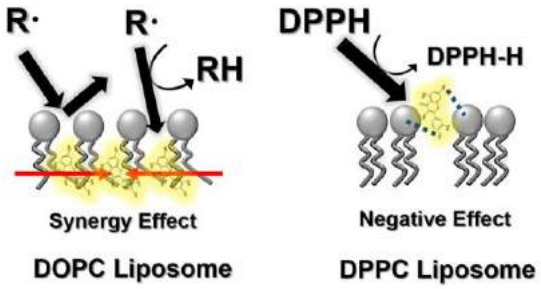

Fig.1 Clarified mechanism of antioxidation by quercetin containing liposomes.

Raman spectroscopy; the distribution coefficient of antioxidants into lipid membrane, UV spectroscopy and second derivative UV spectroscopy. These analysis methods were applied to each lipid membrane before and after the application of magnetic field. The magnetic field was applied with neodymium magnets.

3.RESULTS and DISCUSSION

To evaluate the effect of magnetic field effect on the anti-oxidation, at first, the lipid membrane properties were analyzed before and after the antioxidant (quercetin) was inserted into lipid membrane (**Fig.1**). The distribution coefficient and location of quercetin (antioxidant) was largely different in saturated and unsaturated liposomes. About DPPH radical scavenging assay, even if liposomes contained quercetin, its radical scavenging ability was almost same as that of quercetin in the aqueous solution. By applying the magnetic field, the DPPH radical scavenging ability in some liposome was enhanced. This would be due to deformation and change of membrane properties. Furthermore, the peroxidation of unsaturated lipid could be prevented by quercetin insertion. Based on these result, the enhancement of antioxidation by magnetic field is investigating now for application of liposomes as DDS carrier.

The lipid membrane with dendrimers can be expected to increase the drug loading efficiency and uptake ratio by cells. Therefore, fatty acid conjugated dendrimers were successfully synthesized and applied for liposome preparation. By changing the generation of dendrimers and composition ratio of fatty acid

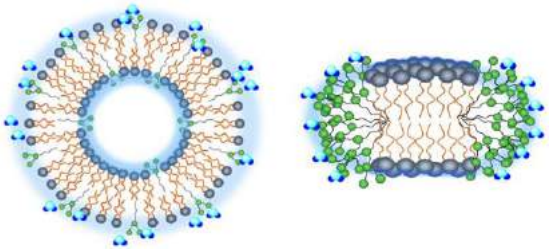

Fig.2 Illustration of self-assembled structures by fatty acid dendrimer/phospholipids.

dendrimers/phospholipids in the lipid membrane, the lipid membrane structures varied from spherical to disk like one (**Fig.2**). The prepared structures kept bilayer and showed more hydrophilic in the surface region in some composition. It is reported that the disk like lipid membrane aligns and is oriented to magnetic field. Therefore, now, the magnetic responsibility of prepared disk like membrane is investigated for fundamental research and application.

Finally, the magnetic field effect on the lipid membrane was investigated with different chemical structure lipids. As a result, some liposomes showed variation of membrane properties after the application of magnetic field. Furthermore, the molecular recognition ability of these liposomes was altered after magnetic field application. Therefore, now, from the viewpoint of lipid molecular and lipid membrane properties, this alteration is studying to clarify the magnetic field effect.

From these results, though these are preliminary one, it can be implied that magnetic field can affect the cell membrane itself and cell activity by changing membrane properties. In addition, as we reported, the combination of lipid membrane coated nanoparticles and magnetic field will be big potential for biomedical application[3)].

Acknowledgement

Y.O deeply acknowledge Watanabe Foundation to perform these research.

Some parts of this report were reported in Membrane Symposium held on 2020/11/12-13 via Internet.

References

1) Jin Han, Misaki Amau, Yukihiro Okamoto, Keishi Suga, Hiroshi Umakoshi; *J. Biosci. Bioeng.*,in press.
2) Jin Han, Yosuke Iimure, Yukihiro Okamoto, Keishi Suga, Hiroshi Umakoshi: Chemistry Letters, **50**, 187-190 (2021).
3) Miftah Faried, Seiya Ando, Keishi Suga, Yukihiro Okamoto, Hiroshi Umakoshi: *Chemistry Letters,* **49**(9), 1107-1110 (2020)

Analysis of bone formation by magnetic field using fish scales (bone model): Elucidation of a new mechanism by eddy currents

Nobuo Suzuki*, Sotoshi Yamada**, Jun Hirayama***, Yoshiaki Tabuchi****
and Makiko Kakikawa*****

*Noto Marine Laboratory, Institute of Nature and Environmental Technology, Kanazawa University, 4-1, Ogi, Noto-cho, Ishikawa 927-0553, Japan

**Faculty of Production Systems Engineering and Sciences, Komatsu University, 1-3, Shicho-machi, Komatsu-city, Ishikawa 923-8511, Japan

***Faculty of Health Sciences, Komatsu University, 14-1, Mukaihon-ori-machi, Komatsu-city, Ishikawa 923-0961, Japan

**** Life Science Research Center, University of Toyama, 2630 Sugitani, Toyama-city, Toyama 930-0194, Japan

***** Institute of Science and Engineering, Kanazawa University, Kakuma-machi, Kanazawa-city, Ishikawa 920-1192, Japan

Abstract

The purpose of this study is to analyze bone formation caused by eddy currents. A culture system has been developed with fish scales in which osteoblasts and osteoclasts coexist on calcified bone matrix protein. In the present study, we examined the effect of extremely low–frequency (ELF) magnetic fields that generate eddy currents for bone formation using cultured fish scales. The static magnetic fields changed neither osteoblastic or osteoclastic activity. However, ELF magnetic fields increased the activities of both osteoblasts and osteoclasts. Therefore, we noted eddy currents generated by ELF magnetic fields. We found that a large amount of eddy currents function to activate both osteoblasts and osteoclasts. This indicates that eddy currents may be related to the activation of both osteoblasts and osteoclasts. On the basis of our present data, we will develop an apparatus for bone therapy with ELF magnetic fields in the future.

Keywords: eddy currents, osteoblasts, osteoclasts, fish scales

1. PURPOSE

It has been known that a magnetic field acts on bone tissue to promote bone formation. However, many points about the mechanism that promotes bone formation are unclear. Due to the lack of an *in vitro* model system that can examine bone formation in detail, research is currently underway. Human bone is composed of osteoblasts (bone formation cells), osteoclasts (bone resorption cells), and bone matrix, including collagen, osteocalcin, and hydroxyapatite. In particular, the bone matrix plays an important role in the response to physical stimuli such as magnetic fields and gravity. It is necessary to co-cultivate all of these components, but such co-cultivation is difficult, and an excellent *in vitro* culture system is eagerly desired.

In order to develop a therapeutic drug for bone

diseases such as osteoporosis, a large investment of time and money is currently underway, using rats from which the ovaries have been removed and whose bones are easily broken. If bone diseases can be treated by physical stimulation, such as by a magnetic field, there would be no need to purchase expensive medicine, and there would be no side effects, which is especially suitable for elderly people.

On the other hand, we focused on the fact that osteoblasts, osteoclasts, and bone matrix proteins coexist in fish scales (Fig. 1). Using fish scales with these characteristics, we have developed an *in vitro* scale culture system as a model for human bones.[1–3)]

In the present study, we compared the action on extremely low–frequency (ELF) magnetic fields (60 Hz) where eddy currents are generated with the action on static magnetic fields where eddy currents are not generated using an *in vitro* culture system for goldfish scales. Furthermore, the effects of different amounts of eddy currents on osteoblasts and osteoclasts were analyzed in the cultured goldfish scales. Additionally, in order to confirm the results obtained by using goldfish scales, we investigated the influence of ELF magnetic fields (60 Hz) on osteoblasts and osteoclasts using the cultured scales of zebrafish.

2. Methods

Goldfish (*Carassius auratus*) was anesthetized with ethyl 3-aminobenzoate, methanesulfonic acid salt, and the scales were taken from the bodies of goldfish under anesthesia and placed in a 2 ml tube. Next, we added 500 µl of medium containing HEPES (20 mM) (pH 7.0) and antibiotics (1%) into the tube. The tube was exposed to ELF magnetic fields (60 Hz) or static magnetic fields using a permanent magnet at 15°C for 24 hours. The effects of ELF magnetic fields and static magnetic fields on both osteoblast and osteoclast activities were investigated. In the present study, tartaric acid-resistant acid phosphatase was used as an index of osteoclastic activity, alkaline phosphatase was used as an index of osteoblastic activity,[1–3)] and the effect of magnetic fields on bone tissue was investigated.

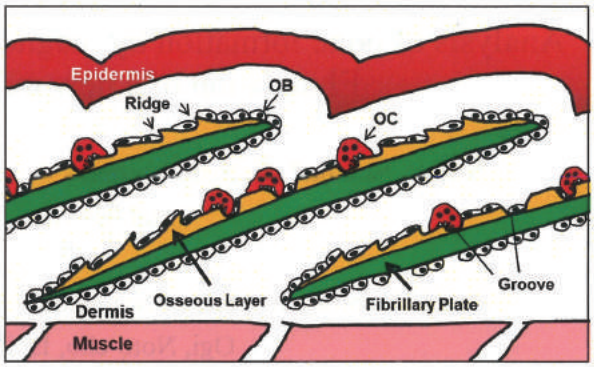

Figure 1 Schema of fish scales
Bone-formation cells (osteoblasts) and bone-resorption cells (osteoclasts) coexist in fish scales. Fish scales can be utilized as a human bone model.

The scales were removed from the goldfish under anesthesia, they were placed in equipment (Fig. 2) made by a 3D printer, and the equipment was exposed to ELF magnetic fields (3 mT) of 60 Hz. Since the scales were placed in holes with different diameters, a larger eddy current flowed through the scales in the holes with a larger diameter as compared to the scales in holes with smaller diameters. We investigated changes in both the activities of osteoblasts and osteoclasts due to the difference in these eddy currents.

Furthermore, the scales of zebrafish were exposed to ELF magnetic fields (60 Hz, 30 mT), and the responses were compared with the scales of goldfish. The scales of the activities of both osteoblasts and osteoclasts in zebrafish were measured according to the example of Suzuki et al. (2016).[4)]

3. Results

Exposure to ELF magnetic fields (60 Hz, 30 mT) for 24 hours revealed a significant increase in both osteoblastic and osteoclastic activities. However, exposure to static magnetic fields (30 mT) for 24 hours did not significantly change neither osteoblastic or osteoclastic activity.

Next, the scales were placed in holes of different diameters, and different amounts of eddy currents were applied. As a result, it was found that the activities of both osteoblasts and osteoclasts increased in the larger holes. On the other hand, this phenomenon did not

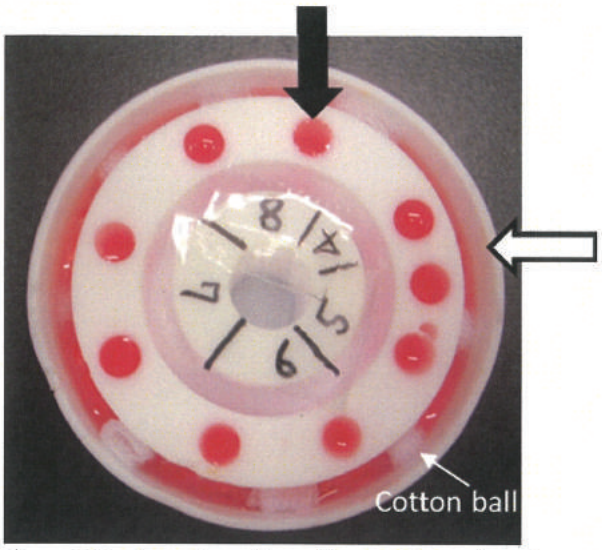

Figure 2 Equipment used for eddy current experiments
Experiments were conducted by inserting scales into the holes indicated by the black and white arrows. Cotton balls were used to partition the scales of each individual.

occur in the smaller holes. It was found that a hole with a large diameter induces a change similar to that of 30 mT, despite the fact that the strength of ELF magnetic fields was 3 mT.

In order to confirm the obtained results by using goldfish scales, we investigated the influence of ELF magnetic fields (60 Hz) on osteoblasts and osteoclasts using the cultured scales of zebrafish. We found that both osteoblasts and osteoclasts in the scales of zebrafish were activated by ELF magnetic fields of 30 mT, as in goldfish scales.

4. DISCUSSION

Our study revealed that both osteoblasts and osteoclasts responded differently to ELF and static magnetic fields, even when exposed to magnetic fields of the same intensity. This difference in response is likely due to differences in eddy currents. Next, scales were placed in holes with different diameters to allow different amounts of eddy currents to flow (Fig. 2). As a result, it was found that when the scales were put into a hole with a large diameter, a similar change to 30 mT was induced, even though the strength of ELF magnetic fields was 3 mT. Therefore, in order to activate both osteoblasts and osteoclasts and promote bone formation, it is important to apply a larger eddy current rather than to increase the magnetic field strength.

On the other hand, the results obtained with the scales of goldfish can be reproduced with the scales of zebrafish. We found that both osteoblasts and osteoclasts in zebrafish scales are activated by ELF magnetic fields of 30 mT. In the future, we plan to examine the effects of eddy currents on both osteoblasts and osteoclasts in detail by *in vivo* experiments using zebrafish.

ACKNOWLEDGEMENT

This study was supported by the Magnetic Health Science Foundation.

REFERENCES

1) Suzuki, N., Suzuki, T. and Kurokawa, T.: Suppression of osteoclastic activities by calcitonin in the scales of goldfish (freshwater teleost) and nibbler (seawater teleost). *Peptides*, **21**, 115-124 (2000)
2) Suzuki, N. and Hattori, A.: Melatonin suppresses osteoclastic and osteoblastic activities in the scales of goldfish. *J. Pineal Res.*, **33**, 253-258 (2002).
3) Suzuki, N., Somei, M., Seki, A., Reiter, R.J. and Hattori, A.: Novel bromomelatonin derivatives as potentially effective drugs to treat bone diseases. *J. Pineal Res.*, **45**, 229-234 (2008).
4) Suzuki, N., Hanmoto, T., Yano, S., Furusawa, Y., Ikegame, M., Tabuchi, Y., Kondo, T., Kitamura, K., Endo, M., Yamamoto, T., Sekiguchi, T., Urata, M., Mikuni-Takagaki, Y. and Hattori, A.: Low-intensity pulsed ultrasound induces apoptosis in osteoclasts: Fish scales are a suitable model for analysis of bone metabolism by ultrasound. *Comp. Biochem. Physiol. Part A*, **195**, 26-31 (2016).

Three-dimensional neuronal magnetic field measurement for the study of thermosensation of *C. elegans* worms

Masazumi Fujiwara*, Eriko Kage-Nakadai**

*Graduate School of Science, Osaka City University
3-3-138 Sugimoto, Sumiyoshi-ku, Osaka 558-8585 Japan
**Graduate School of Human Life Science, Osaka City University,
Sumiyoshi-ku, Osaka 558-8585, Japan.

Abstract

The purpose of this research is to develop a real-time three-dimensional vector magnetic field imaging system that can simultaneously measure the temperature under the microscope. Such a measurement system may probe thermo-sensitive neuronal cells of *C. elegans*, one of the best studied multicellular model organism. By heating the neurons with laser, the action potential of cells can be measured via generated magnetic field, which allows for the precise temperature measurement at the same time. With the magnetic information and temperature information of neuron activities, we will quantify the activity of the neural network of *C. elegans*. To achieve this ultimate goal, we developed an artifact-free temperature method in diamond quantum thermometry. We also tried to label *C. elegans* with fluorescent nanodiamonds.

Keywords: *C. elegans*, nanodiamond, nanothermometry, nanomagnetometry

1. Introduction

Fluorescent nanodiamonds (NDs) are bright and stable fluorescent probes. They are non-toxic and can be introduced in cells and organisms for bioimaging[1]. Further, it has been recently reported that NDs can sense magnetic fields and temperature via the quantum control/measurement of electron spins of nitrogen vacancy (NV) emission centers[2]. In this NV-based quantum sensing, electron spin resonance driven by microwave irradiation can be detected by a change in fluorescence intensity and this resonance frequency is dependent on magnetic field and temperature with a different dependency. Therefore, simultaneous sensing of magnetic fields and temperature is possible in principle. Recently, we have reported applications of this NV-based temperature sensing to evaluate stem cell regeneration function[3] and to the real-time temperature probing in nematode *C. elegans*[4]. Regarding magnetometry, the NV sensor has demonstrated the detection of action potential when the squid axon is activated[5].

By using this multimodal measurement technology of temperature and magnetic filed, it is expected to obtain active biological information. For example, it can probe the thermosensation of neural network of nematodes. In *C. elegans*, thermotaxis has been actively studied[6] and discussed with its fully clarified connectome[7]. However, it has not been clear how much each of neurons spatiotemporally interact one another. The quantitative understanding of neural network is yet to be obtained.

The purpose of this study is to extend our real-time *in vivo* temperature measurement technique to visualize the three-dimensional temperature mapping of the entire nematode at the single cell level. In particular, we have studied the following two issues. (1) Developing a technique to improve the accuracy of

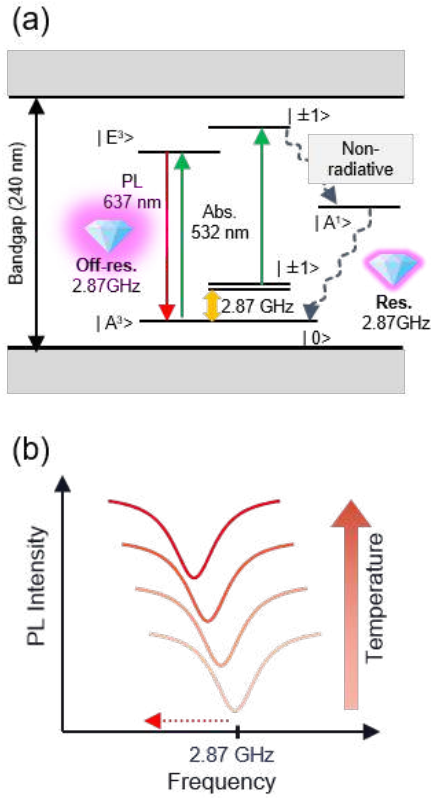

Fig. 1: (a) Schematic of ODMR with NV energy diagram. (b) Schematic of temperature dependent ODMR shift.

temperature measurement in real time *in vivo* where the light transmittance frequently varies. (2) Establishing a protocol to label worms with fluorescent NDs without microinjection.

2. Experiments

The NV-based quantum thermometry utilizes temperature dependence of resonance frequency of ODMR (Figs. 1 (a) and 1 (b)). The simplest way for measuring the ODMR shift is to perform spectral fitting to determine the center frequency. However, this method requires a long measurement time and high measurement accuracy cannot be obtained in a realistic measurement time of seconds. We therefore introduced multipoint ODMR method that measures the fluorescence intensity at four frequency points on the spectrum[8]. Regarding the ND labeling of *C. elegans*, the surface charge state of polyglycerol-grafted fluorescent NDs (PG-ND) was controlled and fed to *C. elegans*.

3. Results and Discussion

Figure 2a shows the temperature measurement profiles of NV sensors when the excitation laser light intensity is intentionally changed while the temperature is kept at 37 °C. An artifact in which the temperature indicates changed even though the temperature was not changed was observed. Detailed measurements of the excitation light intensity dependence of the ODMR spectral shape in separate experiments revealed this origin as a complex effect of electron spin relaxation time and spin mixing between the NV spin sublevels. This artifact can be evaluated in advance of the measurements; it can be removed numerically. The result of applying this numerical filter is shown in Fig. 2 (a). Stable temperature measurement is now possible even under the light intensity change.

For the ND labeling of *C. elegans*, the surface of PG-ND was modified with -COOH and -NH_2 in the manner reported previously[9]. These two types of functional groups make the surface negative and positive, respectively, and it has been reported such surface charge control affects cellular uptake efficiency *in vitro* experiments. These two types of NDs were fed to *C. elegans*. Figure 2 (b) is a fluorescence microscopy image of *C. elegans* fed with the ND-COOH, in which red indicates NDs and blue autofluorescence. Fluorescent NDs were confirmed in the intestinal tract, but it seems there is no ND uptake from intestinal cells. We also found that the 50-nm-sized NDs were too dim to be detected in adult worms because of the worm's background fluorescence in the red region. For the ND-NH_2 having positive charge surface, aggregation of the nanoparticles occurred when it was dispersed in the nematode culture medium at the time of feeding. Currently, we are searching for appropriate conditions to solve this. There is a report that *E. coli*, food for nematodes, aggregates positively charged nanoparticles, which might be the reason of aggregation.

Acknowledgements

The surface treated PG-NDs were supplied from Prof. Naoki Komatsu at Kyoto University. This research is in part supported by Watanabe Foundation and JSPS-KAKENHI (No. 20H00335).

References

1. Masfer H. Alkahtani, Fahad Alghannam, Linkun Jiang, Abdulrahman Almethen, Arfaan A. Rampersaud, Robert Brick, Carmen L. Gomes, Marlan O. Scully and Philip R. Hemmer, *Nanophotonics* **7**, 1423 (2018).
2. Romana Schirhagl, Kevin Chang, Michael Loretz, and Christian L. Degen, *Annu. Rev. Phys. Chem.* **65**, 83 (2014).
3. Hiroshi Yukawa, Masazumi Fujiwara, Kaori Kobayashi, Yuka Kumon, Kazu Miyaji, Yushi Nishimura, Keisuke Oshimi, Yumi Umehara, Yoshio Teki, Takayuki Iwasaki, Mutsuko Hatano, Hideki Hashimoto and Yoshinobu Baba, *Nanoscale Adv.* **2**, 1859-1868 (2020).
4. Masazumi Fujiwara, Simo Sun, Alexander Dohms, Yushi Nishimura, Ken Suto, Yuka Takezawa, Keisuke Oshimi, Li Zhao, Nikola Sadzak, Yumi Umehara, Yoshio Teki, Naoki Komatsu, Oliver Benson, Yutaka Shikano, and Eriko Kage-Nakadai, *Sci. Adv.* **6**, eaba9636 (2020).
5. John F. Barry, Matthew J. Turner, Jennifer M. Schloss, David R. Glenn, Yuyu Song, Mikhail D. Lukin, Hongkun Park, and Ronald L. Walsworth, *Proc. Natl. Acad. Sci. U.S.A.* **113**, 14133 (2016).
6. Tsubasa Kimata, Hiroyuki Sasakura, Noriyuki Ohnishi, Nana Nishio, and Ikue Mori, *Worm* **1**, 31 (2012).
7. Steven J. Cook, Travis A. Jarrell, Christopher A. Brittin, Yi Wang, Adam E. Bloniarz, Maksim A. Yakovlev, Ken C. Q. Nguyen, Leo T.-H. Tang, Emily A. Bayer, Janet S. Duerr, Hannes E. Bülow, Oliver Hobert, David H. Hall & Scott W. Emmons, *Nature* **571**, 63 (2019).
8. Masazumi Fujiwara, Alexander Dohms, Ken Suto, Yushi Nishimura, Keisuke Oshimi, Yoshio Teki, Kai Cai, Oliver Benson, and Yutaka Shikano, *Phys. Rev. Research* **2**, 043415 (2020).
9. Yajuan Zou, and Naoki Komatsu, *Carbon* **163**, 395 (2020).

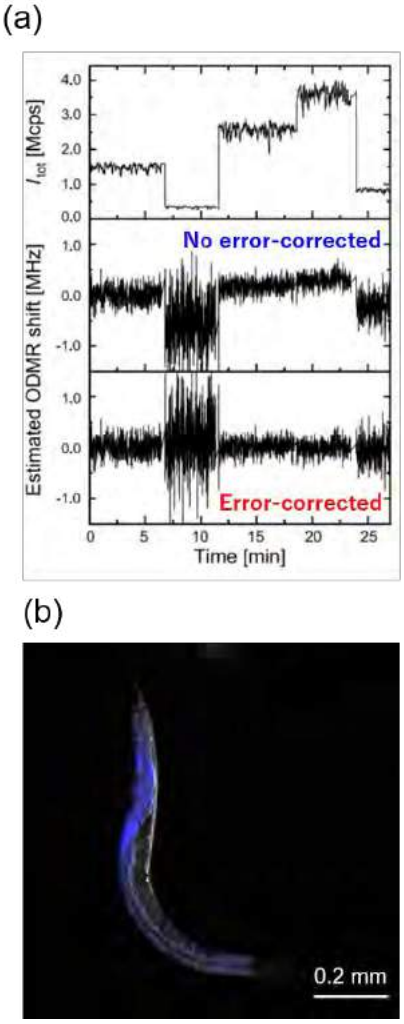

Fig. 2: (a) Temperature indicate profile under intentional changes of laser power, Fluorescence intensity (top), estimated ODMR shift without error-correction (middle), and with error-correction (bottom). (b) Fluorescence microscopy image of ND-labeled *C. elegans* worm (blue: autofluorescence, red: ND, gray: bright-field image).

Development of the high frequency pulse magnetic fields generator for medical applications

Atom Hamasaki

*Faculty of Science, Shinshu University
3-1-1 Asahi, Matsumoto, Nagano 390-8621 Japan

Abstract

An oscillating strong magnetic field can be easily generated compared to the conventional magnetic field generation using an AC power supply by using a pulsed magnetic field. Increasing of the generated magnetic field intensity leads to an increase in the efficiency of heat generation, which can shorten the treatment time. In this study, an oscillating pulsed magnetic field of 3 kHz was generated with a simple circuit and relatively low energy, and heat generation in an aluminum block was observed.

Keywords: oscillating strong magnetic field, pulsed magnet, heat generation

1. PURPOSE

Recently, there has been an increase in the number of therapies using pulsed magnetic fields, such as transcranial magnetic stimulation and hyperthermia. Among them, hyperthermia is a treatment method that selectively heats and kills cells by induction heating with a magnetic field. It has been attracting attention because it reduces the burden on the patient as it can be treated without contact, taking advantage of the characteristics of magnetic fields that penetrate deep into the body. However, there are some problems such as insufficient heating of the affected area by the magnetic field. One of the reasons for this is that the magnetic field strength in the affected area is insufficient. In order to output a high magnetic field strength, the conventional method requires a large power supply, which requires excessive installation space and high installation cost, which may hinder the spread of the system. Therefore, we proposed a method of heating magnetic particles using a pulsed magnetic field instead of using a general AC power supply. In this study, a system that generates an oscillating magnetic field was created, and the characteristics of the generated magnetic field were investigated.

2. METHOD

The circuit diagram of the designed and fabricated pulse magnet system is shown in Figure 1. The system can be divided into a charging circuit, an energy storage circuit, a discharging circuit, and a control circuit. To generate an oscillating magnetic field, the clover circuit was eliminated from the conventional circuit and a diode was installed in the opposite direction to the thyristor; the picture in Figure 2 shows the parts other than the storage facility and discharge switch, which are simple compared to the circuit of an AC power supply. A search coil was used to measure the induced electromotive force generated by the device and to measure the magnetic field strength generated in the coil. The coils were prepared with different shapes in terms of number of turns, wire thickness, and diameter to study the effect of the oscillating magnetic field due to the different shapes of the coils. The temperature change when the magnetic field was generated by placing an aluminum sample with a thermocouple inserted in the diameter of the coil was also investigated.

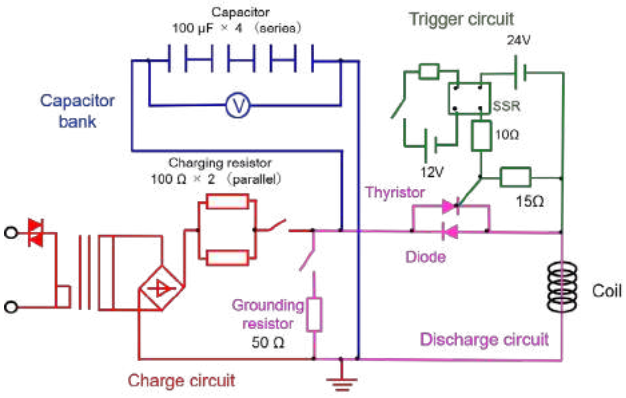

Figure 1. Electric circuit of a oscillating pulsed magnet system.

Figure 2. Constructed oscillating pulsed magnet system.

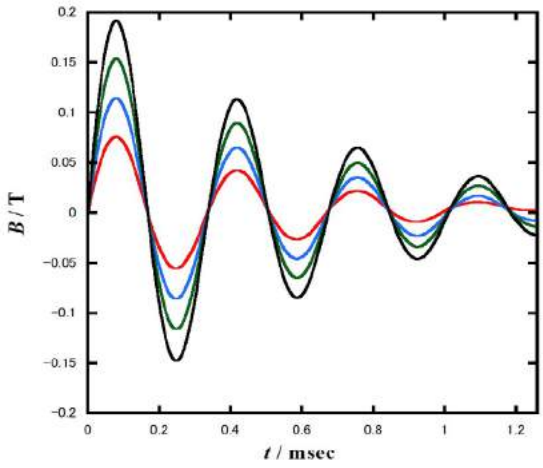

Figure 3. Time course of oscillating magnetic field

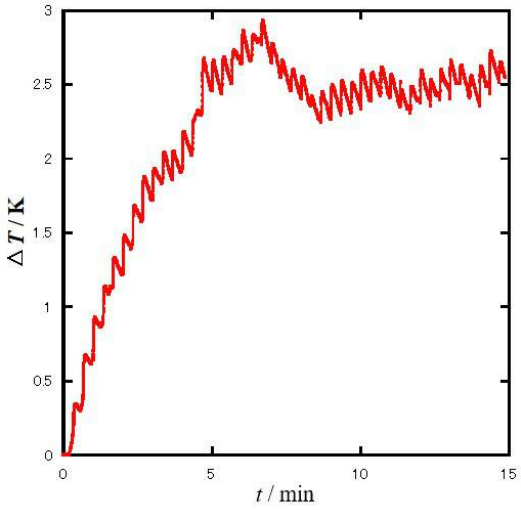

Figure 4. Time course of temperature of Aluminum block.

3. RESULTS

A coil with inductance (L) and resistance of 125 μH and 93 mΩ, respectively, was connected to a capacitor bank of 100 μF. When the discharge switch was turned on after charging with a voltage of 100 V, a magnetic field of up to about 0.2 T was generated four times in a row with a period of about 3 kHz as shown in Figure 3. The frequency did not change with the charging voltage, and the amplitude was proportional to the charging voltage. The temperature rise of the aluminum block (φ8, *l*=10) in the center of the bore was observed by generating oscillating pulsed magnetic fields every 30 seconds at a charging voltage of 100 V. As shown in Figure 4, the temperature rose about 2.5 K in about 5 minutes.

4. DISCUSSION

This time, an oscillating magnetic field of 3 kHz was generated, and it decayed as the second and third cycles progressed, but the decay can be suppressed by reducing the resistance and increasing the inductance. However, the decay can be suppressed by reducing the resistance and increasing the inductance. This can be improved by making the coil wire thicker and the diameter smaller. As for the temperature increase caused by magnetic stimulation, it is necessary to raise the magnetic field strength, but this can also be handled by improving the charging voltage. On the other hand, the improvement of vibration is also effective, and if the frequency is

increased to about 10 times, the saturation magnetization of the magnetic particle is reached. It is necessary to lower the capacitance and charge the battery at high voltage, and this can be achieved by connecting a large capacitor in series to effectively lower the capacitance. In the future, we will continue the development to improve the heat generation efficiency by increasing the number of capacitors under the use of the optical system we have prepared for optical non-contact measurement of heat generation.

.

ACKNOWLEDGMENT

This research was partly supported by The Watanabe Foundation.

REFERENCES

1) Swee Kuan Yen, et al. *Theranostics* 2013, 3, 986-1003

2) Atom Hamasaki, et al., *IEEE Transactions on Magnetics*, 2016, 52, 9401704

3) Atom Hamasaki, et al., *IEEE Transactions on Magnetics*, 2017, 53, 6500504

Detection of disturbances of visual perception processing using magnetoencephalography in patients with Lewy body disease

Moeko Shinohara[1, 2], Masato Koike[1, 3], Hirofumi Morise[3], Kiwamu Kudo[3], Junji Komatsu[1, 2], Chiemi Abe[1, 2], and Masahito Yamada[1]

[1]Department of Neurology and Neurobiology of Aging, Kanazawa University Graduate School of Medical Sciences, Kanazawa University, Kanazawa, Japan
[2]Department of Preemptive Medicine of Dementia, Kanazawa University Graduate School of Medical Sciences, Kanazawa University, Kanazawa, Japan
[3]Medical Imaging Business Center, Ricoh Futures BU, Ricoh Company, Ltd., Tokyo, Japan

Abstract

Lewy body disease (LBD) includes Parkinson's disease and Dementia with Lewy bodies (DLB). DLB is the second most common neurodegenerative disease, which cause dementia, after that due to Alzheimer's disease (AD). Early diagnostic methods of DLB have not been established. Since DLB is characterized by visual processing disturbance, we analyzed the neural responses to the optic flow and evaluated the visual perception processing using magnetoencephalography (MEG). The analysis was performed for patients with LBD (n = 4) and normal controls (n = 6). This study demonstrated that the maximum power in the left lateral occipital significantly correlated with the Trail making test-A score. Further studies are necessary to verify whether MEG during the optic flow task is useful for early diagnosis of DLB, and differentiation of DLB and AD.

Keywords: Lewy body disease, magnetoencephalography, optic flow

1. PURPOSE

Lewy body disease (LBD) includes Parkinson's disease (PD) and Dementia with Lewy bodies (DLB). DLB is the second most common neurodegenerative disease which cause dementia, after Alzheimer's disease (AD). Early diagnosis of DLB is difficult.[1)2)3)] DLB is characterized by visual processing disturbance. The aim of this study was to obtain a better understanding of the mechanisms of cortical processing during the optic flow task in patients with LBD and normal controls (NC) using magnetoencephalography (MEG).

2. METHOD

This study was conducted according to the guidelines of the Declaration of Helsinki and all procedures involving human subjects were approved by the Kanazawa University Medical Ethics Review Board (approval numbers 3041). Written informed consent was obtained from all subjects.

2.1 Subjects

The LBD group included patients with PD and DLB. The NC group had no history of psychiatric or neurological diseases and were receiving no medications that could act on their central nervous system. All subjects were assessed to be cognitively normal.

2.2 Optic flow task

Visual stimuli were presented on the screen in front of a subject. The subjects were required to maintain centered visual fixation throughout the presentation of all visual stimuli. Two types of stimuli, stationary dots and optic flow, were used. To suppress variance of neural responses to the optic flow stimuli, we set the optic-flow stimuli and the stationary-dots stimuli to occur randomly at a ratio of 4:11.

2.3 Data processing

MEG data of 96 optic flow trials were analyzed for each subject using a MATLAB toolbox, Brainstorm. Six regions of interest (ROIs), left/right Lateral Occipital, Inferior Parietal, and Superior Parietal, that covered the dorsal stream, were set based on the Desikan-Killiany atlas.[4] Event-related fields in the epoch-averaged signals were observed from 100 ms to 300 ms in all the subjects. Neural responses of the six ROIs to the optic flow were evaluated by maximum power of source activity within the time interval.

3. RESULTS

A total of 4 PD patients (LBD group) and 6 NC subjects participated in this study. All the patients with PD were diagnosed with clinically established Parkinson's disease, according to the diagnostic criteria of the International Parkinson and Movement Disorder Society (MDS). The median score of the Unified Parkinson's Disease Rating Scale (UPDRS) part III was 26.5 points in the LBD group. Age and gender did not differ between the LBD and NC groups. The Mini-mental state examination (MMSE) scores were significantly lower in the LBD group than in the NC group ($P = 0.019$) (Table 1). No significant difference was noted between the LBD and NC groups for Trail making test (TMT)-A and TMT-B scores (Table 1). All patients with LBD group were diagnosed as normal cognition. Three of 4 patients with LBD represented rapid eye movement sleep behavior disorder, and one of them had visual hallucination.

Regarding the maximum power, statistical difference was not significant between the LBD and NC groups in any ROIs. The maximum power in the left lateral occipital significantly correlated with the TMT-A score ($r = -0.803$, $P = 0.009$) (Figure 1).

4. DISCUSSION

We demonstrated that the maximum power in the left lateral occipital significantly correlated with the TMT-A score. It has been reported that TMT-A score mainly related with visuo-perceptual attention abilities.[5] Our results therefore indicated that the attention ability would be associated with a change in the processing of optic flow stimulations in the left lateral occipital regions. Further studies with large number of subjects as well as various types of dementia, such as DLB and AD, are necessary since the number of subjects in this study was small.

In conclusion, our MEG analysis indicates that visuo-perceptual attention ability would have a relationship with the brain function of the left lateral occipital regions during the optic flow perception.

Acknowledgement

This study was supported by Watanabe foundation and grant from RICOH Co., Ltd.

References

1) McKeith IG, et al. Diagnosis and management of dementia with Lewy bodies: Fourth consensus report of the DLB consortium. Neurology, **89**: 88-100 (2017).
2) Lobotesis K, et al. Occipital hypoperfusion on SPECT in dementia with Lewy bodies but not AD. Neurology, **56**: 643-9 (2001).
3) O'Brien, JT, et al. ^{18}F-FDG PET and perfusion SPECT in the diagnosis of Alzheimer and Lewy body dementias. J Nucl Med, **55**: 1959-1965 (2014)
4) Tobimatsu S and Celesia GG. Studies of human visual pathophysiology with visual evoked potentials. Clin Neurophysiol, **117**: 1414-1433 (2006).
5) Sanchez-Cubillo I, et al. Construct validity of the Trail Making Test: Role of task-switching, working

memory, inhibition/interference control, and visuomotor abilities. J Int Neuropsychol Soc, **15**: 438-450 (2009).

Table 1. Cognitive function of NC and LBD group

	NC (n = 6)	LBD (n = 4)
MMSE (points), median (range)	29.4 (28-30)	27.7 (27-28)*
TMT-A (sec), median (range)	41.0 (25-59)	48.5 (31-94)
TMT-B (sec), median (range)	83.0 (39-129)	93.5 (88-146)

* $P < 0.05$; LBD: Lewy body disease; MMSE: Mini-mental state examination; NC: Normal control; TMT-A: Trail making test-A; TMT-B: Trail making test-B

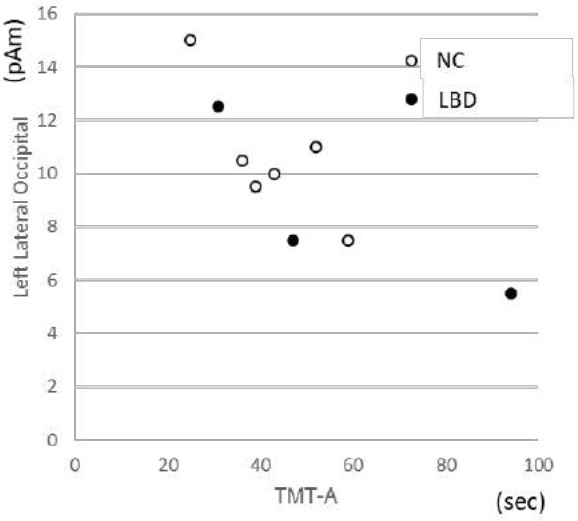

Figure 1. Correlation between the maximum power in the left lateral occipital and TMT-A score.

Development of navigation system for surgical operation of a spinal cord applying low-frequency-band magnetic field detection

Yoshiaki Adachi*, Daisuke Oyama*, Shigenori Kawabata**,
Yoshikazu Nakajima***, Takaaki Sugino***, Miyuji Matsuda***, Masaya Onogi***

*Applied Electronics Laboratory, Kanazawa Institute of Technology
3 Amaike, Kanazawa, Ishikawa 920-1331 Japan
**Department of Advanced Technology in Medicine, Tokyo Medical and Dental University
1-5-45 Yushima, Bunkyo-ku, Tokyo 113-8519 Japan
***Institute of Biomaterials and Bioengineering, Tokyo Medical and Dental University
2-3-10 Kandasurugadai, Chiyoda-ku, Tokyo, 101-0062, Japan

Abstract

Conventional surgical navigation systems mainly rely on infrared stereographic camera technology and cannot track the position of the tools when optical markers are behind the body or hand of the surgeon. Furthermore, the dimensions of optical markers are often problematically large. To solve these inconveniences and satisfy the requirements of surgeons, which include a wide operative field and small markers, we developed a prototype of the new navigation system for spinal surgery based on low-frequency band magnetic field measurements. The developed system was equipped with a coil array implemented in a square frame surrounding the operative field. Instead of optical markers, surface-mounted inductors were used as markers to detect the magnetic fields generated from the coils. Real-time marker localization was successfully performed at approximately 1 Hz. As a result, we could expand the effective operative field to 300 mm×400 mm and reduce the dimensions of the marker to less than 3 mm×3 mm×3 mm.

Keywords: navigation system, marker localization, surface-mounted inductor

1. PURPOSE

Surgical navigation is a system that detects the position of the patient's vertebrae and the position and orientation of the surgical tools during orthopaedic spine surgery, and superimposes them on the previously captured X-ray and/or CT images in real time and displays on the screen. This is an indispensable technology for safe surgery. Most conventional surgical navigation systems are of the optical type, in which optical markers attached to the patient's anatomical fiducial points and surgical tools are imaged by a stereo graphic camera to determine the relative positions between them. However, when a doctor's hand or body is placed between the camera and the markers, imaging is interrupted, and tracking becomes impossible. In addition, the placement of the optical markers was greatly restricted due to the interruption of imaging and the dimensions of the markers themselves.

On the other hand, a radio-wave-based navigation system, which detects the position by transmitting an electromagnetic field from the marker and receiving it by the antenna coil (or conversely, transmitting an electromagnetic field from the coil and receiving it by the marker), does not have the above problem, but it has another problem: when there are metal surgical tools in or near the operative field, the distribution of radio

waves is distorted owing to the skin effect, and the position cannot be detected correctly.

This study aims to develop a new navigation system for spinal surgery based on low-frequency band magnetic field measurements that solve the problems of the conventional optical and radio wave types by using the frequency range of 100 Hz to 1 kHz, which is less affected by the skin effect of metals.

2. METHOD

Before developing the navigation system, we discussed with orthopaedic surgeons who perform the spine surgery what an easy-to-use and effective surgery navigation system would be. Consequently, it was revealed that a wide operative field and small markers were required in addition to uninterrupted marker tracking.

To satisfy these requirements, the developed system was designed with a coil array implemented in a square frame surrounding an operative field to induce magnetic fields and markers equipped with the magnetic flux sensors to capture them. The inner dimensions of the frame were 300 mm×400 mm, which was sufficiently large to cover the entire operative field for spine surgery. The thickness of the frame was 30 mm so that would not interfere with the surgery. In this study, a coil array was equipped with 16 circular coils, and each coil was excited at different frequencies. Under these conditions, a Monte Carlo simulation was applied to various coil arrangements, as shown in Fig. 1(a), to determine the optimal coil configuration. As shown in Fig. 1(b), coil array #0 was selected as the coil array with the largest area where the magnetic flux sensor's localization error was less than 1 mm within a range of ±120 mm above and below the frame. Eight circular coils of ϕ80 mm were placed at each of the four corners of the square frame. The other eight circular coils of ϕ40 mm were placed on the edges of the frame. Each coil had 100 turns.

We applied surface-mounted inductors (100 μH, NLV25T101-PF, TDK, Japan) as markers with magnetic flux sensors. Although their sensitivity is less than that of other types of magnetic flux sensors and

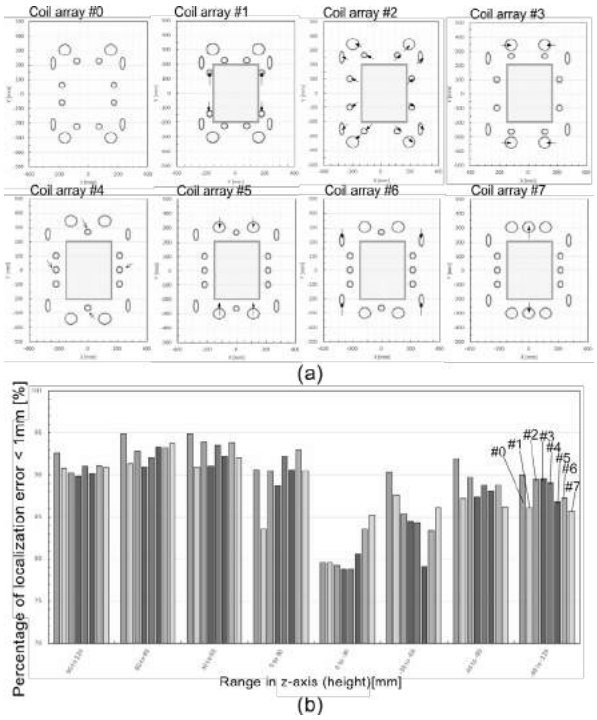

Figure 1. (a) Candidates of the coil arrangements. (b) Percentage of the region in which the localization error would be less than 1 mm for each coil arrangement.

proportional to the signal frequency, which is a significant disadvantage, especially for detecting low-frequency band signals, their small dimensions are a large advantage in reducing the dimensions of the markers, much smaller than those of the other magnetic flux sensors. The proposed coil array in the frame could induce sufficiently large magnetic fields that could be detected by the surface-mounted inductors, and we could reduce the dimensions of the markers to less than 3 mm×3 mm×3 mm.

Multi-channel current amplifiers to apply a specific frequency current to each coil and multi-channel low-noise amplifiers to amplify the magnetic field signals from the magnetic flux sensors were designed and prototyped. We also developed a position-detection software that implements a magnetic sensor position estimation algorithm. Figure 2 shows the appearance of the coil array, electric circuit, and software of the prototype surgical navigation system.

In the preliminary test, 16 coils were excited simultaneously at different frequencies from 780 Hz to 2 kHz, and four magnetic sensors at arbitrary positions

in the frame and digitally recorded the combined magnetic fields. For each sensor, the data were sequentially separated by a time window of a specific width, and Fourier analysis was used to extract the coil-specific frequency components. The position of the magnetic flux sensor was estimated from the extracted frequency components and the positions and orientations of the 16 coils in a manner similar to the calibration for an array of biomagnetic sensors using an array of multiple coils[1]. The obtained positions of the magnetic flux sensors are displayed in real time on the screen and sent to a computer for matching medical images through the LAN.

To superimpose the detected marker position on the previously captured medical image, it is necessary to align the detected position coordinates in three-dimensional (3D) space with the coordinates on the medical image. We developed a software for position matching and display and tested it using a set of optical markers attached to the frame of the coil array. As shown in Fig. 3, the relative positions of the camera, frame, and surgical tools were tested using a combination of a commercially available 3D tracking system (Aurora, NDI) and an optical-type surgical navigation system (Polaris).

3. RESULTS

Figure 4 shows an example of the frequency analysis of the combined magnetic fields from 16 coils obtained using the position estimation software. This indicates that the magnetic fields from each coil can be separated and detected with a sufficient signal-to-noise ratio. Figure 5 shows an example of the simultaneous estimation of the positions of the four magnetic flux sensors based on the frequency components specific to each coil and the positions and orientations of the coils. The positions of the four sensors were sequentially estimated at a frequency of approximately 1 Hz, and it was confirmed that the estimated positions followed the movement of the magnetic flux sensors when they were moved in parallel, assuming that the multipole markers were attached to the surgical tool.

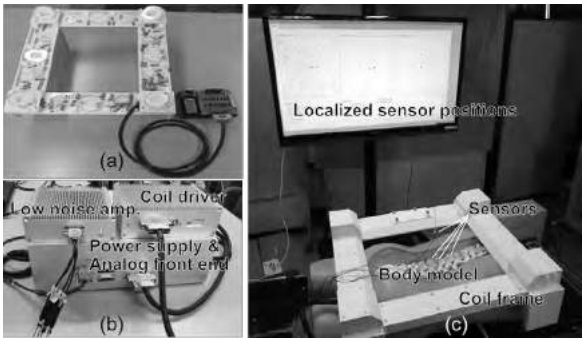

Figure 2. Prototyped navigation system. (a) Inner view of the coil array in the frame. (b) Electronics to drive coils and amplify the signals from sensors. (c) Localization of the sensors.

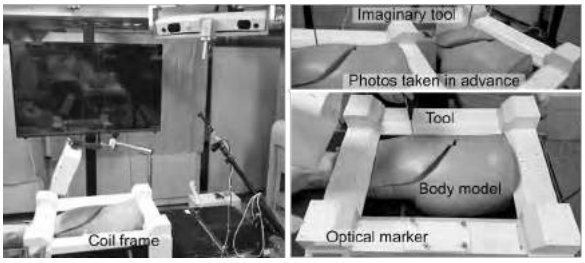

Figure 3. Preliminary test for calibration between the coil frame and the medical image using a set of commercially-available navigation system.

4. DISCUSSIONS

Previously, we proposed a navigation system with the opposite configuration of this study, that is, using a small coil as a marker and a frame-shaped sensor array to detect the magnetic field emitted from the coil and localize the marker[2]. Although the previous navigation system provided a localization frequency of approximately 2 Hz or more, in the prototype of this study, the frequency was only approximately once per second, even in a similar computing environment. One of the reasons is that the theoretical magnetic fields were calculated using an approximate magnetic dipole for marker coils in the previous system, whereas it cannot be approximated using a magnetic dipole for the circular coils used in this study, and a higher computational cost was necessary to calculate the theoretical field. In practice, a circular coil is approximated as a polygon coil to reduce the computational cost. To increase the frequency of position estimation, it is advantageous to approximate with polygons with fewer vertices because

this reduces the computational cost, but it is a tradeoff for the degradation of position estimation accuracy owing to the approximation error.

We also confirmed that it was possible to calibrate the camera image and coil frame using a commercially available surgical navigation system. However, this method requires a separate system to calibrate them other than the coil frame and camera. In principle, it is possible to estimate and calibrate the positions of optical markers on the coil frame from images captured by a camera. However, in actual surgical navigation, the position of the surgical tool should be superimposed on the X-ray image, so it is necessary to align the coil frame, X-ray irradiator, and X-ray imaging panel. Unlike an optical camera, the X-ray image shows little perspective, necessitating the development of a new calibration algorithm. In addition, markers that can be observed in X-ray images are also necessary. These are our future tasks.

5. CONCLUSION

In this study, we prototyped a needs-orientated navigation system for spine surgery using "position detection by magnetic field measurement" as the technological seed, which is based on biomagnetic measurement. The system became easy to use from a doctor's viewpoint through medical-industrial collaboration, providing a wide operational field expanded to 300 mm×400 mm and equipped with small markers with the dimensions of less than 3 mm.

We are also on the verge of developing a software to superimpose the position of the surgical tool on the medical image according to the estimated marker position.

In the future, we will continue to work on various issues for practical use of the system, such as evaluating and optimizing marker localization accuracy, reducing the excitation frequency by improving the signal-to-noise ratio, speeding up marker position localization, calibrating with X-ray images, and improving the use interface of the software.

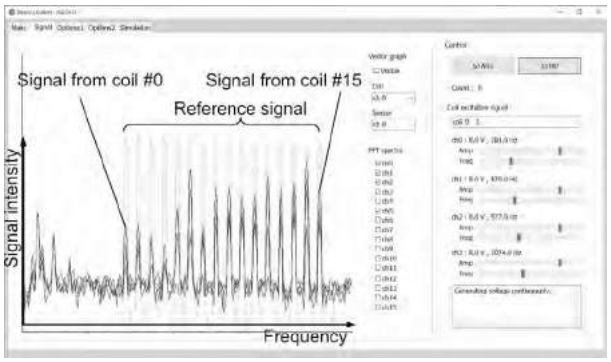

Figure 4. An example of frequency analysis of the combined magnetic fields from 16 coils.

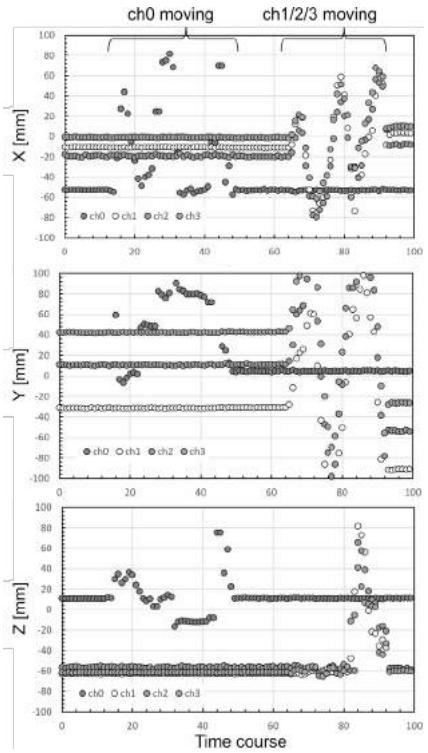

Figure 5. An example of sequential localization of the four magnetic flux sensors.

ACKNOWLEDGMENT

This work was supported by a Watanebe Foundation Research Grant.

REFERENCES

1) Yoshiaki Adachi et al, IEEE Trans Magn, vol. 55(7), 5000506 (2019).
2) Daisuke Oyama et al, IEEE Trans Magn, vol. 50 (11), 5101604 (2014).

Development of magnetic nanomaterials that enable novel bioperspective nanoimaging

Kazuhide Sato*,**

*Nagoya University Institute for Advanced Research (IAR)
**Dept of Respiratory Medicine, Nagoya University
65, Tsuruma-cho, Showa, Nagoya, Aichi, 466-8550, Japan

Abstract

In clinical medicine, diagnosis and evaluation based on imaging are essential for understanding pathological conditions, determining treatment methods, and measuring treatment effects. In this study, we develop the Gd encapsulated carbon nanotube (CNT), and investigate its biocompatible modification. We intend to develop this material for biological application with both Near infrared II (NIR-II) fluorescence and MRI-magnetic imaging.

Keywords: carbon nanotube, NIR-II, peapods, MRI, in vivo imaging

1. Introduction

In clinical medicine, diagnosis and evaluation based on imaging are essential for understanding pathological conditions, determining treatment methods, and measuring treatment effects [1]. In recent years, molecular imaging, which can diagnose and depict only pathological conditions and diseases from anatomical imaging, has become known as a new field and method [2]. Among them, imaging using fluorescence is widely used in detailed biological experiments and genetically modified animal experiments, and is the foundation of today's biological research. Among them, the region of near-infrared light above 1000 nm is called the NIR-II region, and has been attracting attention in recent years [3]. It is characterized by extremely low autofluorescence, allowing observation of the deepest parts of the body, and a signal-noise ratio of 100 times higher at 1320 nm than at 850 nm, making it a promising new area for in vivo imaging. However, compared to other fluorescent materials, there is a lack of fluorescent materials that can be used in vivo.

2. Purpose

The purpose of this research proposal is to develop the world's first metal (Gd) encapsulated carbon nanotubes (CNTs), to investigate their biocompatible modification, and finally to achieve their biological application as NIR-II imaging materials that can simultaneously perform MRI (magnetic imaging). In addition to real time imaging of CNTs using MRI, we will be able to measure real time changes in tumor blood vessels by treatment and the effects of lung diseases by achieving inhalation imaging. In addition, we will develop naturally-derived carbon materials as imaging agents for future clinical and biological applications, such as blood flow in near-infrared ray immunotherapy, which has been reported as an innovative treatment.

3.Methods, Results, and Discussion

A single-walled carbon nanotube, MEIJO eDIPS EC1.0 (Meijo NanoCarbon Co., Ltd.), was prepared. The central diameter of the above single-walled carbon nanotube is 1.0 nm. The numerical value of the central diameter is the median value of the carbon nanotubes contained, and is calculated from the chiral index, but the same value can be confirmed by observation under

an electron microscope [4]. In an electric furnace under an atmospheric atmosphere, the single-walled carbon nanotubes were heated up to 500°C over a period of 6 hours, and when the temperature reached 500°C, the heating was stopped and the tubes were allowed to cool down to room temperature [5]. This operation was used to open the both ends of the single-walled carbon nanotubes. The product was removed from the quartz tube after cooling to room temperature and washed with water. GdI3 that was not involved in the carbon nanotubes and GdI3 that was not encapsulated in the carbon nanotubes but adhered to the outer surface of the carbon nanotubes were removed by this rinsing. The Gd-encapsulated carbon nanotubes after rinsing were used as Gd-encapsulated carbon nanotubes. The Gd-embedded carbon nanotubes were observed by transmission electron microscopy (TEM). The TEM image of the Gd-encapsulated carbon nanotubes of Production Example 1 is shown in Figure 1.

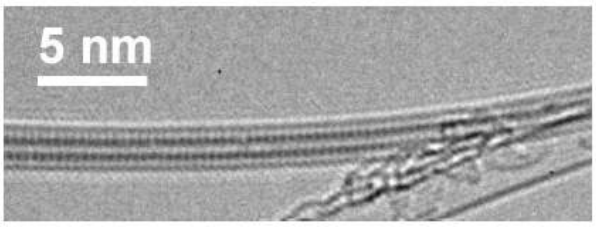

Figure1 TEM Image

From the TEM images in Figure 1, it can be confirmed that Gd-containing materials are encapsulated inside the carbon nanotubes in all of the Gd-encapsulated carbon nanotubes. A wire-like structure with interconnected Gd inside the carbon nanotubes was observed.

According to the TEM observation, it could be judged that Gd-containing substances were encapsulated in approximately half of the carbon nanotubes present in all of the Gd-encapsulated carbon nanotubes.

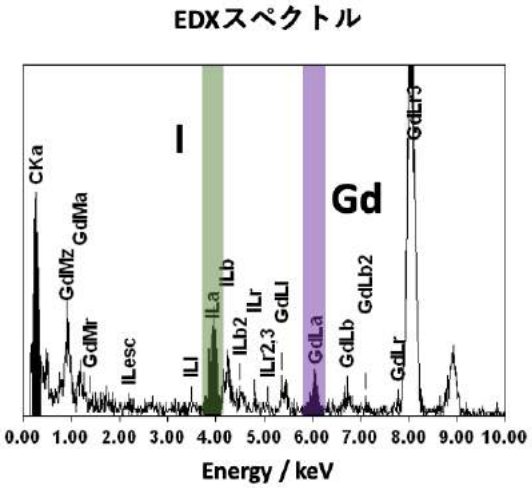

Figure2 EDX spectra

Next, we analyzed the Gd-encapsulated carbon nanotubes that were confirmed to contain GdI3 by TEM-EDX, which combines a transmission electron microscope with an energy dispersive X-ray analyzer (Figure 2). As a result, peaks originating from Gd and Cl were observed in the EDX spectra of the GdI3 encapsulated carbon nanotubes.

Then, 5 mg of Gd-encapsulated carbon nanotubes and 3 mL of 1 mass% sodium cholate solution were mixed and sonicated for 4 hours in a sealed ultrasonic disperser Nanoruptor NR-350 (Tosho Electric Co., Ltd.) to make a dispersion solution. The dispersed liquid was submitted to a small ultracentrifuge CS100GXL (Hitachi Koki Co., Ltd.) for separation and centrifuged at 52,000 rpm for one hour to precipitate carbon nanotube aggregates and other substances. The upper part of the dispersion solution after the centrifugation process was collected and used for the subsequent study.

To evaluate the NIR-II fluorescence of the above preparation, GdI3 solution and water (negative control), the fluorescence was evaluated using SHIMADZU's SAI-1000 (Figure 3) [6]. The results showed sufficient NIR-II fluorescence in GdI3 encapsulated CNTs. Next, we examined the MRI to determine the feasibility of magnetic imaging. Omniscan, a contrast agent, was added as a positive control and water as a contrast

control. The results showed that GdI3 appeared darker than water in both T1- and T2-weighted images, indicating that it could be used as a positive contrast agent.

The above materials were found to have good contrast ability in NIR-II and MRI, and will be investigated in animal models of diseases.

Figure3 Detection of NIR-II fluorescence

4. Conclusions

We have successfully synthesized GdCl2 encapsulated carbon nanotubes and confirmed their imaging performance. In the future, we will investigate its use in animal models.

Acknowledgements

This study was supported by a research grant from the Watanabe Foundation.

References

1) Kobayashi H, Longmire MR, Ogawa M, Choyke PL, Kawamoto S.
Lancet Oncol. 2010 Jun;11(6):589-95.

2) Kobayashi H, Choyke PL, Ogawa M.
Curr Opin Chem Biol. 2016 Aug;33:32-8.

3) Wang S, Li B, Zhang F.
ACS Cent Sci. 2020 Aug 26;6(8):1302-1316.

4) Nakanishi Y, Omachi H , Fokina NA , Schreiner PR , Becker J , Dahl JEP , Carlson RMK , Shinohara H .
Chem Commun (Camb). 2018 Apr 12;54(31):3823-3826.

5) Nagata M, Shukla S, Nakanishi Y, Liu Z, Lin YC, Shiga T, Nakamura Y, Koyama T, Kishida H, Inoue T, Kanda N, Ohno S, Sakagawa Y, Suenaga K, Shinohara H.
Nano Lett. 2019 Aug 14;19(8):4845-4851.

6)https://www.an.shimadzu.co.jp/bio/sai-1000.htm

The Subjects for the 2020 Research Grants

Here are the subjects (5 Basic Researches, 3 Application Researches, 3 Specific Researches and 2 Special Research 2020) that the 2020 Research Grants are subsidized.

Ⅰ. Basic Research

Ⅰ-1. Magnetic Field Effects on Photodynamic Therapy
Sojo University／Hiroaki YONEMURA

Ⅰ-2. Amelioration of pathological states by mitophagy induced by extremely low frequency fluctuation of extremely weak fields
Division of Neurogenetics, Nagoya University Graduate School of Medicine／Kinji OHNO

Ⅰ-3. Fabrication of artificial bone substitute applied to cell orientation characteristics by magnetic stimulation
Kyushu Institute of Information Sciences／Takaaki ARAHIRA

Ⅰ-4 The difference of the beige adipose tissue between the subcutaneous and visceral adipose tissues
Nippon Sport Science University／Madoka OGAWA

Ⅰ-5 How would pulse magnetic field influence differentiation of cultured myoblast to obtain contractile function?
Tohoku University Graduate School of Biomedical Engineering／Ryoichi NAGATOMI

Ⅱ. Application Research

Ⅱ-1. Application of TMS-EEG as a novel biomarker of epilepsy
Department of Neurology, The University of Tokyo Hospital／Satoshi KODAMA

Ⅱ-2. Optimazation of magnet shape for compact magnetic probe with nitrogen-vacancy center
The University of Tokyo／Akihiro KUWAHATA

Ⅱ-3. Elucidation of Sodium Metabolism Disorders in Systemic Sclerosis using Na-MRI
Department of Stem Cell and Reguletion, Yokohama City University Graduate School of Medicine／Kaoru MINEGISHI

Ⅲ. Specific Research

Ⅲ-1. Investigation of stimulation parameters for plastic changes in the central nervous system by paired associative stimulation of magnetic stimulation and transcutaneous spinal cord stimulation
Graduate School of Arts and Sciences, The University of Tokyo／Naotsugu KANEKO

Ⅲ-2. Inhibitory effects of magnetic stimulation on the onset of psychiatric symptoms and elucidation of the mechanism
National Defense Medical College Department of Psychiatry／Minori KOGA

Ⅲ-3. Relation of Nervous System and Magnetic Field
Osaka University, Department of Cardiovescular surgery, Graduate School of Medicine／Eri KANEKO
<This study was selected for OKAI Special Grant>

Ⅳ. Special Reseach Grant 2020

Ⅳ-1. <Basic Research>Magnetic heating of nanoparticles for tissue/organ cryopreservation
Tokai National Higher Education and Research System, Nagoya University／Akira ITO

Ⅳ-2. <Application Research>Effect of upper and lower limbs rehabilitation with concomitant peripheral magnetic stimulation below the motor threshold
Department of Rehabilitation Medicine I , School of Medicine, Fujita Health University／Hitoshi KAGAYA

Note: Affiliations above are at the time of the grants were subsidized.

THE REPORT OF STUDY RESULT BY SUBSIDY
助 成 研 究 成 果 報 告 書
第26回

発　行　日　　令和3年9月1日
発　行　所　　公益財団法人 渡邉財団
福岡県福岡市中央区天神1-13-17
TEL 092-724-3605
FAX 092-724-3690
印　　刷　　三栄印刷株式会社

より明瞭なカラーデータの図表をご希望の方はサイト(https://watanabe-zaidan.or.jp/)に掲載しておりますのでご覧下さい。